

NATIONAL TRANSPORTATION SAFETY BOARD

Office of Research and Engineering
Materials Laboratory Division
Washington, D.C. 20594



September 18, 2014

MATERIALS LABORATORY FACTUAL REPORT

Report No. 14-052

A. ACCIDENT INFORMATION

Place : New York (Bronx), New York
Date : July 18, 2013
Vehicle : CSX freight train
NTSB No. : DCA13FR009
Investigator : Cy Gura, RPH-10

B. COMPONENTS EXAMINED

Five used concrete ties and 1 unused exemplar concrete tie.

C. DETAILS OF THE EXAMINATION

An overall view of the concrete ties is shown in figure 1. The five used concrete ties were labeled S5, S4, S3, N10, and N16. The ties had been numbered starting at the point of derailment and counting to the south and independently counting to the north. The letters "S" and "N" precede the tie numbers for ties south and north of the point of derailment, respectively. Thus, the used ties shown were the third, fourth, and fifth ties south of the point of derailment, and the remaining used ties were the tenth and sixteenth ties north of the point of derailment.

The train that derailed was northbound at the time of the derailment. The point of derailment was located in a left-hand curve (northbound direction). The west end of the ties (end supporting the low rail) were labeled on-scene with the green-colored paint visible on the used ties shown figure 1.

The ties were examined at the Metro-North Railroad Highbridge rail yard in New York, New York. Representatives from the Federal Railroad Administration, the VOLPE National Transportation Systems Center, CSX Transportation, and Metro-North Railroad participated in the examination. After the examination at the rail yard, the ties were shipped to Wiss Janney Elstner (WJE), Northbrook, Illinois, for mechanical testing and petrographic analysis.

The letters KSA or KOPPERS were observed cast in raised letters in the middle of the ties. Codes stamped on the shoulder inserts were matched to manufacturing records for the ties as provided by the tie manufacturer. Records indicated the used ties were manufactured in June, 1994, and the exemplar tie was manufactured in September, 1993.

Multiple transverse cracks were observed by visual inspection in the middle portion of each of the used ties. A closer view of ties S3 and S4 is shown in figure 2 where arrows indicate the transverse cracks. Ties S4 and N16 had 8 cracks, and the remaining used ties had 7 cracks. For reference, the cracks were labeled from west to east with lower-case letters a through g or h. The spacing between the cracks was measured at the tie centerline, and results of the measurements are listed in table 1.

The crack depths were determined by close visual inspection on both the north and the south faces of the ties. The measured crack depths from the top surface are listed in table 1. The cracks were oriented approximately in a vertical transverse plane near the top surface, and the tips of many of the cracks curved toward a longitudinal plane orientation consistent with bending deflections (top surface in tension) and interaction with the stress field of the reinforcement. A view of the south faces of ties S3 and S4 is shown in figure 3. A yellow paint marker was used to outline the locations of the cracks, as can be seen in figure 3.

Material was missing from the lower portions of the used ties. The lower side of tie N16 is shown in figure 4, showing typical features observed on the lower portion of the ties. The lower portion of the ties had rounded shape with a rough surface texture similar to that shown in figure 4. Material was also missing from the lower portion of the end faces of the ties, as shown for tie S3 presented in figure 5. The material loss was greater at the west ends of the ties relative to the east ends. As shown in figure 5, the ends of the reinforcement were exposed by the material loss.

Overall dimensions of the ties were measured including length at the top and bottom of the ties, width at the middle and at the rail seats, and depth at the middle and at the rail seats. Results of the measurements are listed in Table 2. On average, the used ties were missing 1.0 inch, 0.8 inch, 0.7 inch of depth relative to the engineering drawing at the low rail seat, the middle of the tie, and the high rail seat, respectively.

Ties N16, S3, and S4 were selected for scanning using a Faro QUANTUM FaroArm coordinate measurement device fitted with a Faro Laser ScanArm. A partial scan of tie N16 was completed outdoors at the Highbridge rail yard. Scans of ties S3 and S4 were completed indoors at a nearby New York Metropolitan Transportation Authority facility. The resulting scans were assembled into a 3D models, and the models were exported to interactive 3-dimensional (3D PDF) portable document files. The interactive 3D PDF models are included in Appendix A in the electronic copy of this report.¹

The 5 used ties and 1 exemplar tie were subsequently shipped to Wiss, Janney, and Elstner Associates, Inc., in Northbrook, Illinois, for mechanical testing and petrographic analysis. The ties were tested using the tie center negative moment test (tie upper surface in tension) per the American Railway Engineering and Maintenance-

¹ Adobe Reader 9 or later software is required to view 3D PDF files.

of-Way Association's *Manual for Railway Engineering*.² During the tests, deflection was measured at the middle of the tie, and strain evolution was mapped using Digital Image Correlation (DIC).

After the flexure tests were completed, samples were selected for conducting compression strength tests, splitting tensile strength tests, underwater abrasion tests, and petrography. The compression strength tests, splitting tensile strength tests, and petrography were conducted in accordance with ASTM standards C 39, C 496, and C 856, respectively.³ During the compression strength tests, elastic modulus and Poisson's ratio were determined in accordance with ASTM standard C 469, *Standard Test Method for Splitting Tensile Strength of Cylindrical Concrete Specimens*.

Underwater abrasion tests were conducted using a modified ASTM C 1138, *Standard Test Method for Abrasion Resistance of Concrete (Underwater Method)*. The standard test was modified due to limitations on specimen size and quantity that could be extracted from the ties. The standard test was used with the following modifications to adjust for the specimen size and quantity limitations.

- Two samples were cored from each tie tested instead of three specimens required per the standard.
- The inside diameter of the test container was 9 inches \pm ¼ inch instead of 12 inches required per the standard.
- Diameter of the agitation paddle (not including shaft diameter) was scaled to approximately ¾ the size shown in ASTM C 1138.
- The height of the water in the test chamber was adjusted to the top of the paddle (height D in figure 1 of ASTM C 1138).
- The number of balls listed in table 1 of ASTM C 1138 was reduced. The abrasive charge contained 5 balls with a nominal diameter of 1.00 inch, 20 balls with a nominal diameter of 0.75 inch, and 14 balls with a nominal diameter of 0.50 inch.

Specimens for the compression strength tests, splitting tensile strength tests, and the underwater abrasion tests were selected from areas between the outer shoulder insert and the end of the tie (area outside the loading points from the bend tests). Petrography of the used ties was conducted on areas near the middle of the ties where cracks had been observed prior to testing.

A brief summary of the mechanical test and petrographic examination results is provided below. For a more detailed documentation of the results of the mechanical testing and petrographic analysis, see the WJE report included in Appendix B.

² *Manual for Railway Engineering*, Ch. 30, Part 4, Concrete Ties, American Railroad Engineers and Maintenance-of-Way Association.

³ ASTM International; C 39, *Standard Test Method for Compressive Strength of Cylindrical Concrete Specimens*; C 496, *Standard Test Method for Splitting Tensile Strength of Cylindrical Concrete Specimens*; and C 856, *Standard Practice for Petrographic Examination of Hardened Concrete*

During the bend tests, the exemplar tie was initially tested to a load of 14,400 pounds, held for 3 minutes, then unloaded. No cracks were detected by visual inspection after this initial test. Next the exemplar tie was loaded to failure with a maximum load of 32,304 pounds and a corresponding mid-span deflection of 0.398 inch. The used ties were tested to failure without interruption. The maximum loads supported by the used ties ranged from 23,725 pounds (tie S3) to 30,854 pounds (tie N16) with an average of 27,167 pounds. The mid-span deflections at maximum load in the used ties ranged from 0.397 inch (tie N10) to 0.450 (tie S5) with an average deflection of 0.421 inch.

Compressive strength was tested on two specimens from the exemplar tie and 1 specimen from each of the used ties. A view of a typical compression test specimen after testing is presented in figure 6. The compressive strength of the specimens from the new tie measured 9,772 psi and 10,505 psi. Compressive strength of specimens from the used ties ranged from 10,609 psi (tie S5) to 12,618 psi (tie N10) with an average compressive strength of 11,654 psi.

Splitting tensile strength was tested on two specimens from the exemplar tie and 1 specimen from each of the used ties. A view of a typical compression test specimen after testing is presented in figure 6. The splitting tensile strength of the specimens from the new tie measured 910 psi and 1,115 psi. Splitting tensile strength of specimens from the used ties ranged from 1,005 psi (tie S5) to 1,130 psi (tie N10) with an average splitting tensile strength of 1,061 psi.

Underwater abrasion tests were conducted on specimens from the exemplar tie and ties S5, N10, and N16. A view of a typical test specimen after testing is presented in figure 8. Threaded steel inserts were present in the ends of the ties where test specimens could be taken, which resulted in the inserts being present in the test specimens as indicated in figure 8. The inserts had an outer diameter of 0.9 inch and were located at the center of each test specimen. A threaded rod was installed in the inserts to prevent media and debris from being trapped in the insert during testing. Tests lasted for 72 hours for each specimen, and volume lost was measured by gravimetric analysis. Results from the testing showed the average total volume lost from specimens from the exemplar tie was 3.11 in³ (50.9 cm³). The average total volume lost from specimens from the used ties was 3.33 in³ (54.5 cm³), 3.15 in³ (51.6 cm³), and 3.61 in³ (59.1 cm³) for ties S5, N10, and N16, respectively.

Results of the petrographic examination indicated the concrete from all samples was well consolidated and showed no evidence of deleterious chemical reactions between the aggregates and the constituents of the paste. Paste quality appeared to be good as it was hard, had low water absorbancy, and had subvitreous luster on fresh fracture faces. A tight paste-aggregate bond was noted, and no evidence of freeze-thaw related deterioration was observed. Air content in the exemplar tie measured 7.8%. Measured air content in the used ties ranged from 3.1% (tie S3) to 5.9% (tie N16) with an average of 4.8%. The vertical cracks observed in the used ties showed negligible amounts of carbonation (depth generally less than 0.02 inch).

Matthew R. Fox
Senior Materials Engineer

Table 1. Transverse Crack Locations and Depths

Tie Label	Crack letter	Distance from West End of Tie (inch)	Distance from Adjacent Crack to the West (inch)	Crack Depth Measured at the South Face of the tie (inch)	Crack Depth Measured at the North Face of the tie (inch)
S5	a	33.0		2.8	3.0
S5	b	38.0	5.0	3.0	2.5
S5	c	42.5	4.5	3.0	3.5
S5	d	49.5	7.0	3.3	3.0
S5	e	55.5	6.0	3.0	3.5
S5	f	63.5	8.0	3.0	2.3
S5	g	68.5	5.0	4.0	4.5
S4	a	30.0		3.3	2.8
S4	b	36.5	6.5	2.4	3.8
S4	c	42.3	5.8	2.8	3.5
S4	d	46.3	4.0	4.0	3.5
S4	e	55.3	9.0	4.0	3.5
S4	f	60.3	5.0	2.5	3.8
S4	g	64.8	4.5	2.8	3.0
S4	h	68.8	4.0	2.5	2.3
S3	a	33.5		1.8	3.0
S3	b	39.5	6.0	2.8	2.5
S3	c	43.5	4.0	3.5	3.8
S3	d	51.5	8.0	3.5	3.8
S3	e	58.5	7.0	3.5	4.8
S3	f	62.5	4.0	3.0	2.3
S3	g	67.0	4.5	2.4	2.5
N10	a	34.0		3.0	3.0
N10	b	37.5	3.5	2.8	2.4
N10	c	41.5	4.0	3.3	2.8
N10	d	47.8	6.25	3.0	2.5
N10	e	55.8	8.0	3.0	3.0
N10	f	61.8	6.0	3.0	3.0
N10	g	67.8	5.5	1.0	0.8
N16	a	33.0		2.5	3.5
N16	b	37.5	4.5	2.3	3.5
N16	c	44.0	6.5	2.8	3.3
N16	d	49.5	5.5	2.8	3.3
N16	e	52.5	3.0	3.3	3.2
N16	f	59.5	7.0	3.3	3.0
N16	g	63.8	4.3	3.8	3.3
N16	h	69.8	6.0	3.0	2.8

Table 2. Tie Dimensions

Tie Label	Width at the Rail Seats (inch)	Width at the Middle (inch)	Length at the Top (inch)	Length at the Bottom (inch)	Depth at the Low (West) Rail Seat (inch)	Depth at the Middle (inch)	Depth at the High (East) Rail Seat (inch)
S5	10.0	10.0	102.0	101.3	7.3	6.5	7.8
S4	10.0	10.0	101.9	100.0	6.8	6.0	7.5
S3	10.0	10.0	101.5	99.3	6.8	6.0	6.8
N10	10.0	9.8	101.8	96.0	6.8	6.3	7.0
N16	10.0	10.0	101.9	98.0	7.4	6.4	7.8
Drawing	10.0	10.0	102.0	102.0	8.0	7.0	8.0



Figure 1. Overall view of the concrete ties.



Figure 2. Middle portions of ties S3 and S4 showing multiple transverse cracks as indicated with arrows.



Figure 3. View of the south faces of ties S3 and S4 showing crack features outlined with yellow paint as indicated with arrows on tie S3.



Figure 4. View of the lower surface of tie N16 showing typical features observed on the lower side of the ties.

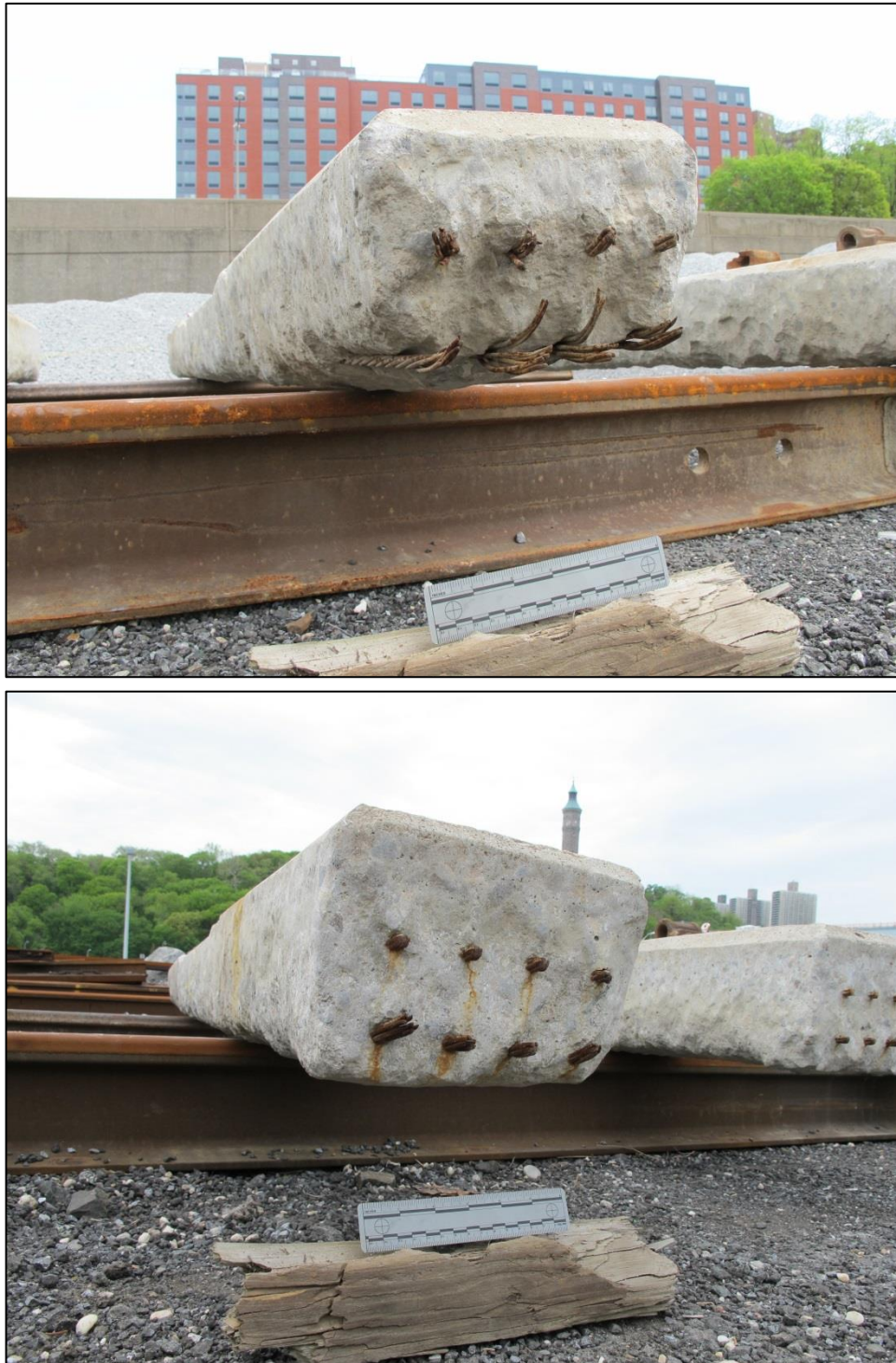


Figure 5. Views of the west (upper image) and east (lower image) ends of tie S3.



Figure 6. View of the compression test specimen from tie S3 shown after testing.



Figure 7. View of splitting tension test specimen from tie S3 shown after testing.

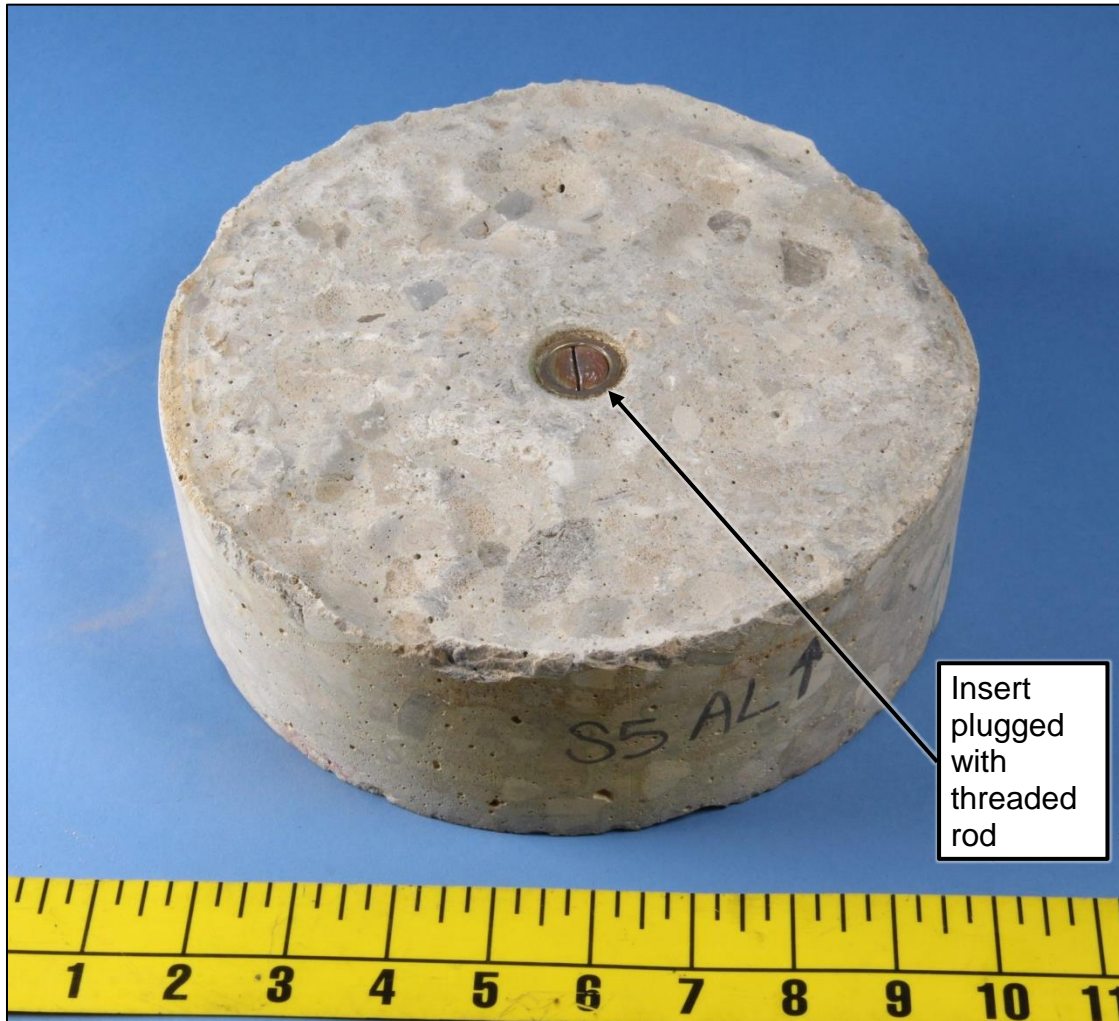
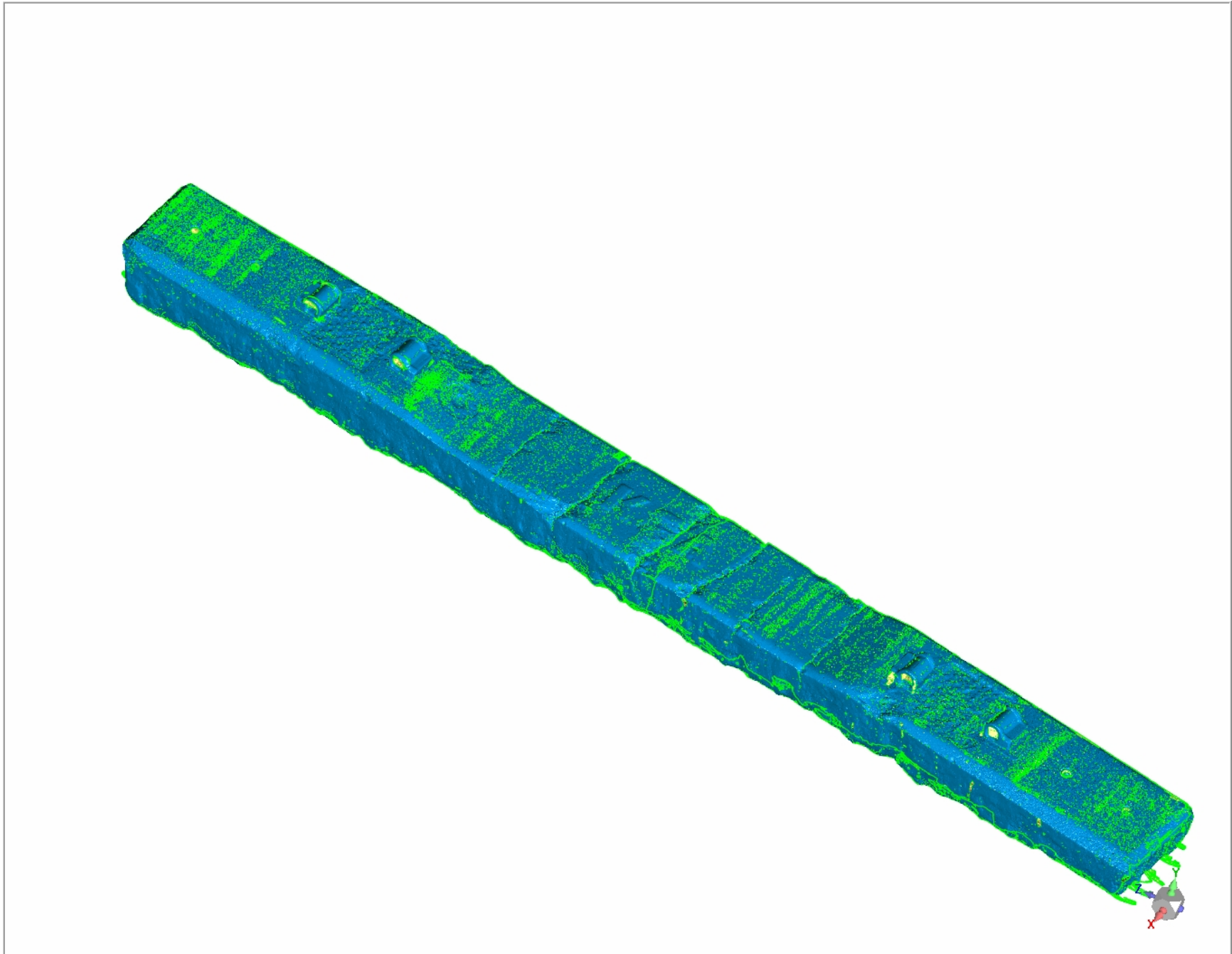
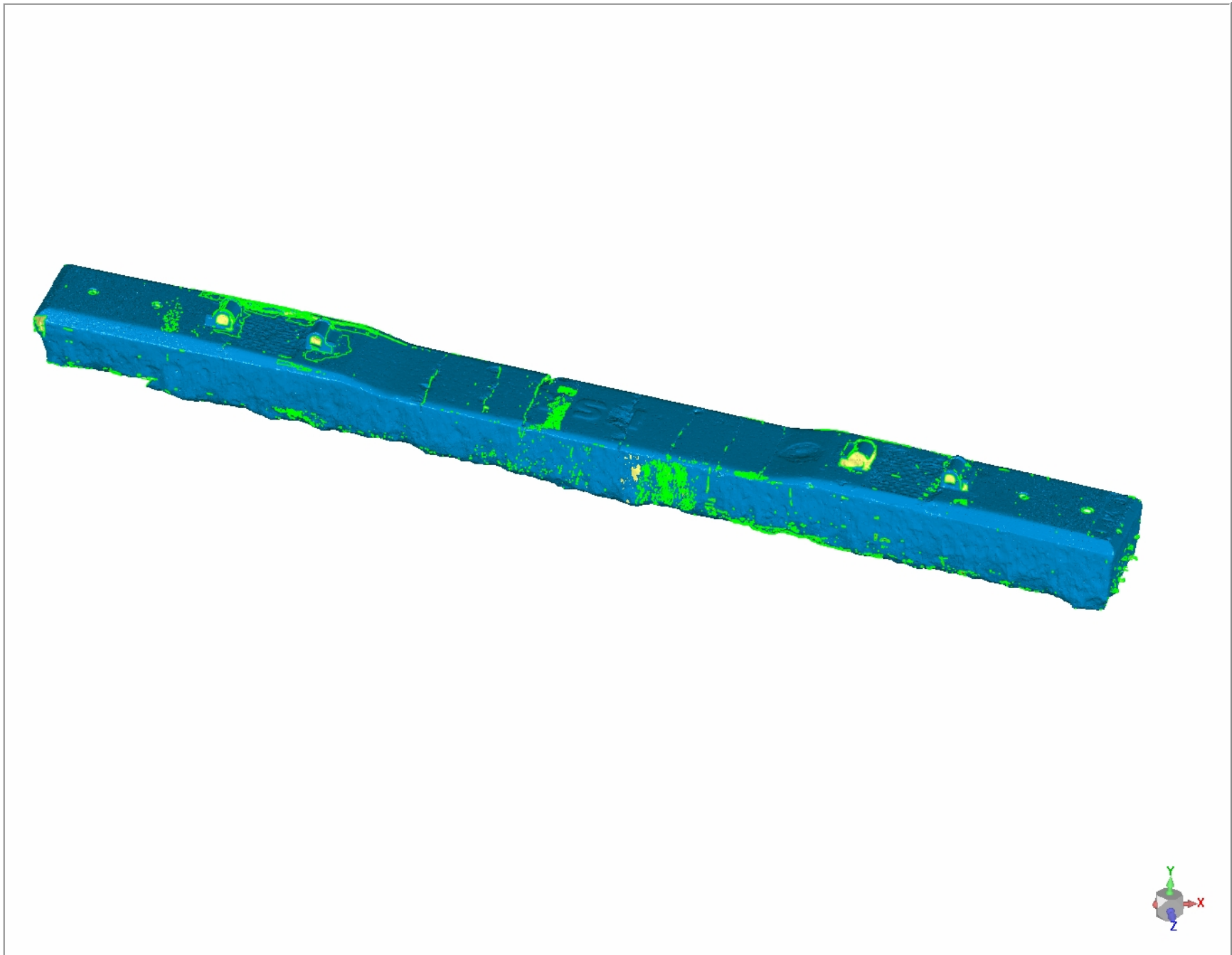


Figure 8. Overall view of one of the underwater abrasion test specimens from tie S5. The threaded insert at the center of the test specimen was plugged with a threaded rod.

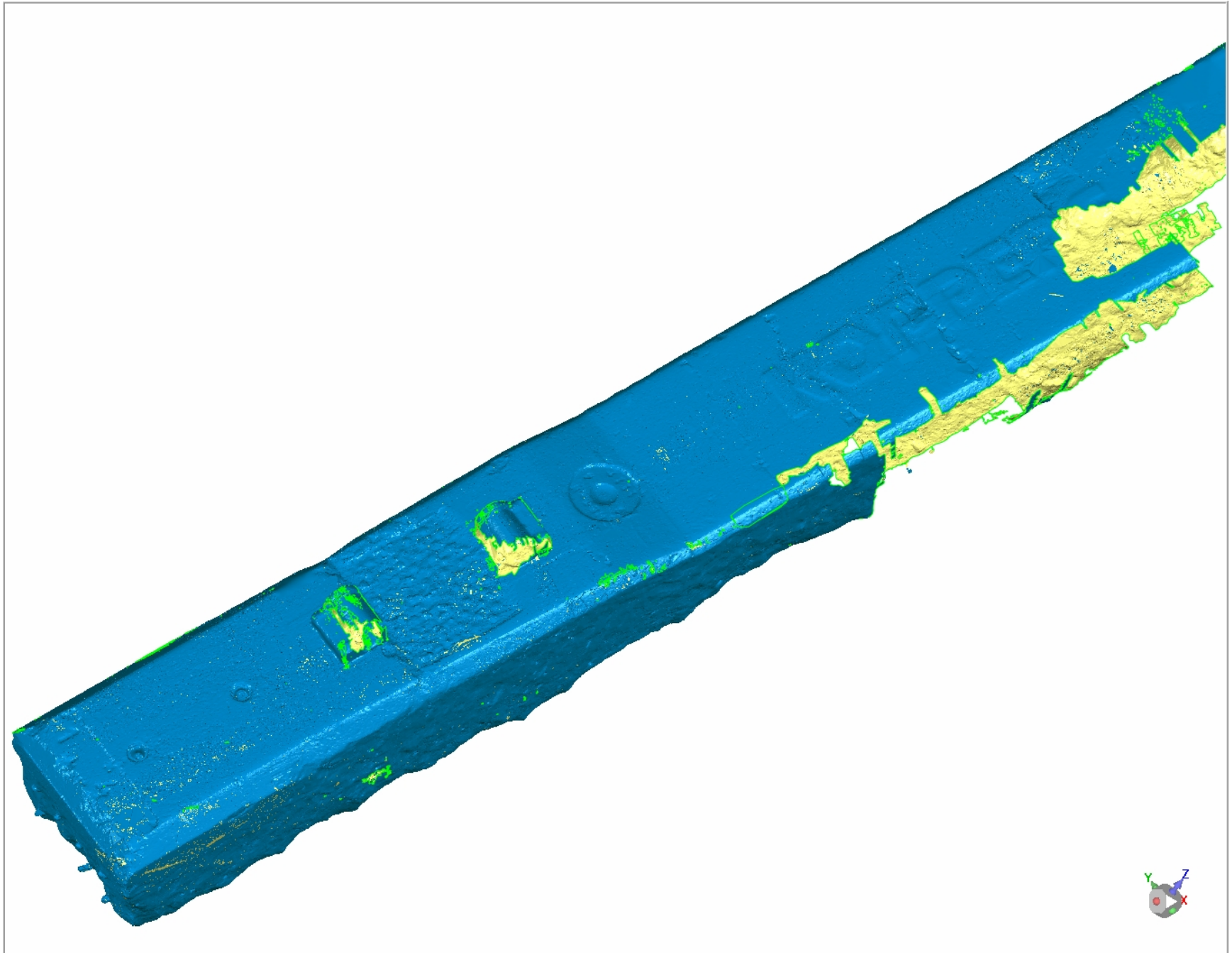
D. APPENDIX A. 3D PDF IMAGES OF TIES S4, S3, AND N16



Click on the image to activate the 3D Model.



Click on the image to activate the 3D Model.

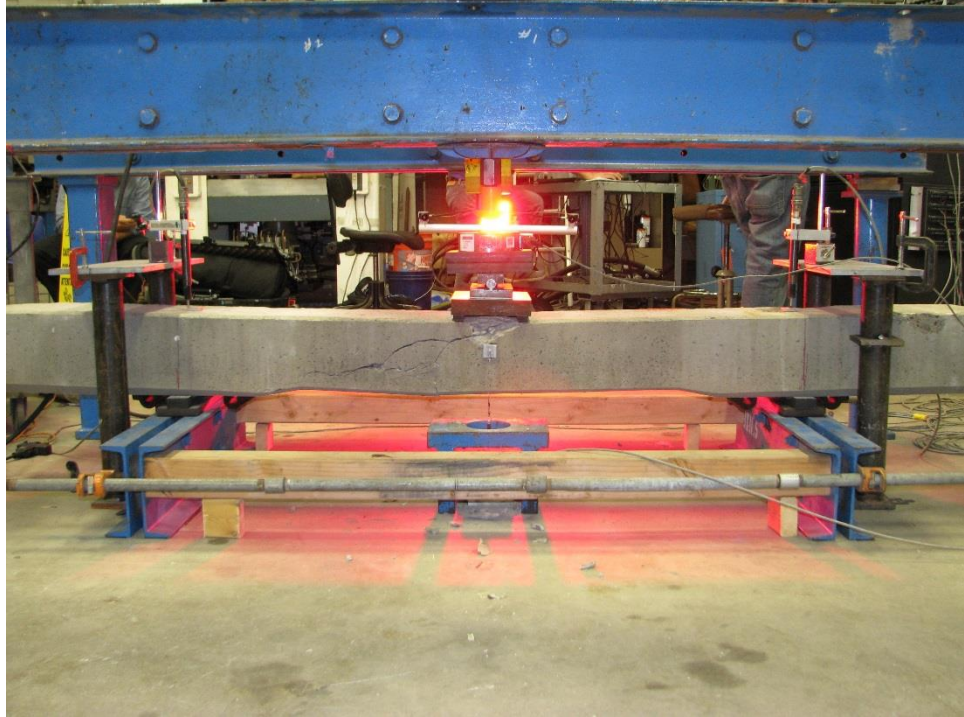


Click on the image to activate the 3D Model.

E. APPENDIX B. WJE REPORT



NTSB-R-140003
Concrete Tie Testing and Petrographic Services



Final Report
July 18, 2014
WJE No. 2014.2701



Prepared for:
Mr. Matthew Fox, Ph.D.
National Safety Transportation Board
Materials Laboratory Division (RE-30)
490 L'Enfant Plaza, SW
Washington D.C., 20594

Prepared by:
Wiss, Janney, Elstner Associates, Inc.
330 Pfingsten Road
Northbrook, Illinois 60062
847.272.7400 tel | 847.291.5189 fax



NTSB-R-140003
Concrete Tie Testing and Petrographic Services



A. Koray Tureyen, Ph.D., PE

Final Report
July 18, 2014
WJE No. 2014.2701



Prepared for:
Mr. Matthew Fox, Ph.D.
National Safety Transportation Board
Materials Laboratory Division (RE-30)
490 L'Enfant Plaza, SW
Washington D.C., 20594

Prepared by:
Wiss, Janney, Elstner Associates, Inc.
330 Pfingsten Road
Northbrook, Illinois 60062
847.272.7400 tel | 847.291.5189 fax

TABLE OF CONTENTS

Introduction.....	1
Scope of work	1
Bend Tests.....	2
Test Setup and Procedure.....	2
Test Results.....	3
Abrasion Tests	4
Compression and Splitting Tensile Strength Tests	5
Petrographic Examinations	6
Tables	
Figures	
Appendices	

NTSB-R-140003 Concrete Tie Testing and Petrographic Services

INTRODUCTION

Wiss, Janney, Elstner Associates, Inc. (WJE) has completed all testing and petrographic examinations in compliance with the requirements of the National Transportation Safety Board (NTSB) Solicitation No. NTSB-R-14-0003 entitled, “Concrete Tie Testing and Petrographic Services” issued May 14, 2014. The objective of this study was to determine the load/deflection response of submitted concrete railroad ties, qualitatively compare the wet abrasion resistance of used ties relative to a new (un-used) tie, assess the concrete using petrographic examination, and conduct physical and mechanical testing of concrete samples removed from the ties. The testing program was developed by NTSB to assist in their investigation of a train derailment incident. Technical consulting services in regards to interpretation of test results as they relate to the train derailment incident will be performed by others. All of the testing and petrographic examination work was conducted at WJE’s Janney Technical Center (JTC) in Northbrook, Illinois.

Six railroad ties, designated Ties N16, N10, S3, S4, S5, and New, were shipped by the NTSB to WJE’s laboratories and were received on June 11, 2014. Photographs of as received specimens were provided separately in digital format to Mr. Mathew Fox of NTSB. Five of the ties were used and reportedly had been in service for approximately 20 years. These used railroad ties had visible cracks that were previously marked by others and exhibited concrete section loss, particularly on the in-service bottom surface and side surfaces that are in contact with the ballast. Typical abraded conditions of the used railroad ties and crack markings are provided in Figures 1 through 5. In addition, it was observed that Tie S4 had a concrete spall extending across one of the rail hold downs as seen in Figures 6 and 7. The New Tie was reportedly made at or around the same time as the used ties but not used. Detailed shop drawings for the new tie, which were provided by the tie manufacturer, are provided in Appendix A.

SCOPE OF WORK

In accordance with the solicitation requirements, the following specific tests have been performed:

1. **Bend Tests.** Five used ties and one unused tie were tested to produce negative moment in the upper surface of ties per designated American Railway Engineering and Maintenance-of-way Association (AREMA) protocol. Load, displacement and strains using Digital Image Correlation (DIC) were monitored for each test.
2. **Abrasion Tests.** Tests were performed on eight core samples removed from four ties in accordance with applicable provisions of ASTM C1138, *Standard Test Method for Abrasion Resistance of Concrete (Underwater Method)*.
3. **Compression and Splitting Tensile Tests.** Seven cores from received ties were tested to determine their compressive strength, static modulus, Poission’s ratio and splitting tensile strength in accordance with specified ASTM standard test methods.
4. **Petrography.** Petrographic examination and air content determinations of cores from each of the six received ties were performed in accordance with specified ASTM standard test methods.

In accordance with the terminology utilized in the NTSB solicitation, flexure tests are referred to as Bend Tests in this report. After all Bend Tests were completed, concrete core samples were obtained from

locations identified by Mr. Matthew Fox of NTSB for the required physical and petrographic examinations.

Raw load/deflection data and movies of strain evolution acquired using DIC during the Bend Tests are provided separately in digital format to Mr. Fox of NTSB. In addition, raw stress/strain data from the modulus of elasticity and Poisson's ratio tests are also provided.

Bend Tests

Test Setup and Procedure

All Bend Tests were conducted using the Tie Center Negative Moment Test configuration per American Railway Engineering and Maintenance-of-way Association (AREMA) Manual for Railway Engineering, Chapter 30, Part 4, Concrete Ties (AREMA Manual). Test setup requirements in the AREMA Manual, such as the support and loading conditions used for the tests are provided in Figure 8.

The required protocol for testing of the used ties was as follows:

- Load applied at a rate no greater than 5 kips/minute.
- Load and vertical displacement measured; vertical displacement measured at tie center relative to the rail seat centerline.
- Strains measured on one side of the tie using a digital image correlation (DIC) system.
- Tests conducted until a vertical displacement of 2.5 inches at the tie center relative to the rail seat centerline was achieved or a load of 40 kips, whichever occurred first.

For the New Tie, the required test procedure was as follows:

- Load applied at a rate no greater than 5 kips/minute.
- Load and vertical displacement measured; vertical displacement measured at tie center relative to the rail seat centerline.
- Strains measured on one side of the tie using a digital image correlation (DIC) system.
- Load applied to 14.4 kips and held for 3 minutes, then unloaded and inspected for cracks. Load applied until a vertical displacement of 2.5 inches at the tie center relative to the rail seat centerline was achieved or a load of 40 kips, whichever occurred first.

AREMA's test set-up required the railroad ties be tested upside down, supported 5 feet apart on supports placed between the two rail hold downs, and loaded at mid-span by a concentrated load. Because of the significant roughness of the abraded bottom surfaces of the used ties, WJE applied a thin capping compound to create a smooth and level surface beneath the loading point so that the applied load was uniformly distributed across the width of the ties (Figures 9 through 11). The capping compound was prepared using the gypsum-based material, Hydrostone, which is manufactured by United States Gypsum Corporation. Since the used ties also had significant abrasion on their sides, precise location of the geometric centerlines relative to the sides was obscured. Accordingly, the centerlines were determined relative to the centroid of the prestressing strands visible in each used tie.

Views of the loading hardware and test setup are provided in Figures 12 through 15. Load was applied using a 30-ton calibrated hydraulic jack, with a 50 kip capacity load cell placed between the specimen and the hydraulic jack. The hydraulic pump was equipped with a flow rate control manifold to facilitate application of load and reduce sudden changes that may occur when cracks form or start to open up. Deflections were measured at each support using Linear Voltage Differential Transducers (LVDT). The

deflection at mid-span was measured using a cable-extension transducer, more commonly referred to as a “stringpot”. An Agilent Technologies model 34970A Data Acquisition/Switch unit with a computer-controlled data acquisition system was utilized to capture and record load and displacement measurements during the tests. A complete listing of certificate of calibrations for the measurement equipment utilized for all tests is presented in Appendix B.

A Dantec Dynamics Q-400 Digital Image Correlation (DIC) system was used to make displacement and strain measurements on the ties during testing. The DIC system was equipped with two 5 Megapixel FireWire CCD cameras with lenses from Schneider Kreuznach, and an LED illumination source. The Q-400 is a non-contact, full-field system capable of measuring contour and displacement on any material or component. DIC equipment, operation, image capture and subsequent data reduction were performed by Dantec Dynamics Inc., Holtsville, New York.

For the DIC setup utilized, the displacement resolution is approximately 0.001 in. and the corresponding strain resolution is 100-200.microstrain ($\mu\text{in./in.}$). The measured results were evaluated and graphically presented using the ISTR4 4D software. The software allows for the derivation of full-field measured strain, as well as creation of so-called “virtual gauges”. A virtual gauge allows localized strain determination between any two designated points or regions within a measured field. For the current tie testing, locations either side of selected pre-existing cracks were designated, allowing subsequent computations of overall displacement and strains during loading.

Specimens were photographed before, during and after testing for documentation purposes. All photographs of specimens during and after testing were provided in digital format to Mr. Fox of NTSB. Also, as required by the solicitation, strain maps were provided in digital format to Mr. Fox. Strain maps measured using DIC were provided at:

- Load stages when formation of new cracks or opening of existing cracks occurred
- Maximum, or near-maximum achieved load was reached
- Maximum deflection before failure

Video files documenting strain evolution developed using DIC for all specimens were provided in digital format to Mr. Fox of NTSB.

Test Results

The New Tie was loaded to 14.4 kips and the applied load held constant for 3 minutes, with the actual load during the three minute constant loading period varying between 14.17 kips and 14.57 kips. Due to a loading irregularity, applied load after the hold period was initially slightly increased up to 15.2 kips before the specimen was gradually unloaded for crack observation and documentation. After unloading the new tie was closely examined for cracks by Brian Marquis of Volpe; no cracks were visible to the unaided eye. Load versus mid-span deflection relative to the support centerlines for the initial loading and unloading of the New Tie is provided in Figure 16.

Load versus deflection curves for each specimen tested to failure are presented in Figure 17. The maximum load that was recorded during testing and corresponding mid-span deflection for each specimen is provided in Table 1. Overall photographs of each face of each specimen after failure are provided in Figures 18 through 29.

Strain maps showing principal strains of the optically-scanned face of the tested specimens at a time corresponding to immediately before failure are provided in Figures 30 through 35. Strain maps immediately after the New Tie specimen was loaded to 14.4 kips and immediately before the conclusion of the 3 minute period when the load was held at 14.4 kip are provided in Figures 36 and 37. Although no cracks could be visually observed after the initial loading and unloading regimen for the New Tie, the strain maps presented in Figures 36 and 37 suggest some initial cracking may have occurred, as suggested by strain concentrations in the figures. However, correlation between cracking implied by strain maps in Figures 36 and 37 and strain mapping immediately before failure of the New Tie (Figure 30) does not result in precise matching of discrete crack locations.

To further analyze crack formation during the initial loading of New Tie, the data was further analyzed by designating virtual gages at the three potential crack locations as shown in Figure 38. Measured load versus computed strains indicated by the virtual gages are plotted in Figure 39. The plots of the strains indicated by the virtual gages at locations “2” and “3” exhibit some variability up to an applied load of approximately 10 kips. It is likely that these variable and elevated strain measurements at locations marked 2 and 3 are associated with inherent DIC system stabilities rather than formation of cracks. Based on the strain measurement trends for the virtual gage at location 1 in Figure 39, a flexural crack may have formed near mid-span at location marked as “1” in Figure 38 at a load of approximately 12.2 kips.

All crack locations indicated by DIC system strain measurements are shown in Figures 30 through 35 and are numbered consequentially from left to right. Virtual gauges were designated at these locations to estimate the load at which each crack formed or existing cracks started to open up during loading to failure of the specimens. The indicated strains at cracks for each specimen are plotted in Figures 40 through 51. Based on a review of these strain data, the estimated loads to initiate cracking, or to cause opening of existing cracks are provided in Table 2. The “step” numbers cited in Table 2 are DIC measurement numbers, which also correspond to time steps in the electronically provided strain movies and raw data for each virtual gage. Due to the noted variability in the strain measurements, particularly in the low strain ranges associated with crack opening loads, the provided crack opening loads and step numbers in Table 2 should be considered accurate to approximately +/-3 kips.

Abrasion Tests

Two nominal 9 inch diameter (actual 8-5/8 inch diameter) concrete cores were extracted from the tops of each of the New Tie, N16, S5 and N10 ties at specific locations determined by Mr. Fox of NTSB. The cores were subsequently trimmed to a 3 inch nominal height, preserving the original top-of-tie surface. Preexisting stainless steel inserts in the areas from which the cores were extracted were plugged using matching threaded rods.

All abrasion tests were conducted in general accordance with procedures outlined in the ASTM C 1138 - *Standard Test Method for Abrasion Resistance of Concrete (Underwater Method)*. Four test apparatuses, shown in Figures 52 and 53, were specially constructed for the tests. A Genesis Model GFDP160 drill press capable of achieving 1195 revolutions per minute was used as the rotary driving motor. Because the railroad ties were not wide enough to accommodate the required standard 12 in. diameter sample size, the solicitation called for the testing apparatus to be scaled to approximately 3/4 the size shown in ASTM C 1138. Therefore, the inside diameter of the container used for the tests was 8.835 inches instead of 12 inches per ASTM C 1138. The agitation paddles, obtained from JiffyMixer Co., Inc., were precisely scaled to 3/4 the size shown in ASTM C 1138. The number of balls required to be used as abrasive charge per the standard was also reduced in accordance with the solicitation requirements. The abrasive charge

for each test contained 5 balls with a nominal diameter of 1.00 inch, 20 balls with a nominal diameter of 0.75 inch, and 14 balls with a nominal diameter of 0.50 inch. All balls were Grade 1000 chrome steel. Three 1-3/4" long 1 inch x 1 inch x 1/8 inch aluminum tubes were used to seat each specimen. While ASTM C 1138 requires three samples to be tested and results to be averaged, only two core samples per tie were tested as modified per the solicitation.

Test results for the abrasion tests are presented in Table 3. Volume loss versus time plots for each specimen and average volume loss from the two companion specimens for each test are provided in Figures 54 and 55, respectively.

Compression and Splitting Tensile Strength Tests

WJE conducted compressive strength, static modulus of elasticity, Poisson's ratio, and splitting tensile strength tests on concrete core specimens removed from each tie. Compressive strengths of the specimens were measured in accordance with ASTM C 39 - *Standard Test Method for Compressive Strength of Cylindrical Concrete Specimens*, with necessary adjustment factors for the final trimmed specimen size applied per the standard. Elastic modulus in compression and Poisson's ratio were measured in accordance with ASTM C 469 - *Standard Test Method for Static Modulus of Elasticity and Poisson's Ratio of Concrete in Compression*. Due to the small size of the test specimens, WJE used bonded electrical resistance strain gauges for the measurement of both the static modulus of elasticity and Poisson's ratio. Splitting tensile strengths were measured in accordance with ASTM C 496 - *Standard Test Method for Splitting Tensile Strength of Cylindrical Concrete Specimens*.

Following completion of the Bend Tests, one nominal 3-inch diameter concrete core was extracted from intact portions of each of the used ties and two nominal 3-inch diameter concrete cores were extracted from intact portions of the New Tie at locations designated by Mr. Fox of NTSB. All cores were horizontally drilled and each core was approximately 10 inches long. The cores were cut as necessary to produce required specimen lengths for each type of test.

Compressive strength, static modulus of elasticity and Poissons's ratio testing was conducted on trimmed and capped cores, whereas splitting tensile strength tests were conducted on remaining segments from each extracted core. Splitting tensile strength test samples extracted from the New Tie and N10 were further prepared by lath to achieve surface straightness required by ASTM C 42 - *Standard Test Method for Obtaining and Testing Drilled Cores and Sawed Beams of Concrete*. The remainder of the splitting tensile strength test samples did not require further preparations. All tests were performed utilizing WJE's SATEC Model MKIII 120 HVL Universal Test Machine with a maximum compressive load capacity of 120,000 lbs.

The ASTM C 469 standard requires that the modulus of elasticity and Poisson's ratio be calculated using measured longitudinal strain at 50 micro-strains and the applied stress corresponding to 40 percent of the ultimate compressive strength of the specimen. ASTM C 469 further requires the modulus of elasticity and Poisson's ratio be reported as the averages obtained from two tests conducted on the same specimen. Since the actual compressive strength of the cores was not known prior to the conduct of the tests, the strength was assumed to be approximately 8000 psi for the first test (Tie S5). This maximum load corresponds to approximately 30 percent of the strength for the first of the two companion test runs on the specimen obtained from Tie S5. The second test on this specimen was conducted up to compressive failure. For the remainder of the modulus of elasticity and Poisson's ratio tests, a running average of the

compressive strengths obtained from the previous tests was used for the first of the two companion tests required by the ASTM C 469. The second of the two companion tests was always conducted up to failure.

Test results are presented in Tables 4 and 5. The reported moduli of elasticity and Poisson's ratios represent the average of two companion tests for the specimens identified as New1 and New2. The remainder of the reported moduli of elasticity and Poisson's ratios were obtained from the second test of the two companion tests conducted on the concrete core, due to the first test not being loaded up to 40 percent of the failure stress. The stress-strain data obtained during the tests were submitted to Mr. Fox of NTSB in electronic format.

Petrographic Examinations

For the petrographic studies, one nominal 4 inch diameter core was extracted vertically through the full depth of each tie following completion of Bend Testing at locations designated by Mr. Fox of NTSB. As requested, all petrographic examinations were performed in accordance with the ASTM C 856 - *Standard Practice for Petrographic Examination of Hardened Concrete*; air-void analyses were performed in accordance with ASTM C457 - *Standard Test Method for Microscopical Determination of Parameters of the Air-Void System in Hardened Concrete*. As described in the solicitation, the objectives of the petrographic studies were to assess the general characteristics of the concrete with specific focus on aggregate types, air-void system parameters, depth of paste carbonation, and deterioration that may affect the durability of the ties.

Detailed descriptions of extracted core samples and the petrographic studies that were conducted are provided in Appendix C to this report. Principal findings from the studies are summarized below:

- Concrete mixtures represented by the cores were similar. Concrete in each core contained crushed carbonate rock (mainly dolostone) coarse and fine aggregates uniformly distributed in air-entrained portland cement paste. Maximum nominal top size of the aggregate was 3/4 inch. The aggregates appeared to be well graded and consisted of fairly hard, dense, durable stone.
- The concrete represented by the cores was well consolidated.
- No evidence of deleterious chemical reactions involving the aggregates and constituents of the paste was observed in any of the core samples. Secondary deposits of calcium hydroxide, ettringite, or a mixture of calcium hydroxide and ettringite frequently lined the air voids. None of these deposits are associated with distress.
- The depth of paste carbonation was essentially negligible, typically less than 0.02 inch, and locally up to 0.3 inch around a few near-top aggregates, based on thin-section examinations.
- Paste quality in all cores appeared to be good, with tight paste-aggregate bonds. Estimated average water-to-cementitious ratio (w/cm) in all cores was estimated to be less than 0.38.
- No evidence of freeze-thaw related general deterioration was observed in any of the core samples.
- Measured air-void system parameters are presented in Table 6, along with applicable limits recommended by ACI 201.2R-08 for concretes with nominal maximum aggregate size of 3/4 inch and moderate exposure to freezing and thawing. Measured total air contents ranged from 3.1 to 7.8 percent.
- The vertical and sub-horizontal cracks located near the top surface of the ties removed from service appear to have formed after the concrete had gained significant strength and paste-to-aggregate bond. Features consistent with early age, plastic-stage cracks were not observed. Vertical cracks in cores from all of the in-service ties contained a crack-filling material composed of angular mineral and rock

particles dispersed in a very fine-grained matrix. The mineral and rock particles are not constituents of the tie concrete, suggesting that the source of the crack-filling material is external to the concrete.

- Examined concrete in cores representing the top and bottom surfaces of all used ties exhibited surface erosion of varying extents. Generally, no extensive concrete loss was observed from the top surface. Polished aggregate particles observed on the bottom surfaces of the in-service ties appeared to be indicative of abrasion-related erosion. The loss of concrete section in the cores taken from the in-service ties ranged from 0.1 inch to 0.5 inch.
- Horizontal cracks were observed in core samples corresponding to levels of prestressing strand, which were likely caused by the core removal process and/or the flexural loading tests.

TABLES

Table 1. Bend Test Results

Specimen	Max Load (lbf)	Max Deflection (in.)
New	32,304	0.398
N16	30,854	0.432
S5	30,131	0.450
S4	25,916	0.426
N10	25,209	0.397
S3	23,725	0.404

Table 2. Estimated Crack Opening Loads Determined by DIC

Specimen	Crack #	Load* (lbs)	Step #	Specimen	Crack #	Load* (lbs)	Step #
NEW	1	22,416	82	N10	1	15,072	49
	2	17,549	64		2	12,765	43
	3	12,394	48		3	13,919	46
	4	17,549	64		4	9,784	35
	5	21,347	78		5	21,759	71
N16	1	15,165	64		6	97,84	35
	2	12,049	55		7	13,919	46
	3	13,439	59	S3	1	15,679	56
	4	13,439	59		2	14,828	53
	5	12,049	55		3	9,210	35
	6	18,357	73		4	12,293	45
S5	1	21,212	69		5	12,655	46
	2	17,153	58		6	15,679	56
	3	14,407	53	* The resolution of the stain measurement system is +/- 100 to 200 micro-strains. Therefore, listed loads should only be considered approximations. It is believed that the actual loads when new cracks form or existing ones open may be as much as +/- 3 kips of the estimated loads in this table.			
	4	12,563	47				
	5	29,752	125				
	6	12,563	47				
	7	17,700	59				
	8	19,974	65				
	9	21,523	70				
S4	1	15,207	76				
	2	14,087	73				
	3	14,634	75				
	4	10,870	63				
	5	22,812	102				
	6	12,495	68				
	7	11,484	66				
	8	15,257	78				

Table 3. Abrasion Test Results

Time (hrs)	NEW1				NEW2				Average Volume Loss (m ³)	Grinding Media Weight (gr)
	Weight (gr)		Volume (m ³)	Volume Loss (m ³)	Weight (gr)		Volume (m ³)	Volume Loss (m ³)		
	In-water	SSD			In-water	SSD				
0	3,948.2	6,904.5	2.96E-3	0	3,912.3	6,863.9	2.95E-3	0	0	1015.7
12	3,944.4	6,893.5	2.95E-3	7.20E-6	3,910.9	6,856.5	2.95E-3	6.00E-6	6.60E-6	
24	3,936.5	6,874.4	2.94E-3	1.84E-5	3,906.9	6,843.6	2.94E-3	1.49E-5	1.67E-5	
36	3,937.1	6,872.0	2.93E-3	2.14E-5	3,908.2	6,841.7	2.93E-3	1.81E-5	1.97E-5	
48	3,929.8	6,856.4	2.93E-3	2.97E-5	3,903.9	6,830.6	2.93E-3	2.49E-5	2.73E-5	
60	3,922.3	6,835.1	2.91E-3	4.35E-5	3,901.5	6,818.2	2.92E-3	3.49E-5	3.92E-5	
72	3,908.2	6,809.7	2.90E-3	5.48E-5	3,887.1	6,791.7	2.90E-3	4.70E-5	5.09E-5	1011.8
	N16-AL				N16-AH					
0	4,120.9	7,110.1	2.99E-3	0	4,087.0	7,083.5	3.00E-3	0	0	1015.7
12	4,117.3	7,097.7	2.98E-3	8.80E-6	4,082.7	7,071.1	2.99E-3	8.10E-6	8.45E-6	
24	4,115.6	7,086.2	2.97E-3	1.86E-5	4,075.3	7,051.3	2.98E-3	2.05E-5	1.96E-5	
36	4,114.9	7,082.4	2.97E-3	2.17E-5	4,073.3	7,045.3	2.97E-3	2.45E-5	2.31E-5	
48	4,108.0	7,067.9	2.96E-3	2.93E-5	4,061.6	7,022.7	2.96E-3	3.54E-5	3.24E-5	
60	4,103.6	7,053.0	2.95E-3	3.98E-5	4,053.0	6,999.6	2.95E-3	4.99E-5	4.49E-5	
72	4,088.5	7,025.7	2.94E-3	5.20E-5	4,032.3	6,962.7	2.93E-3	6.61E-5	5.91E-5	1012.4-L/ 1012.5-H
	S5-AL				S5-AH					
0	3,895.6	6,796.7	2.90E-3	0	3,815.9	6,639.9	2.82E-3	0	0	1012.4-L/ 1012.5-H
12	3,891.1	6,781.9	2.89E-3	1.03E-5	3,808.1	6,620.5	2.81E-3	1.16E-5	1.09E-5	
24	3,890.3	6,774.6	2.88E-3	1.68E-5	3,803.7	6,608.5	2.80E-3	1.92E-5	1.80E-5	
48	3,894.3	6,766.0	2.87E-3	2.94E-5	3,800.0	6,590.9	2.79E-3	3.31E-5	3.13E-5	
60	3,889.0	6,751.3	2.86E-3	3.88E-5	3,791.8	6,571.9	2.78E-3	4.39E-5	4.13E-5	
72	3,882.9	6,733.6	2.85E-3	5.04E-5	3,778.6	6,544.0	2.77E-3	5.86E-5	5.45E-5	1007.1-L/ 1007.8-H
	N10-AL				N10-AH					
0	3,953.8	6,812.5	2.86E-3	0	3,922.0	6,775.2	2.85E-3	0	0	1011.8
12	3,953.0	6,803.8	2.85E-3	7.90E-6	3,920.1	6,765.5	2.85E-3	7.80E-6	7.85E-6	
24	3,952.7	6,798.3	2.85E-3	1.31E-5	3,920.7	6,760.7	2.84E-3	1.32E-5	1.31E-5	
48	3,947.7	6,778.9	2.83E-3	2.75E-5	3,914.6	6,738.3	2.82E-3	2.95E-5	2.85E-5	
60	3,937.8	6,758.0	2.82E-3	3.85E-5	3,902.9	6,714.6	2.81E-3	4.15E-5	4.00E-5	
72	3,930.5	6,741.0	2.81E-3	4.82E-5	3,891.4	6,689.5	2.80E-3	5.51E-5	5.16E-5	1007.3-L/ 1007.1-H

The suffixes “AL” and “AH” after the tie specimen names and the “L” and “H” suffix after some of the reported grinding media weights refer to cores taken from the high and low sides, respectively, of the railroad ties as they were in service. The ties were obtained from a super-elevated curved portion of the railroad tracks.

Table 4. Splitting Tensile Strength Test Results

Sample ID	Length 1 (in.)	Length 2 (in.)	Average Length (in.)	Top Diameter (in.)	Middle Diameter (in.)	Bottom Diameter (in.)	Average Diameter (in.)	Max. Load (lbf)	Splitting Tensile Strength (psi)
S3	3.951	3.956	3.96	2.750	2.750	2.751	2.75	18,550	1,085
S4	4.267	4.268	4.27	2.766	2.764	2.766	2.77	19,560	1,055
S5	3.978	3.980	3.98	2.749	2.750	2.750	2.75	17,290	1,005
N10	3.947	3.960	3.96	2.718	2.721	2.725	2.72	19,160	1,130
N16	3.957	3.951	3.95	2.761	2.760	2.763	2.76	17,690	1,030
NEW1	3.958	3.966	3.97	2.765	2.765	2.766	2.77	15,660	910
NEW2	3.957	3.965	3.97	2.728	2.730	2.729	2.73	18,910	1,115

Table 5. Compressive Strength, Modulus of Elasticity and Poisson's Ratio Results

Sample ID	Capped Length (in.)	Diameter, (in.)			Area (in. ²)	Correction		Max. Load (lbf)	Density (lb/ft ³)	Corrected Strength (psi)	Modulus of Elasticity	Poisson's Ration
		D1	D2	Average		L/D	Factor					
S3	4.625	2.753	2.751	2.752	5.95	1.68	0.974	68,300	144.4	11,189	5,803	0.220
S4	4.250	2.766	2.767	2.767	6.01	1.54	0.963	74,100	142.5	11,870	5,414	0.202
S5	4.930	2.754	2.751	2.753	5.95	1.79	0.983	64,200	141.2	10,609	5,218	0.203
N10	5.000	2.752	2.753	2.753	5.95	1.82	0.985	76,200	143.5	12,618	5,316	0.237
N16	4.750	2.763	2.766	2.765	6.00	1.72	0.977	73,600	144.1	11,985	5,690	0.204
NEW1	4.750	2.766	2.767	2.767	6.01	1.72	0.977	60,100	139.0	9,772	4,842	0.194
NEW2	5.125	2.764	2.765	2.765	6.00	1.85	0.988	63,800	142.0	10,505	5,040	0.210

Table 6. Constituent Percentages and Air-Void System Parameters of Cores

Core	New	S3	S4	S5	N10	N16	ACI 201.2R-08 [#]
Air Content (A)	7.8	3.1	5.3	5.0	4.8	5.9	5.0 ± 1.5
Paste Content (p) %	30.7	29.6	27.4	31.8	29.7	28.6	
Fine Aggregate Content %	21.7	25.4	26.0	30.4	22.4	23.1	
Coarse Aggregate Content %	39.8	41.9	41.2	32.9	43.1	42.5	
Total Aggregate %	61.5	67.3	67.2	63.3	65.5	65.6	
Void Frequency (n, per inch)	11.4	5.4	6.1	7.3	6.8	6.9	
Paste-Air Ratio (p/A)	3.9	9.6	5.1	6.4	6.2	4.9	
Avg. Chord Length (inch)	0.0068	0.0057	0.0087	0.0068	0.0070	0.0085	
Specific Surface (in ² /in ³)	586	702	458	587	572	471	630 Min.
Spacing factor (inch)	0.0067	0.0089	0.0103	0.0088	0.0089	0.0097	0.008 Max.

#ACI 201.2R-08 recommended limits for concretes with nominal maximum aggregate size of 3/4 inch and moderate exposure to freezing and thawing.

FIGURES



Figure 1. Overall view showing in service top face of as received railroad ties S3, N16, S4 and N10, from left to right. Tie S5 and new tie are seated on their side.



Figure 2. Overall view showing in service bottom face of railroad ties S3, N16, S4, N10 and S5, from left to right. The un-used specimen is seen seated on its side. Note the significantly abraded bottom and side surfaces of the used specimens

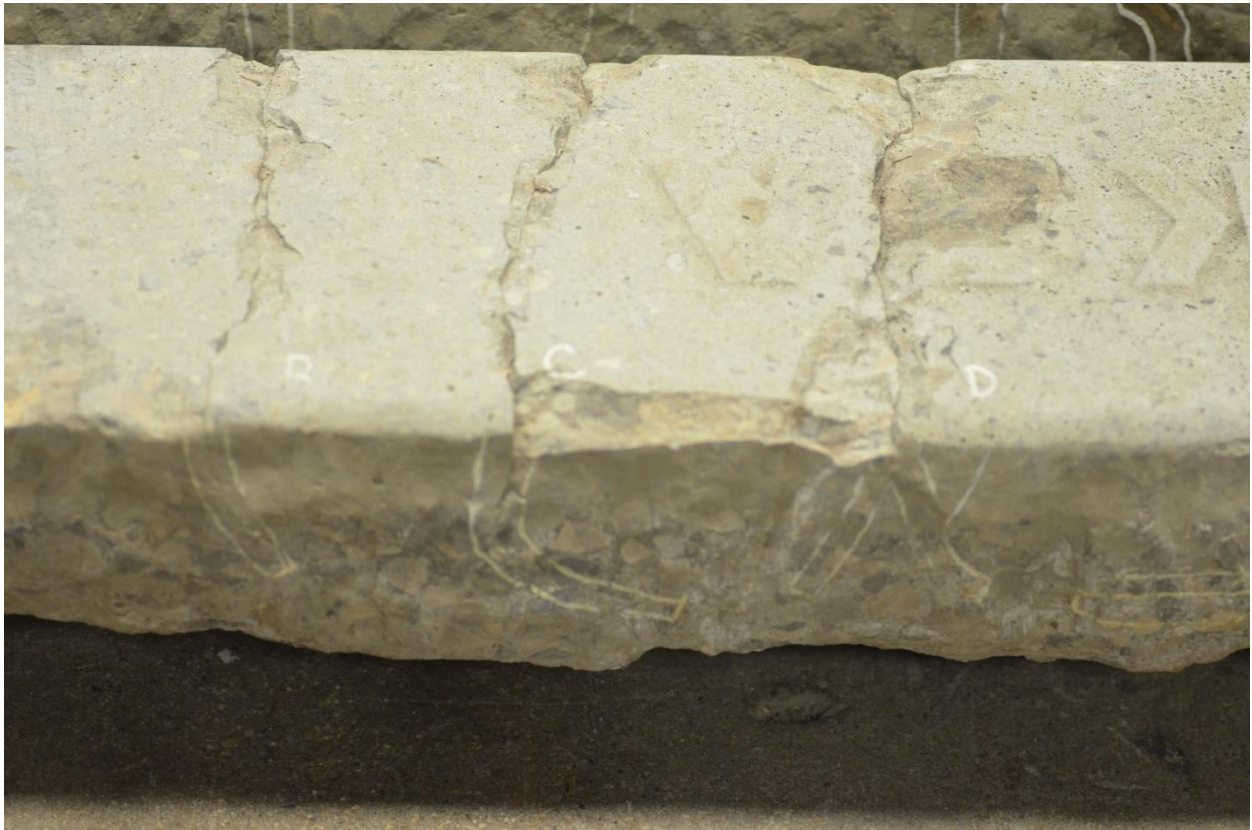


Figure 3. Example of observed in-service top surface conditions. Railroad tie S3 shown in the photo. Note the crack tracings on the side of the tie by others.



Figure 4. Example of abrasion typically observed at the ends of the railroad ties that sit at the lower elevation side of the curve (Specimen S3).



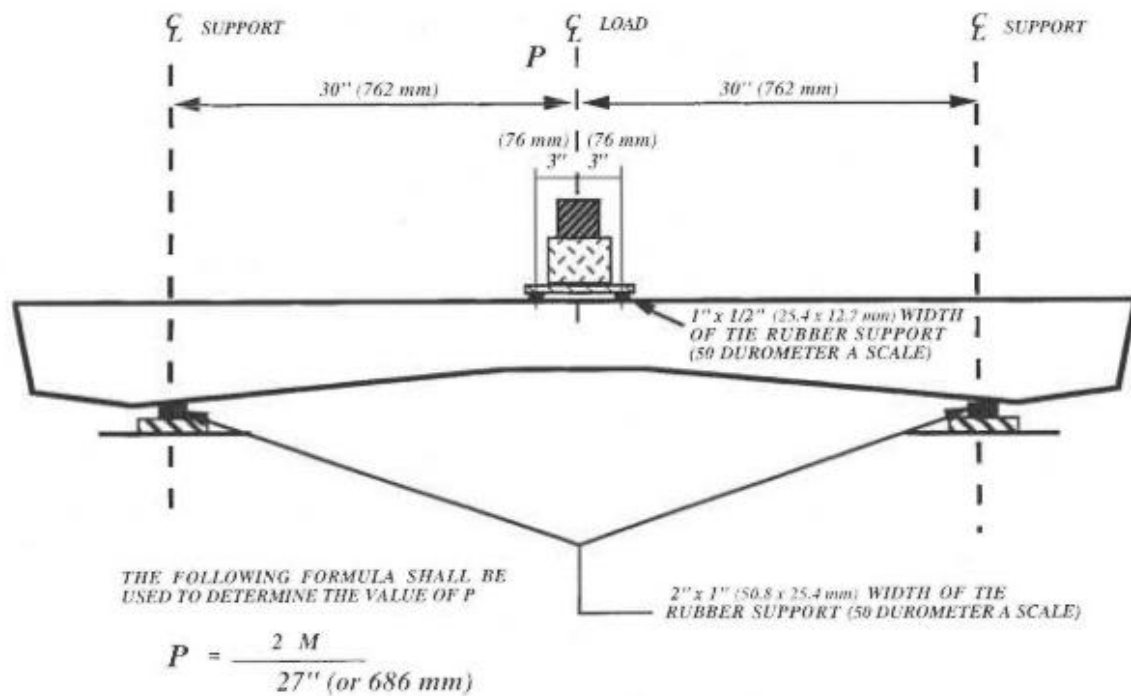
Figure 5. Example of abrasion typically observed at the ends of the railroad ties that sit at the higher elevation side of the curve (Specimen S3).



Figure 6. View of freshly broken off concrete area on Specimen S4.



Figure 7. View of freshly broken off concrete area on Specimen S4.



M = NEGATIVE MOMENT AT THE CENTER OF THE TIE AS REQUIRED IN ARTICLE 4.4.1

Figure 8. Tie Center Negative Moment Test setup reproduced from the AREMA Manual.

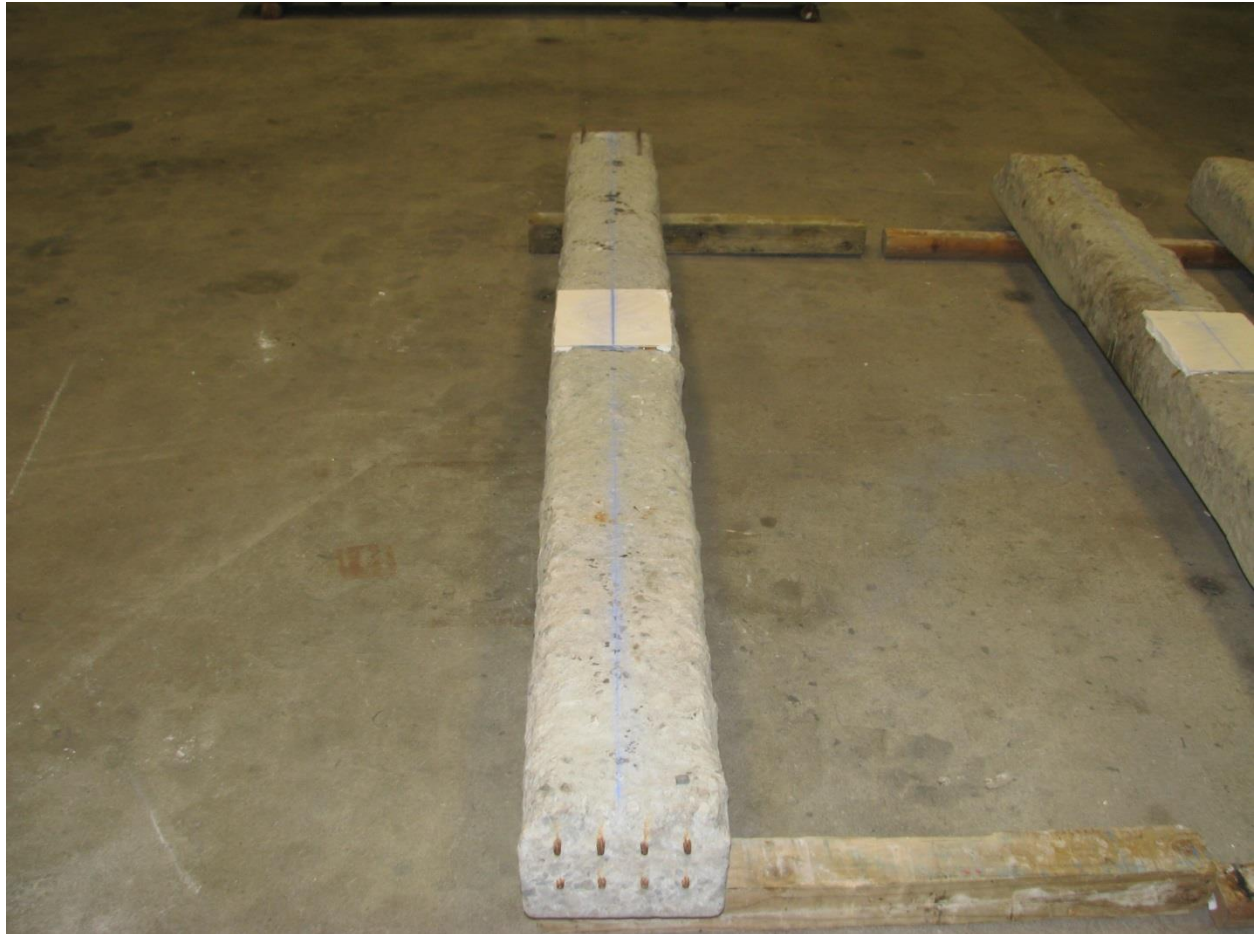


Figure 9. Hydrostone capping used at the loading area on used railroad tie S3.



Figure 10. Hydrostone capping used at the loading area on used railroad ties N16 (left) and S4 (right).



Figure 11. Hydrostone capping used at the loading area on used railroad ties N10 (left) and S5 (right).

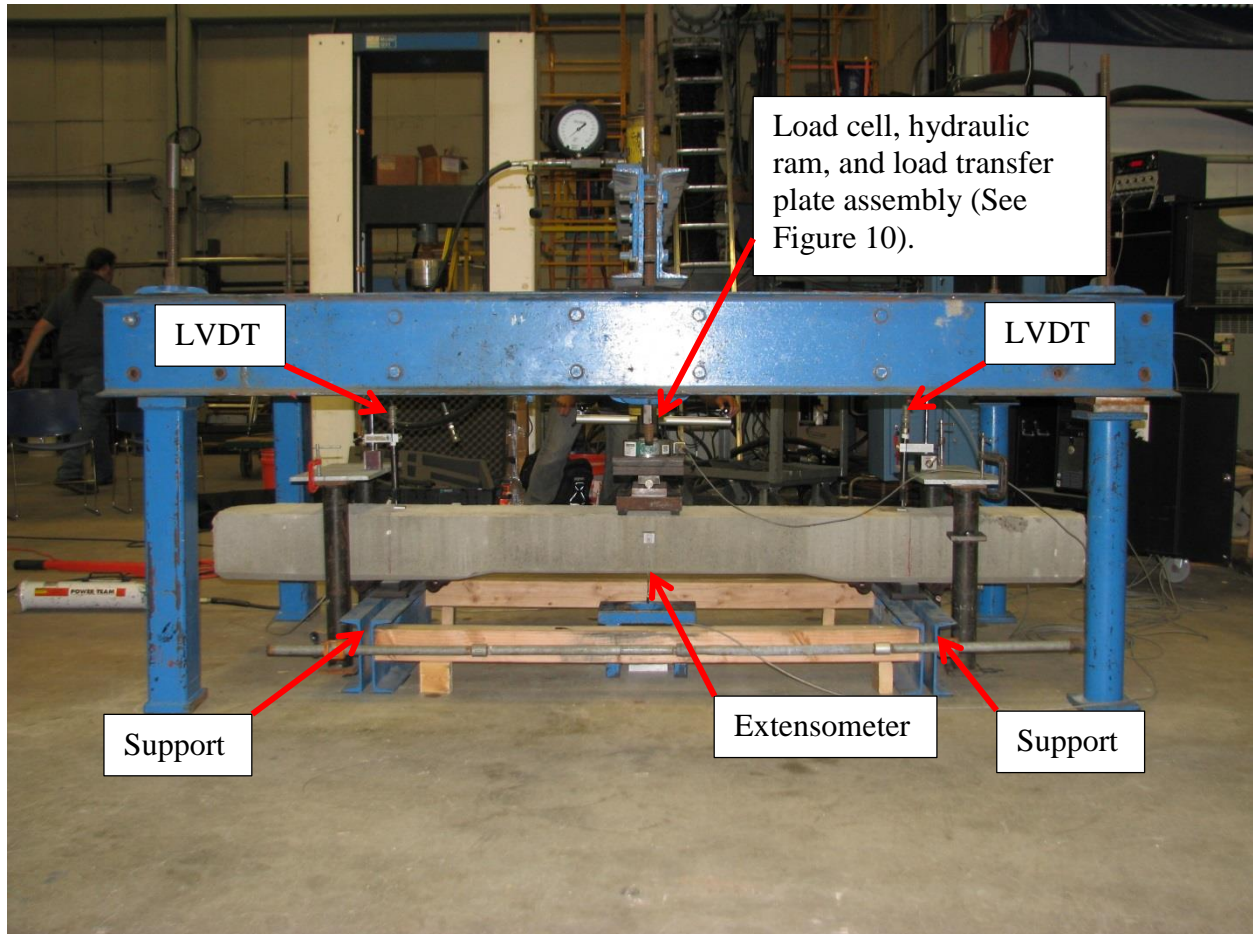


Figure 12. View of actual test setup with new railroad tie in place.

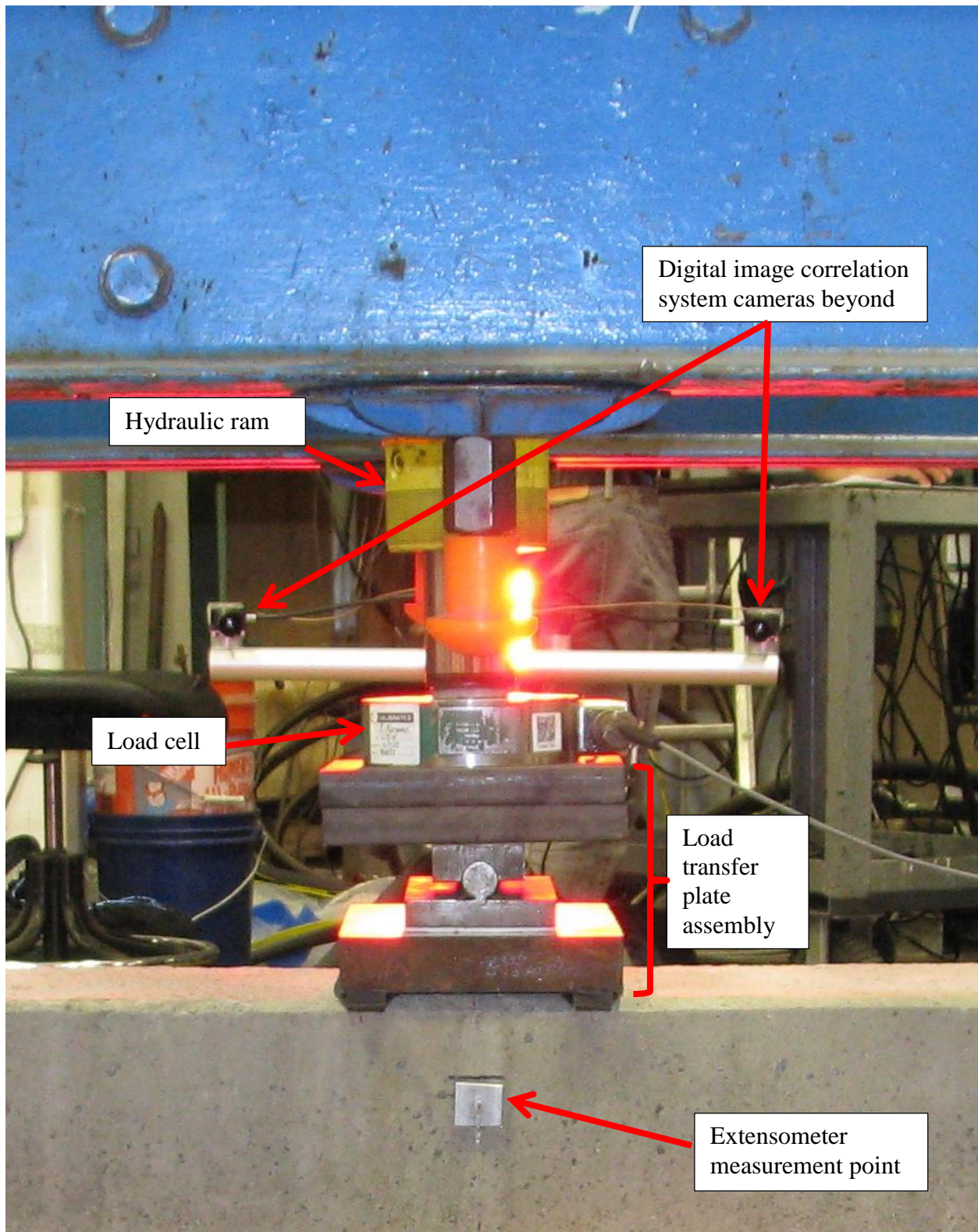


Figure 13. Close-up view of the load transfer assembly.

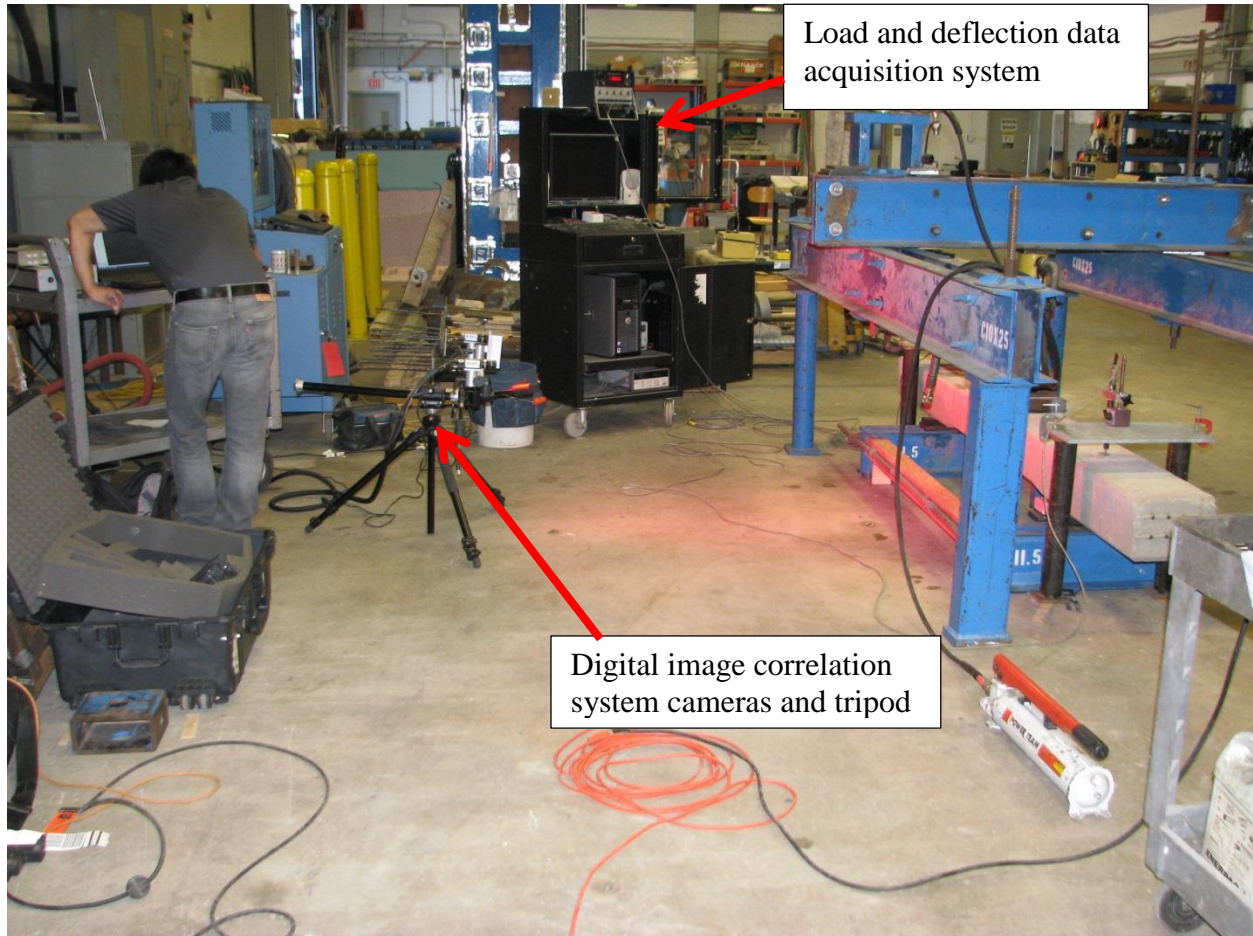


Figure 14. View of test setup with digital image correlation system cameras in place and the system in the process of being calibrated.

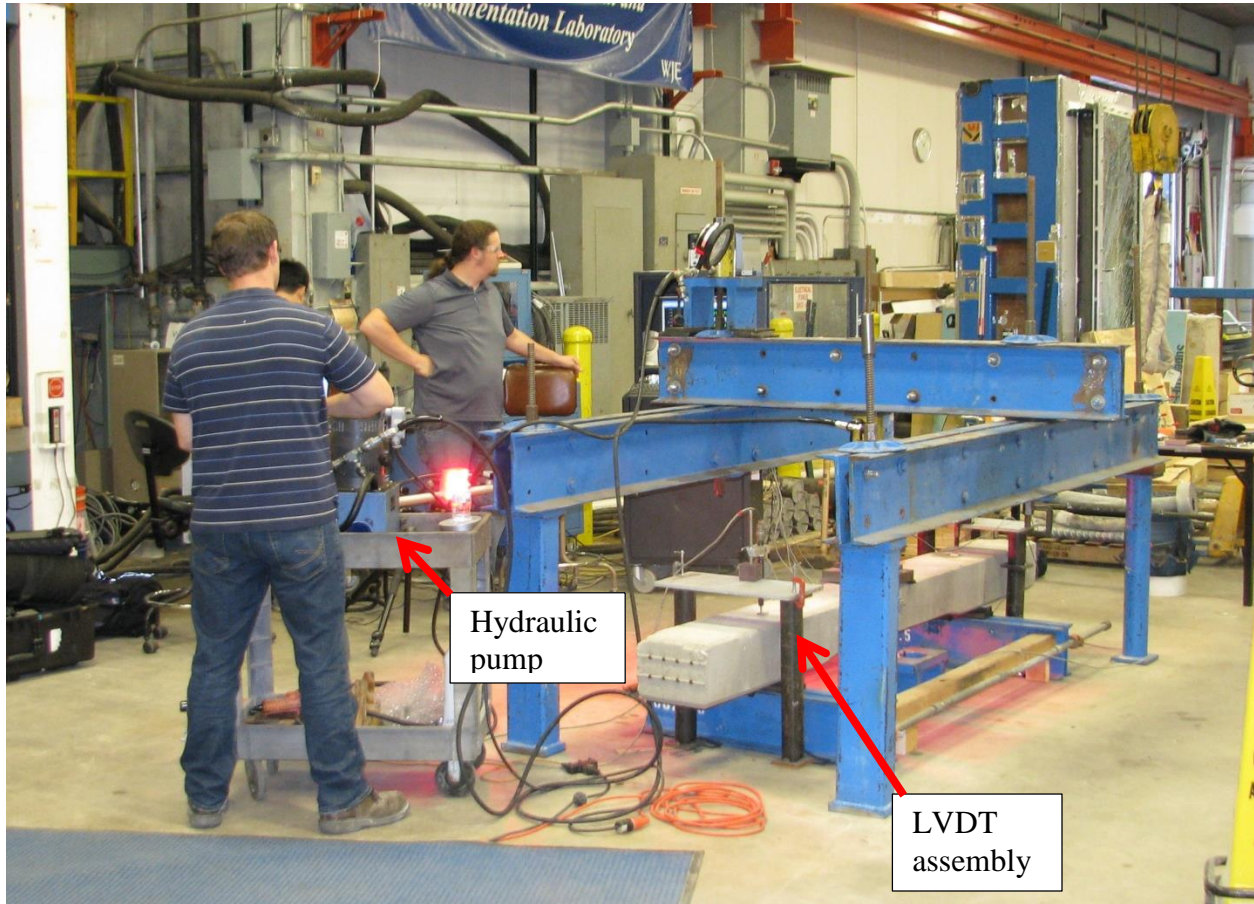


Figure 15. View of test setup during when testing is in progress.

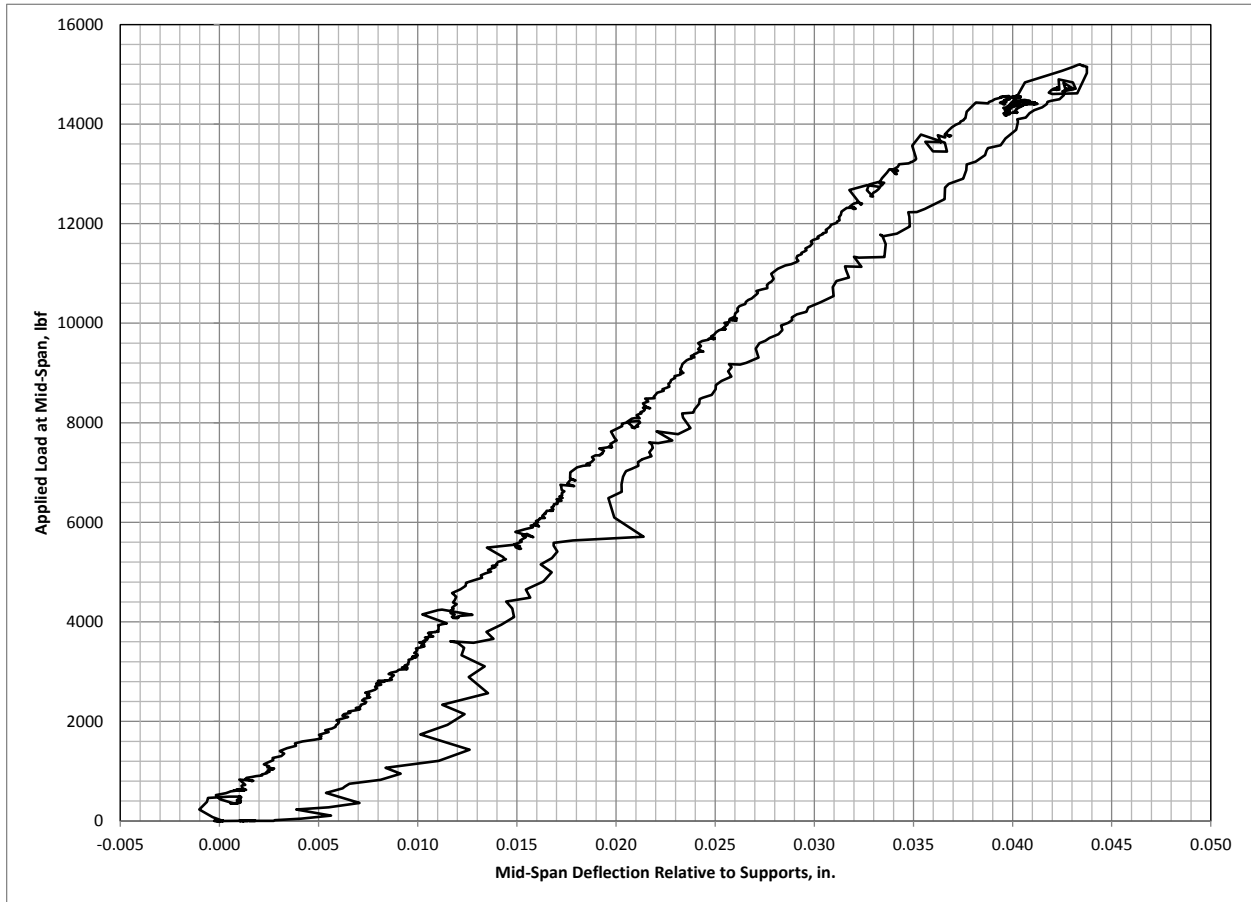


Figure 16. Load versus mid-span deflection relative to supports for the New Tie during initial loading and unloading protocol.

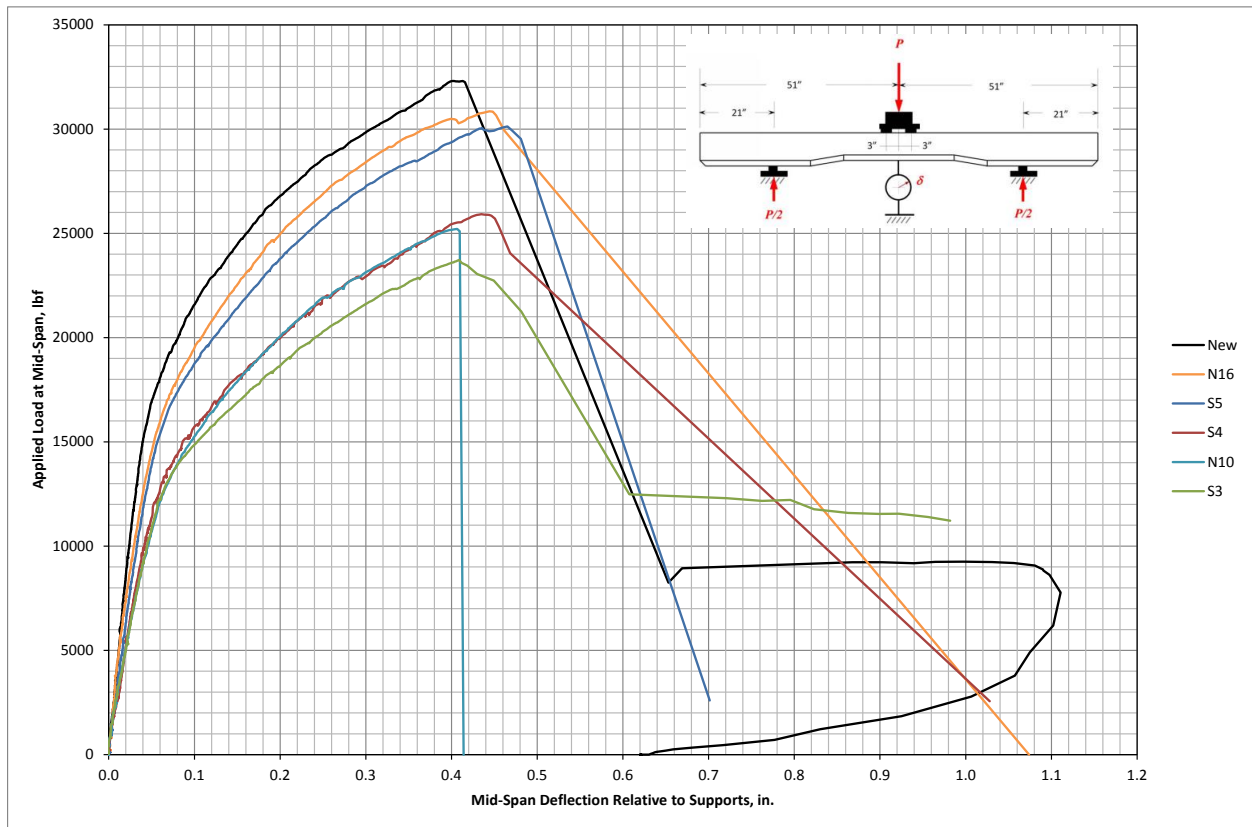


Figure 17. Load deflection curves for all specimens that were tested to failure.



Figure 18. View of east face of New Tie after failure.



Figure 19. View of west face of New Tie after failure.



Figure 20. View of east face of tie N16 after failure.



Figure 21. View of west face of tie N16 after failure.



Figure 22. View of east face of tie S5 after failure.



Figure 23. View of west face of tie S5 after failure.

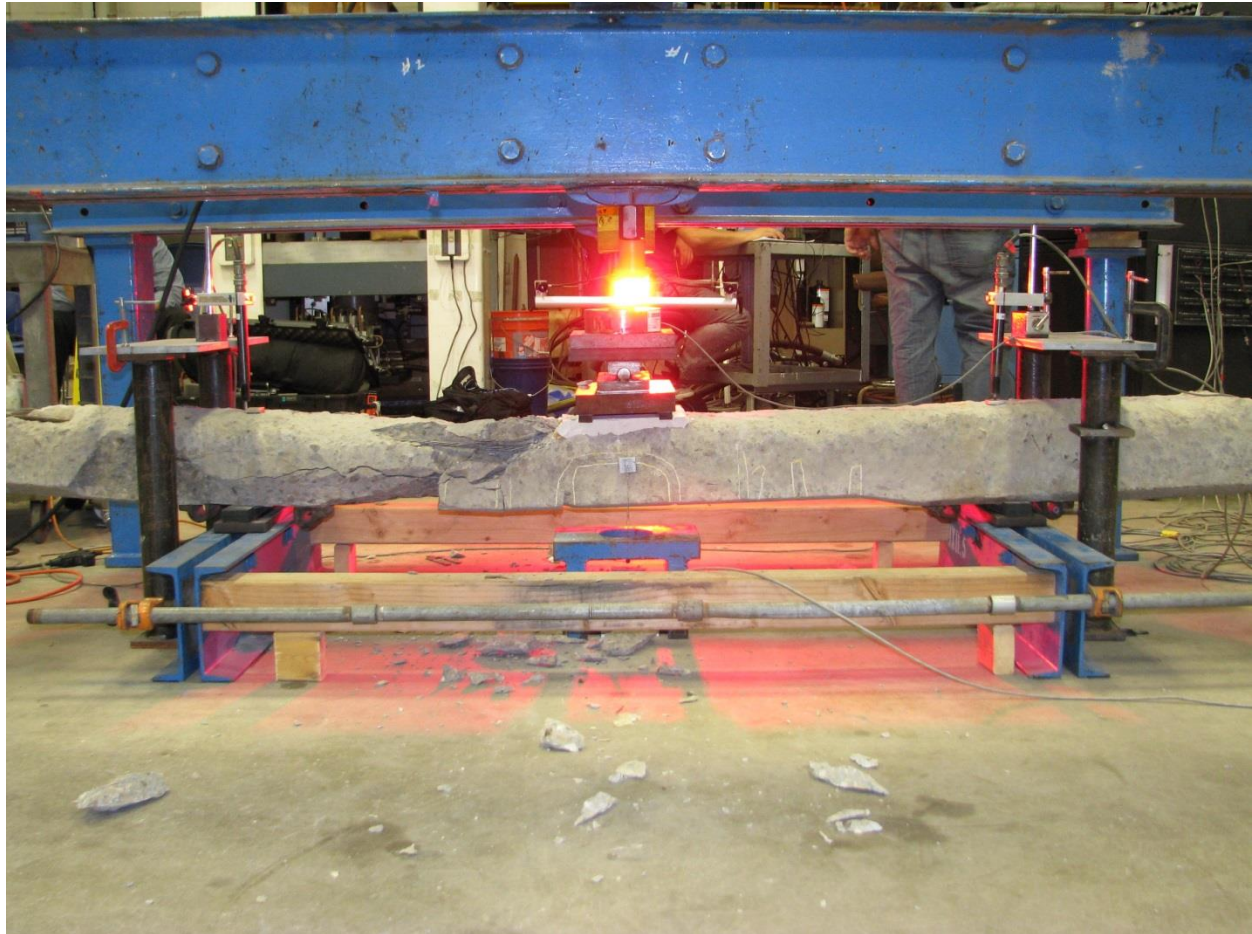


Figure 24. View of east face of tie S4 after failure.



Figure 25. View of west face of tie S4 after failure.



Figure 26. View of east face of tie N10 after failure.



Figure 27. View of west face of tie N10 after failure.



Figure 28. View of east face of tie S3 after failure.



Figure 29. View of west face of tie S3 after failure.

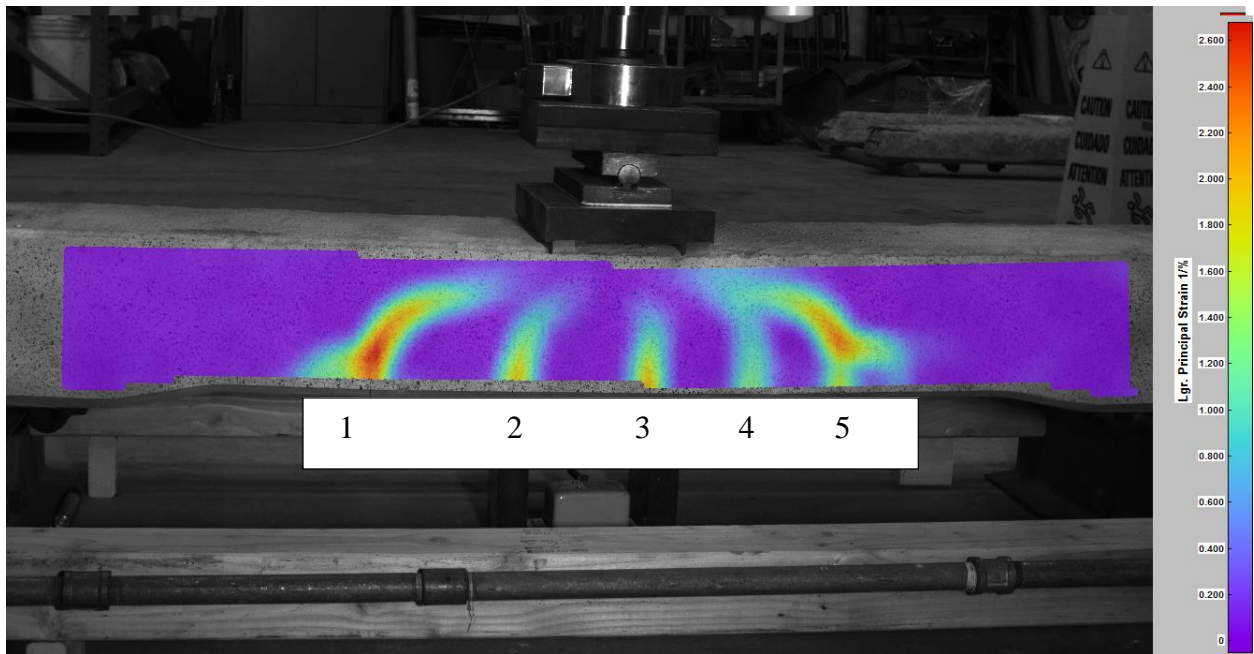


Figure 30. Principal strain map immediately before failure of New Tie.

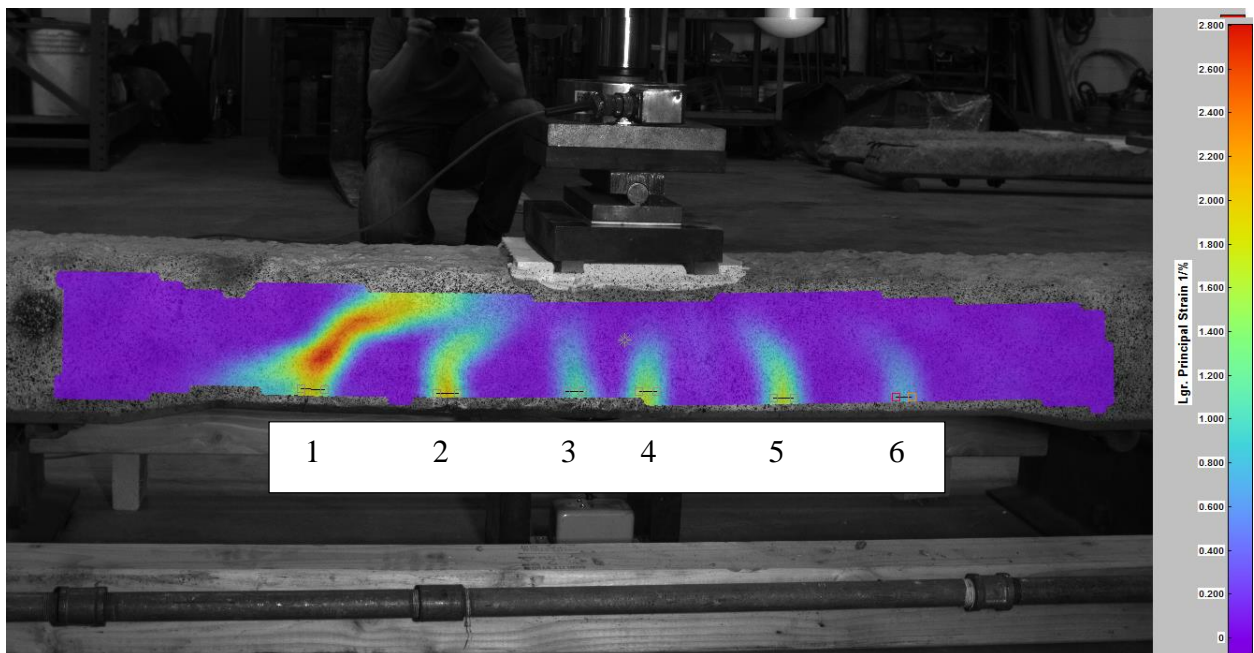


Figure 31. Principal strain map immediately before failure of Tie N16.

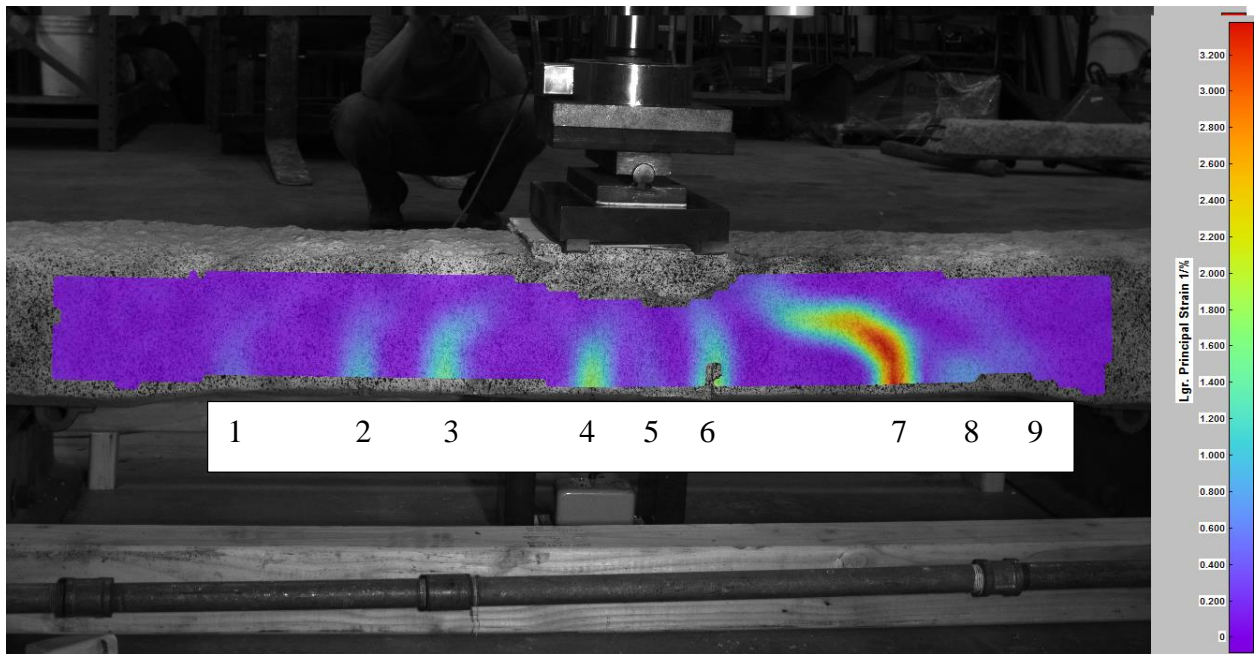


Figure 32. Principal strain map immediately before failure of tie S5.

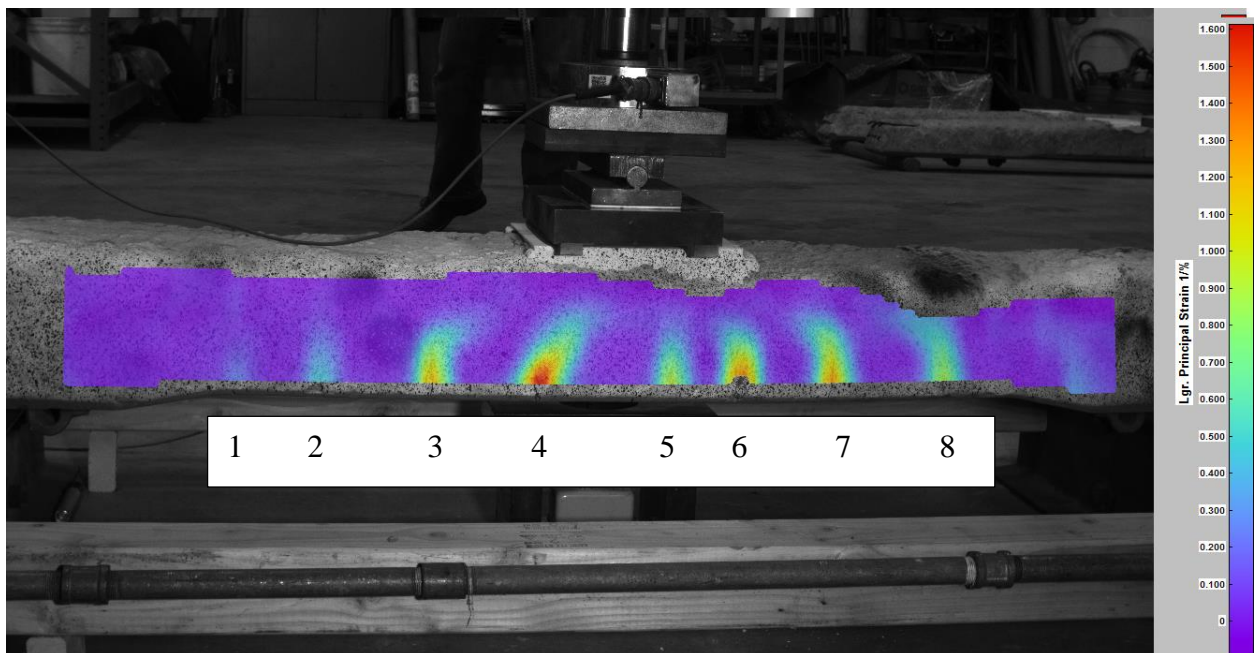


Figure 33. Principal strain map immediately before failure of tie S4.

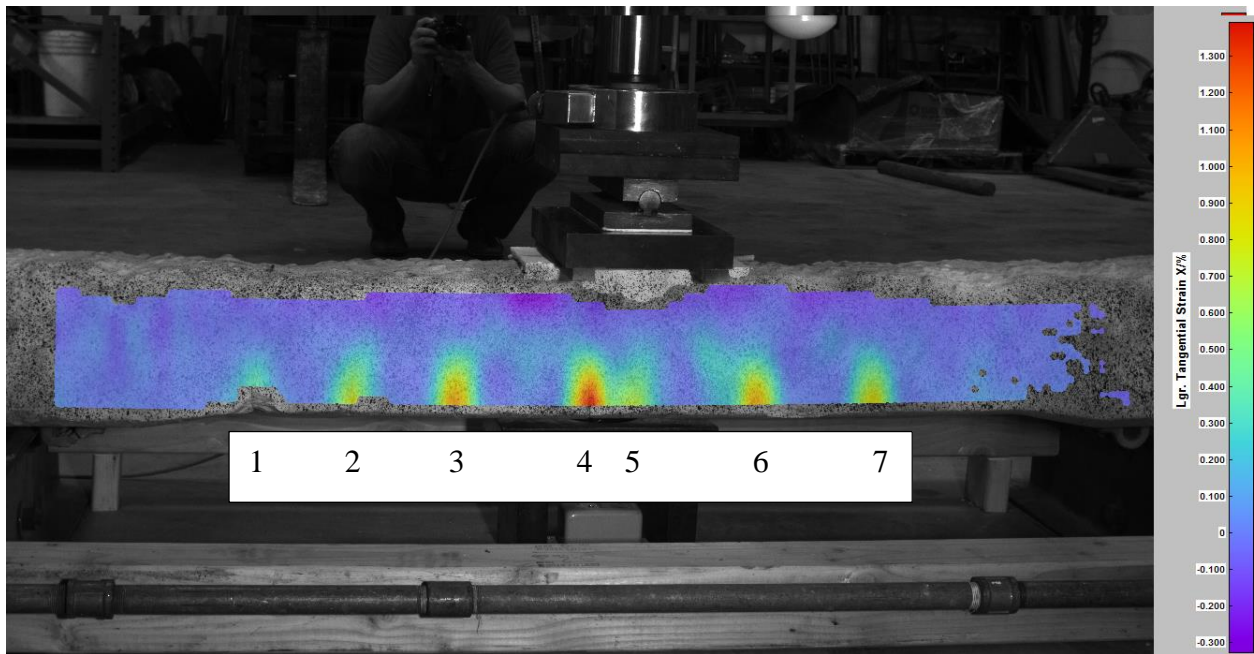


Figure 34. Principal strain map immediately before failure of tie N10.

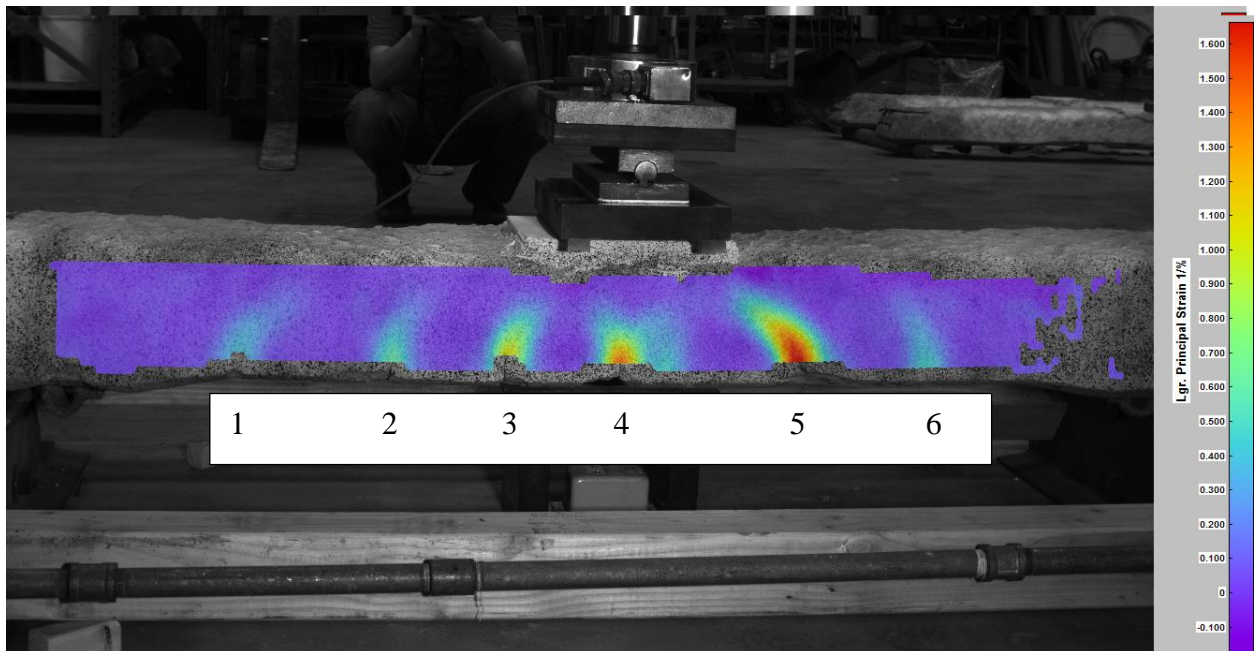


Figure 35. Principal strain map immediately before failure of tie S3.

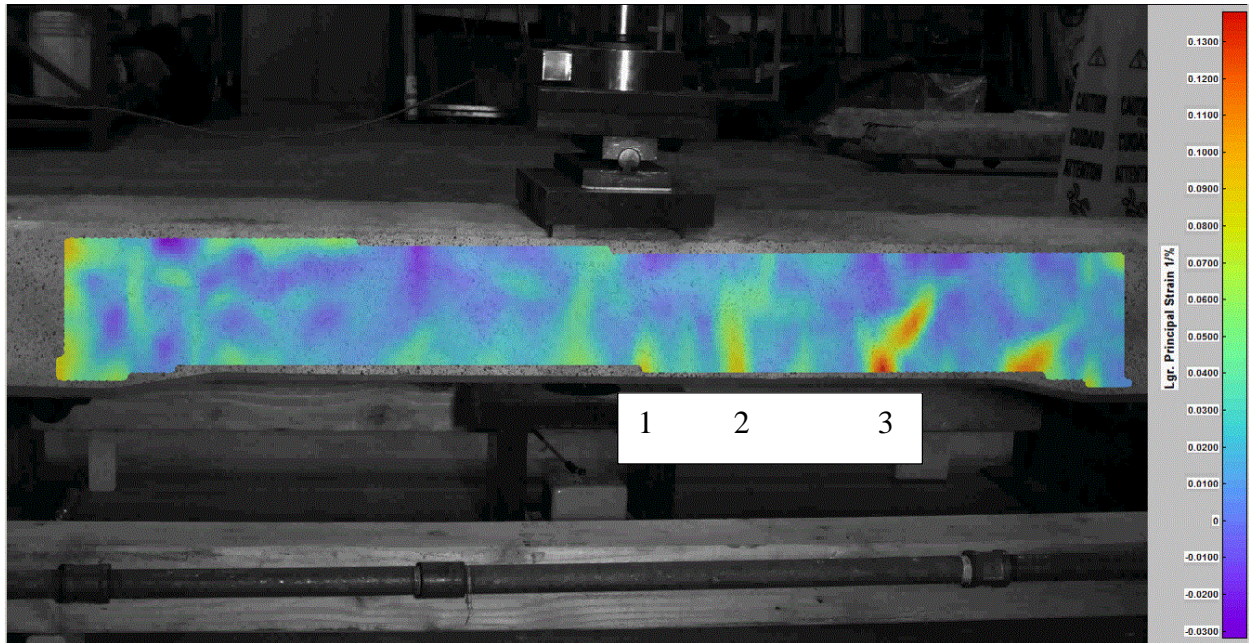


Figure 36. Strain map measured using DIC on New Tie when the applied load first reached the target load of 14.4 kips (actual measured load is 14.55 kips).

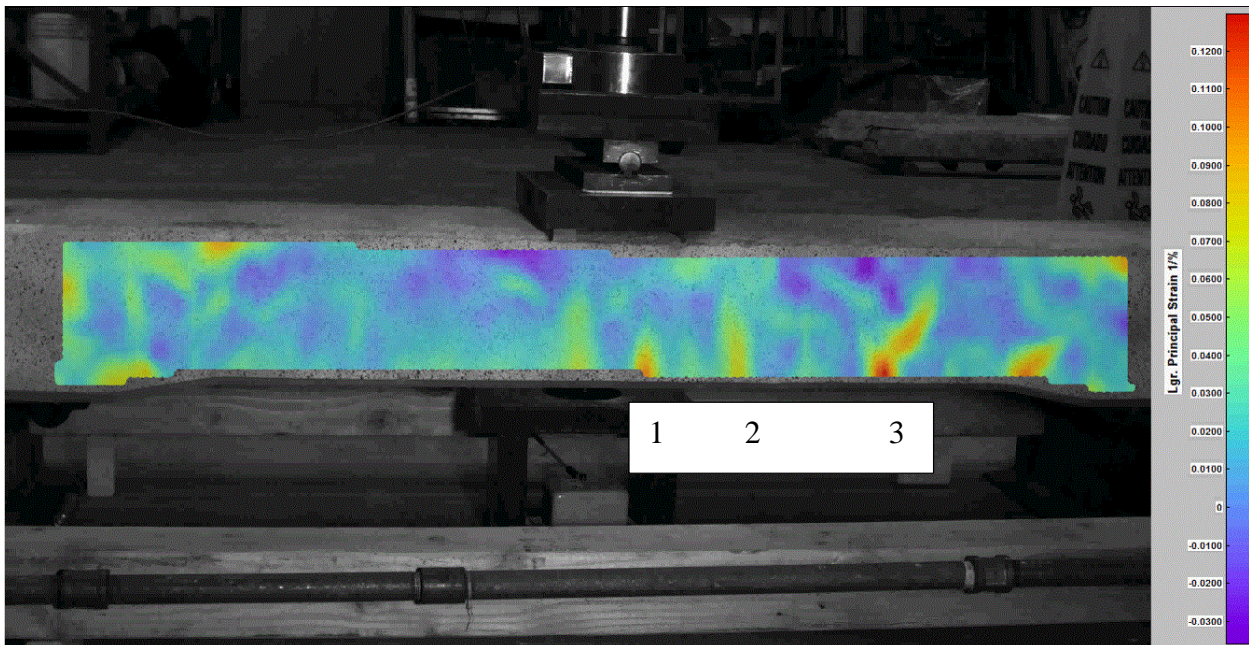


Figure 37. Strain map measured using DIC on New Tie near the end of the 3-minute constant load regimen when the load was kept at approximately 14.4 kips (actual measured load is 14.42 kips).

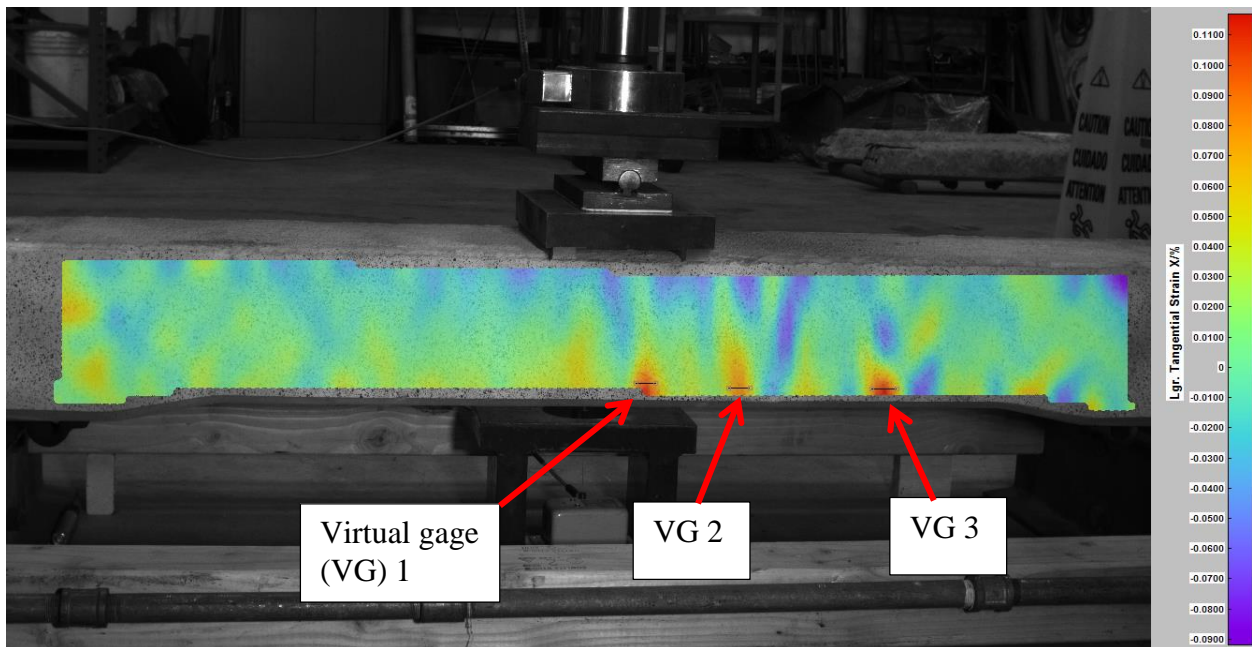


Figure 38. Tangential strain map of New Tie during initial testing regimen showing virtual gauge locations.

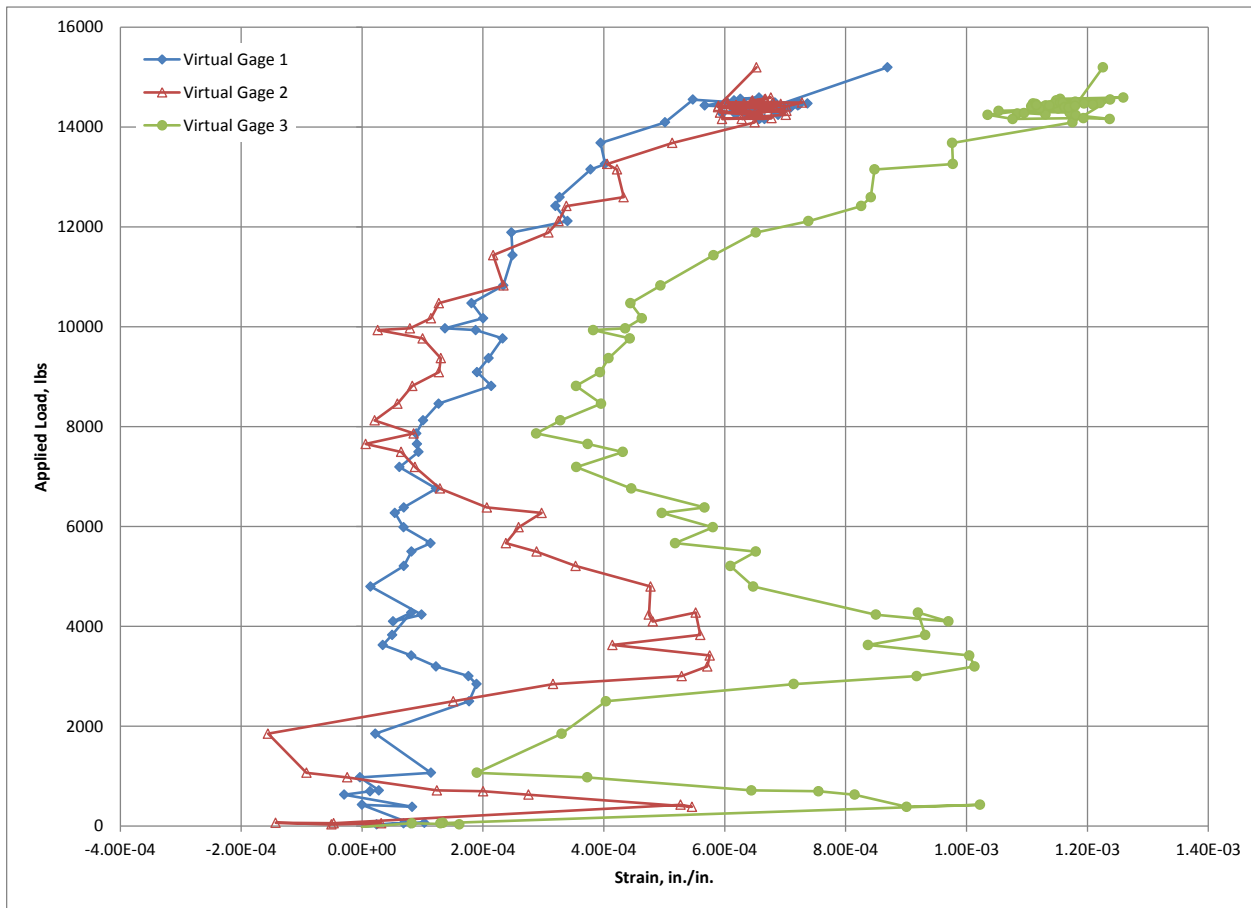


Figure 39. Strains measured using the DIC system at virtual gauge locations on New Tie illustrated in Figure 38.

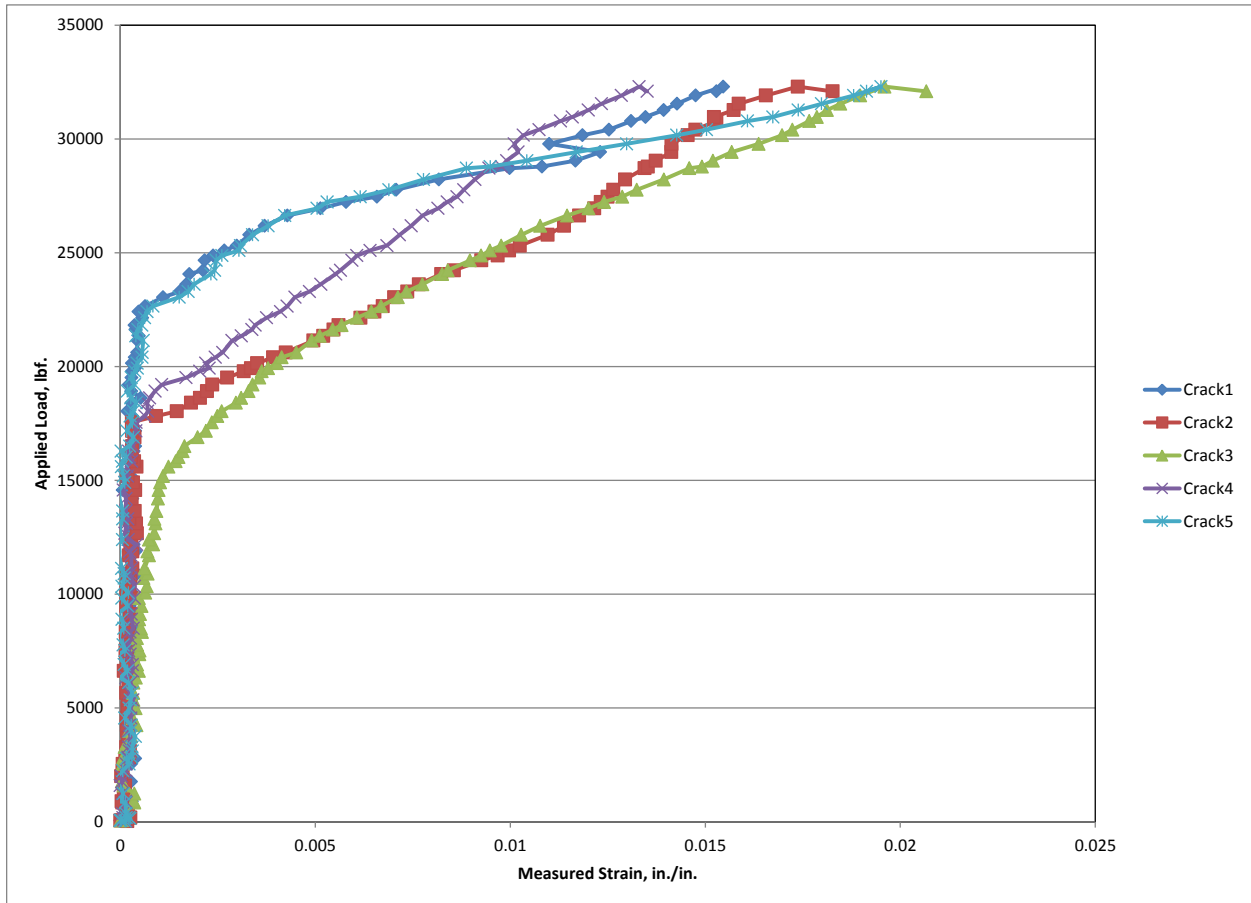


Figure 40. Virtual gage measurements across cracks indicated on the New Tie strain map in Figure 30.

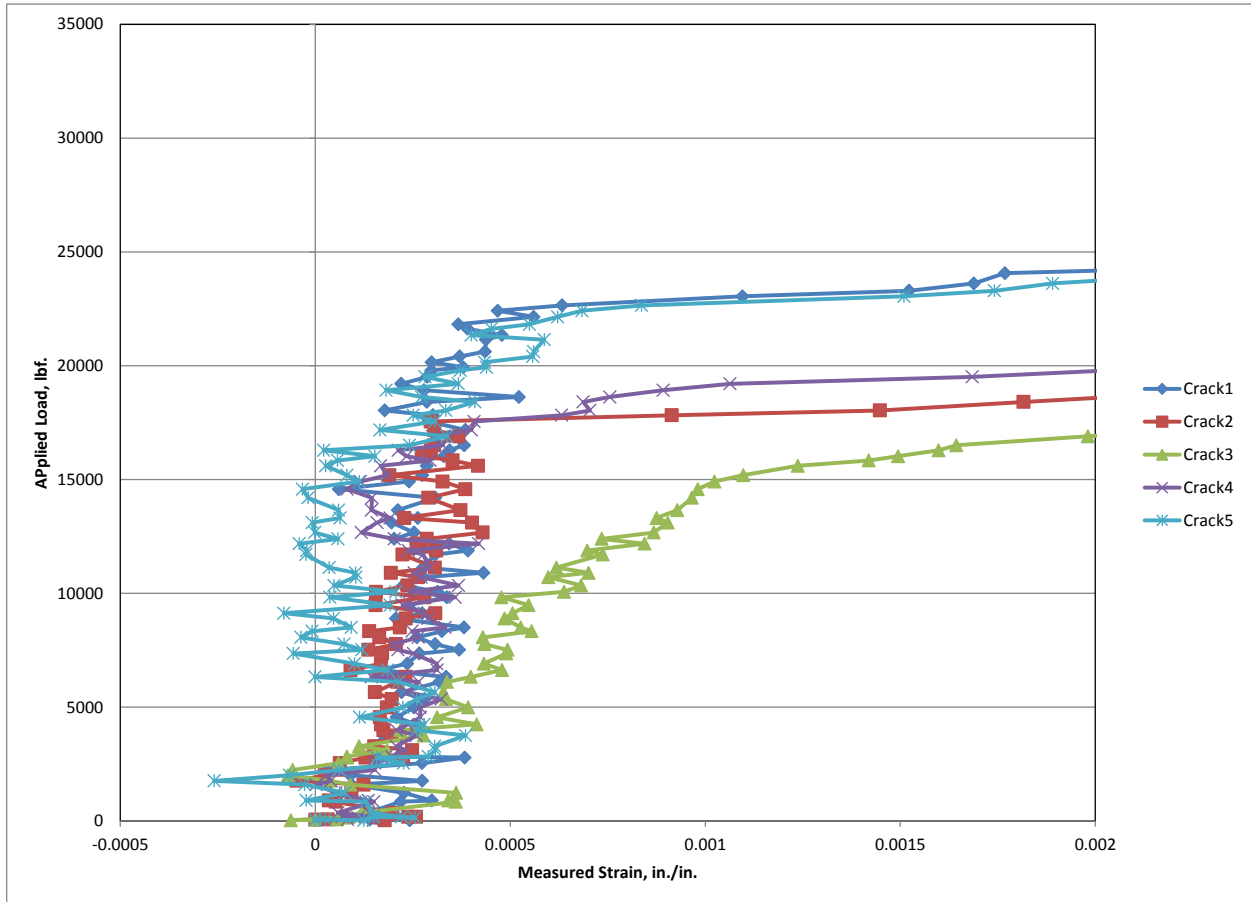


Figure 41. Virtual gage measurements across cracks indicated on the New Tie strain map in Figure 30 zoomed to a lower strain range.

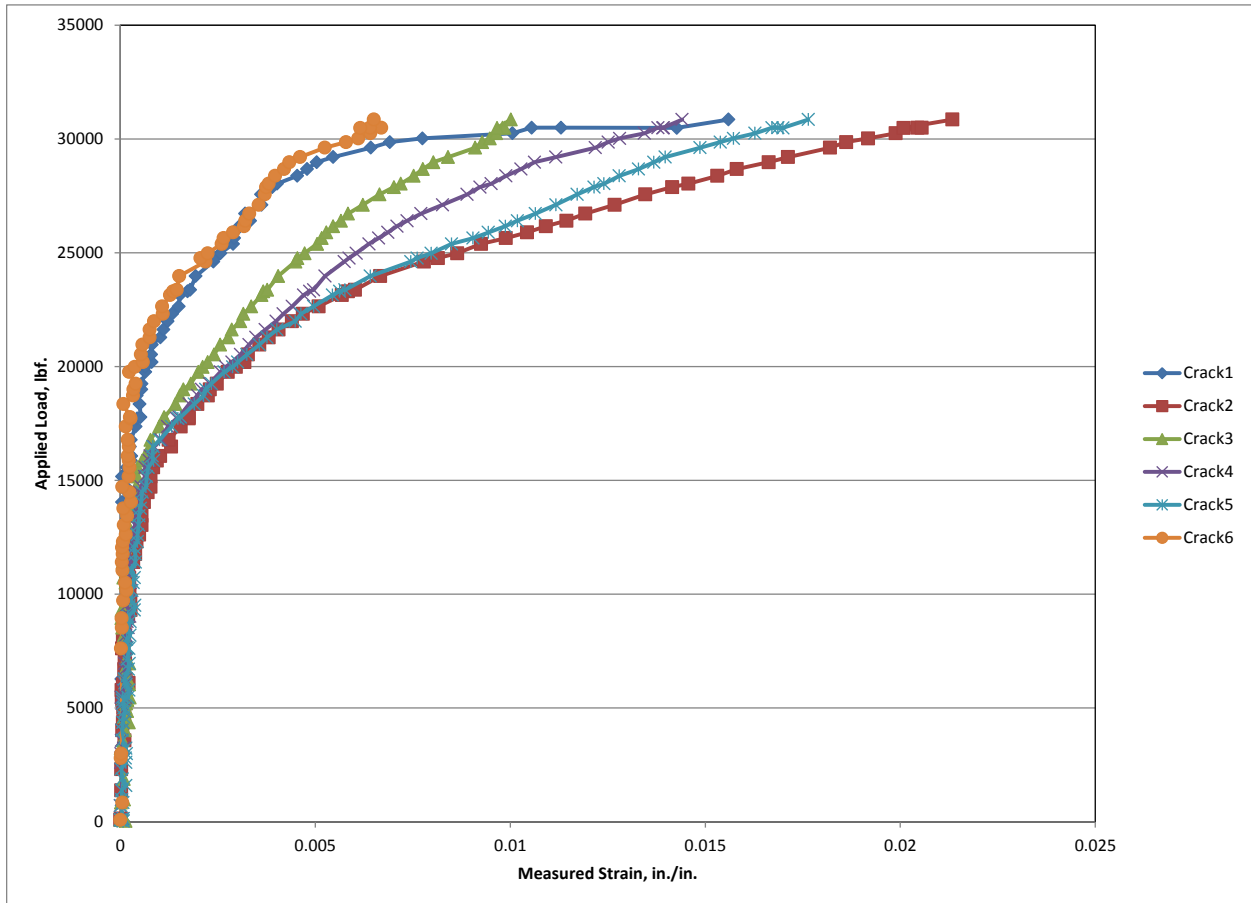


Figure 42. Virtual gage measurements across cracks indicated on Tie N16 strain map in Figure 31.

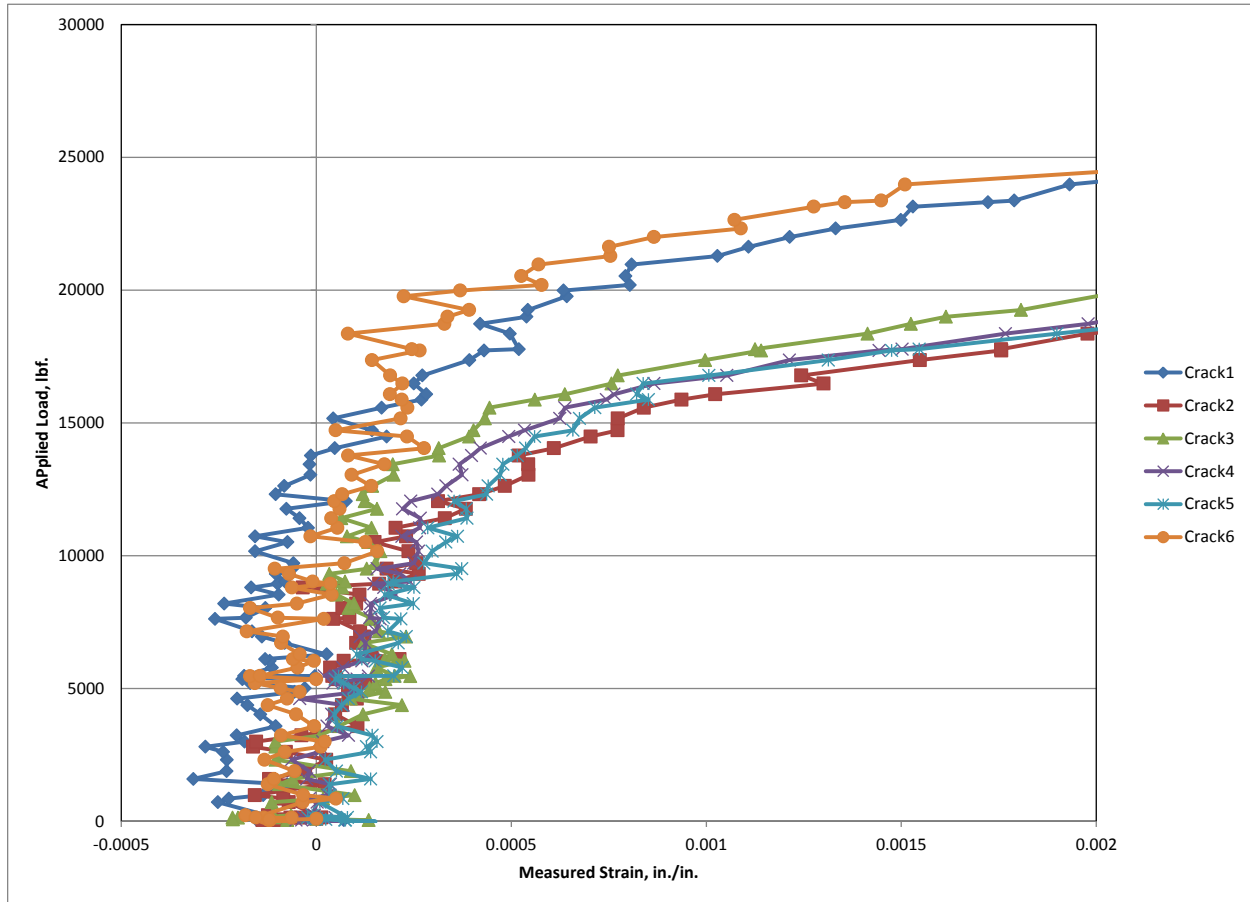


Figure 43. Virtual gage measurements across cracks indicated on Tie N16 strain map in Figure 31 zoomed to a lower strain range.

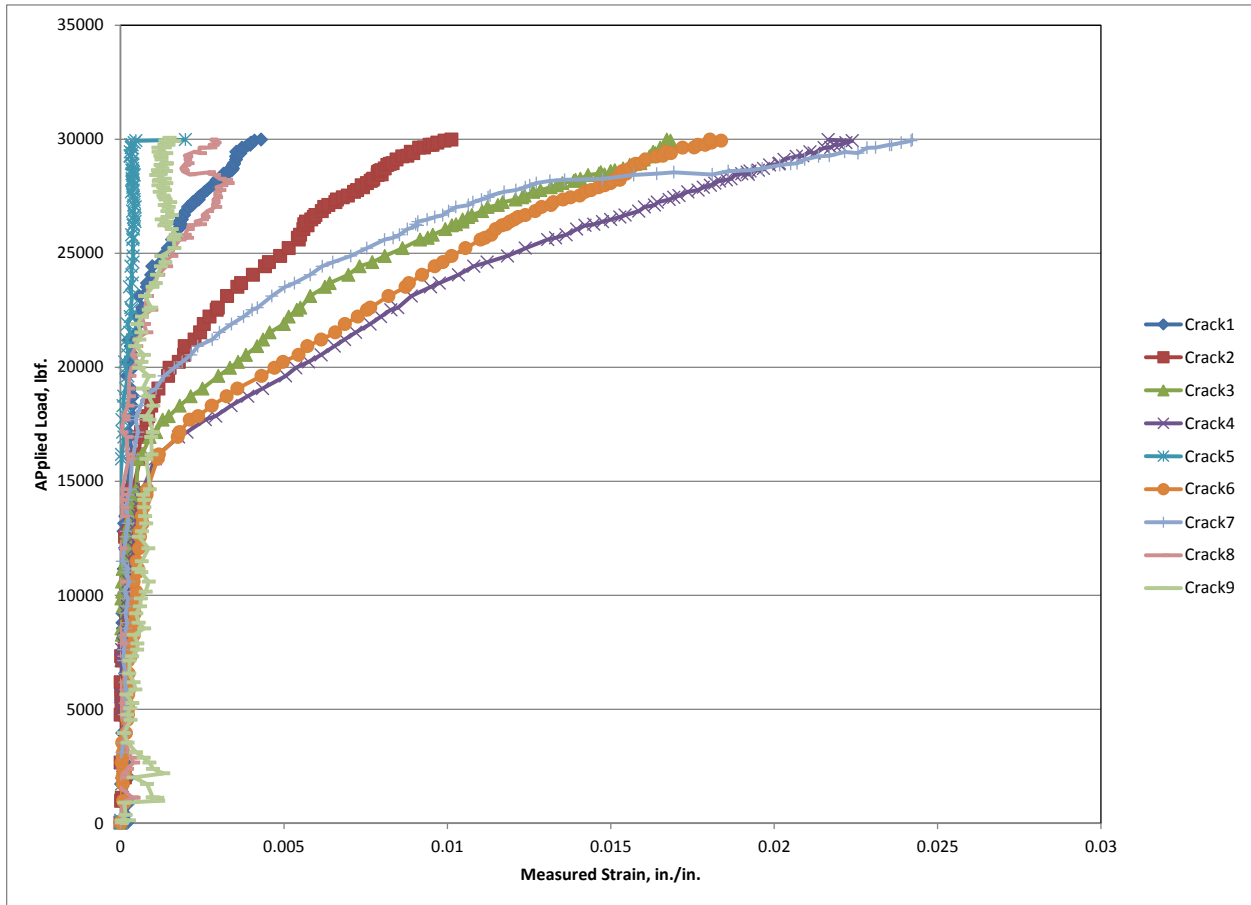


Figure 44. Virtual gage measurements across cracks indicated on Tie S5 strain map in Figure 32.

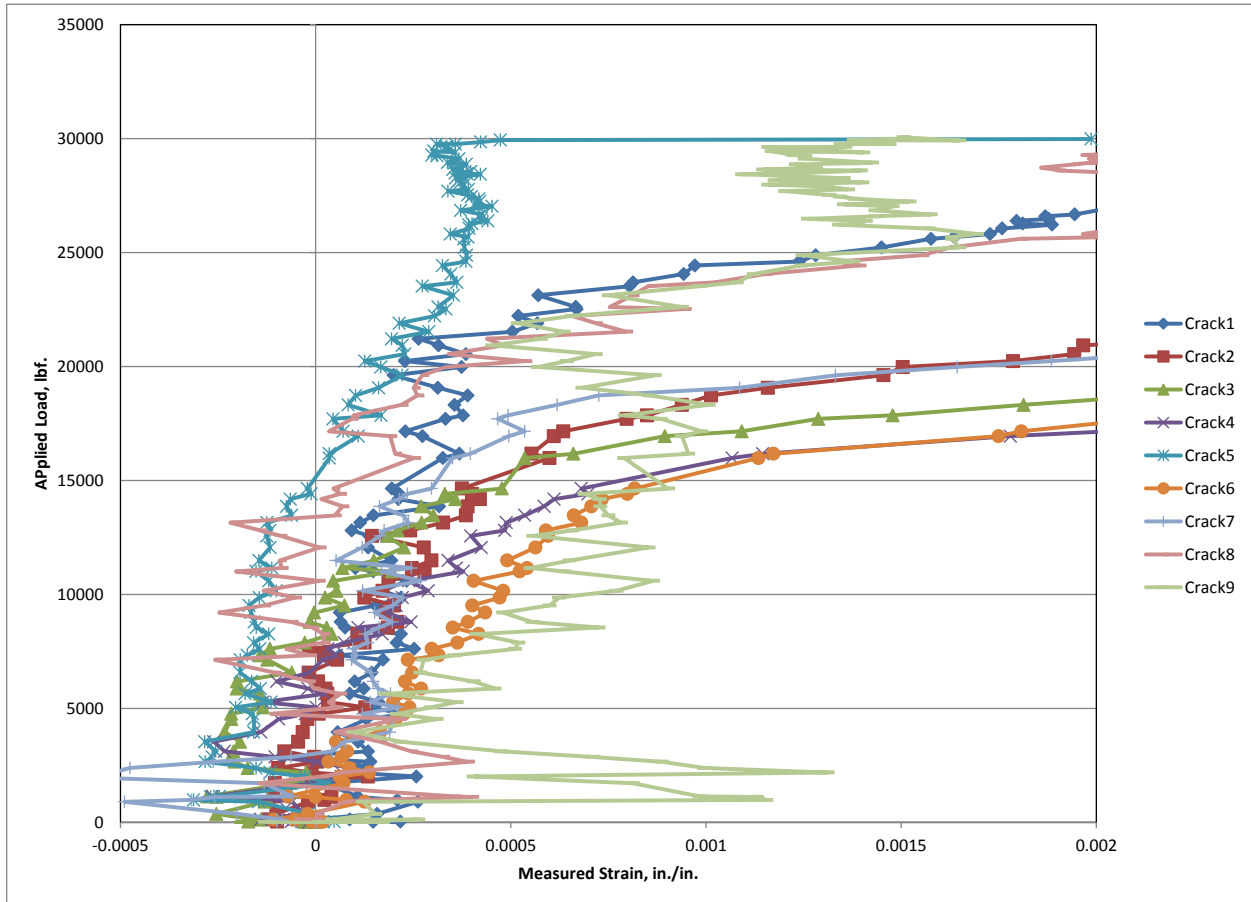


Figure 45. Virtual gage measurements across cracks indicated on Tie S5 strain map in Figure 32 zoomed to a lower strain range.

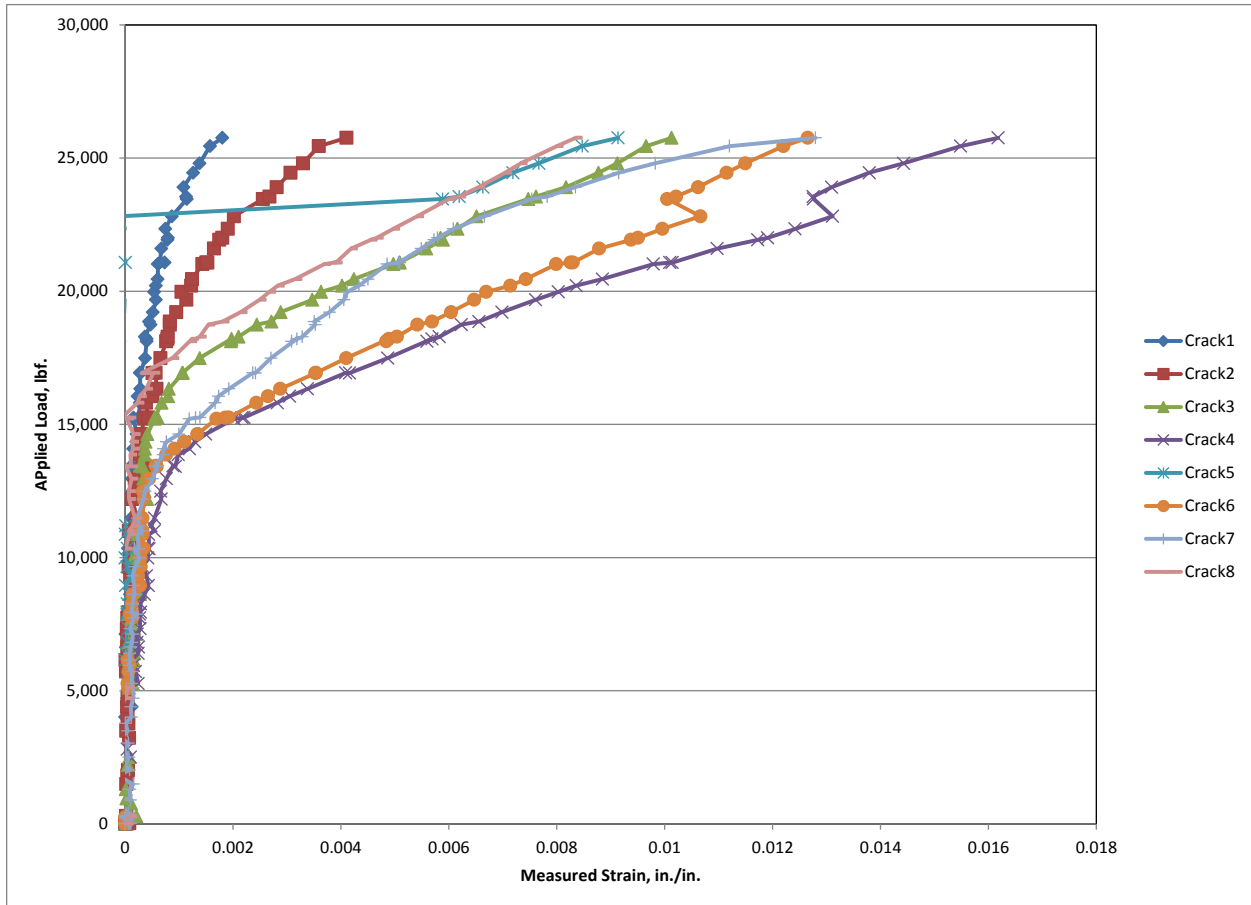


Figure 46. Virtual gage measurements across cracks indicated on Tie S4 strain map in Figure 33.

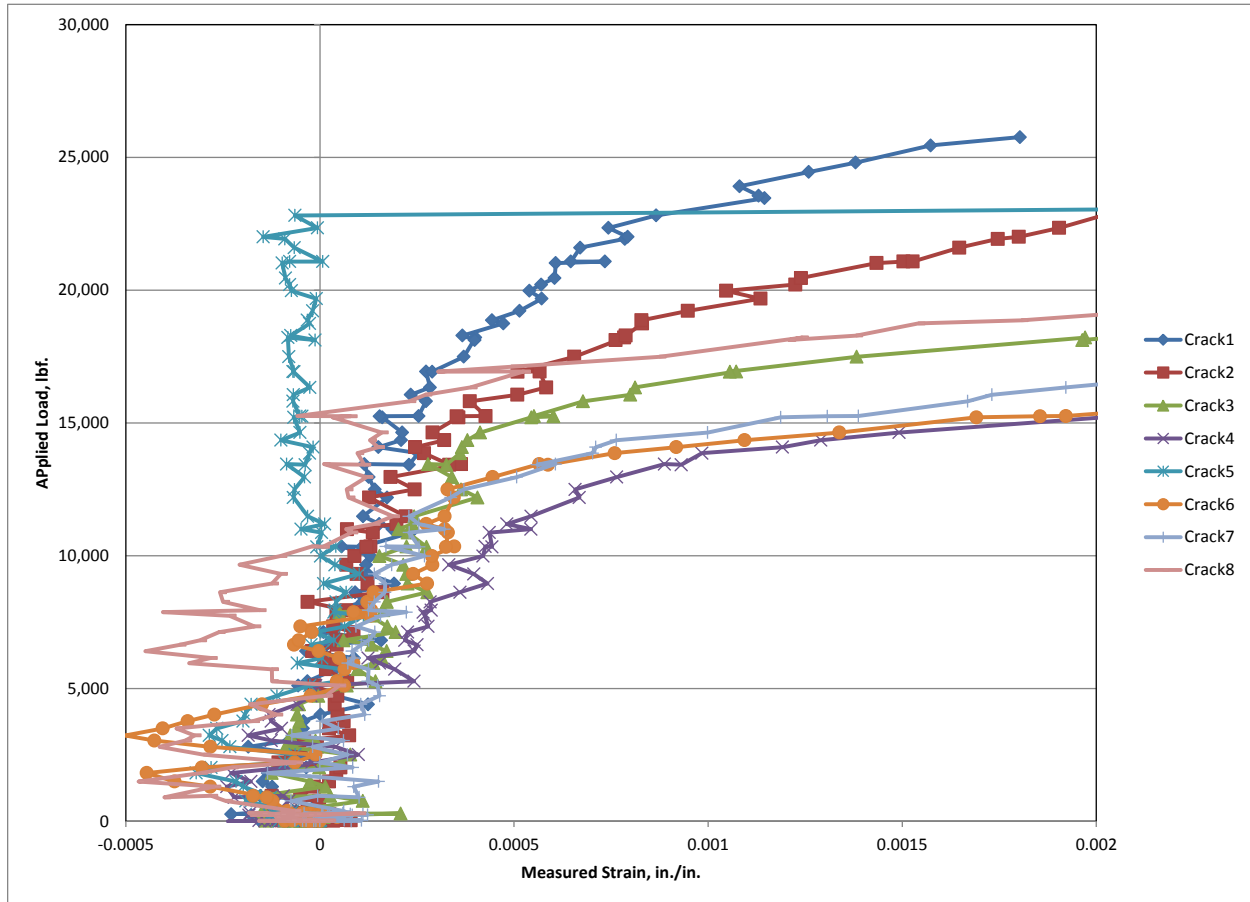


Figure 47. Virtual gage measurements across cracks indicated on Tie S4 strain map in Figure 33 zoomed to a lower strain range.

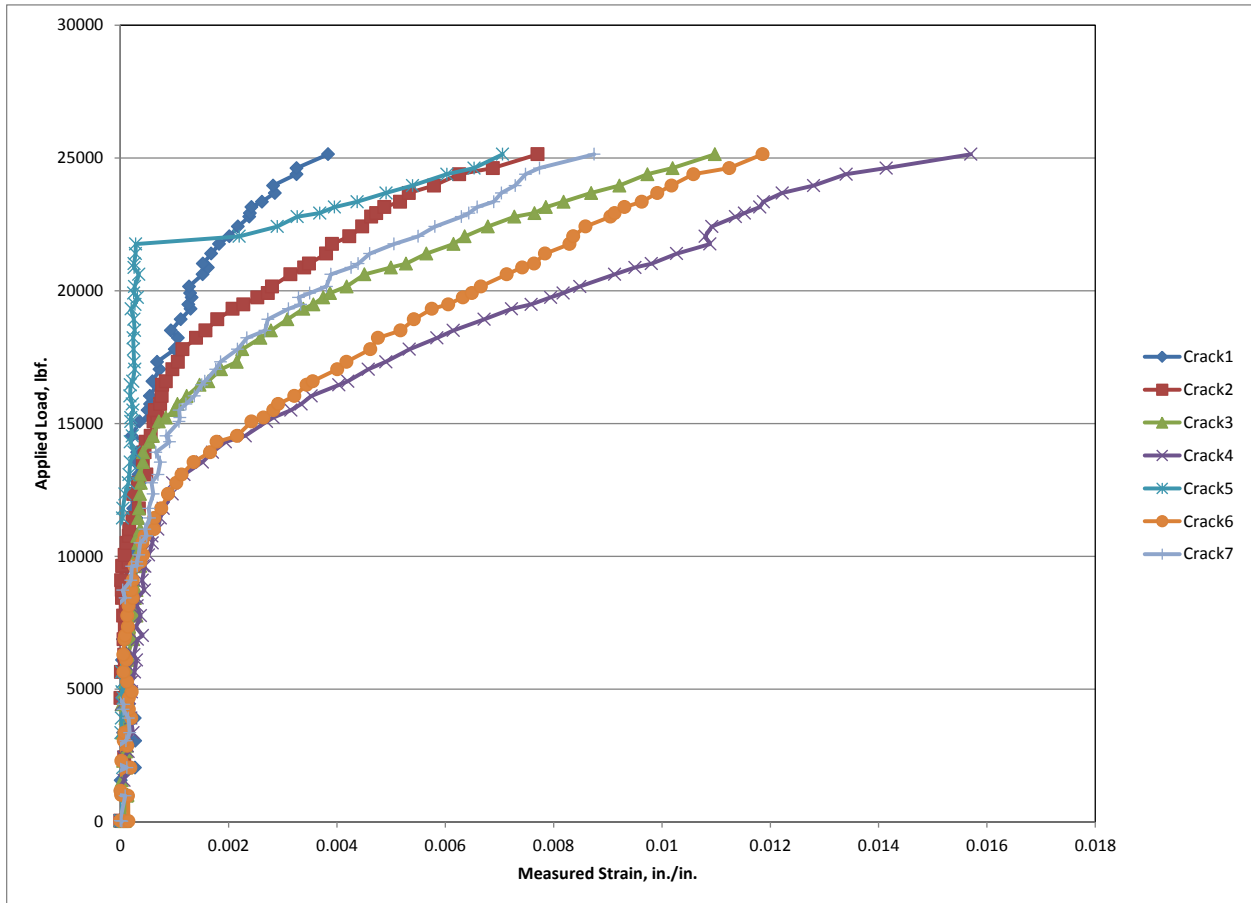


Figure 48. Virtual gage measurements across cracks indicated on Tie N10 strain map in Figure 34.

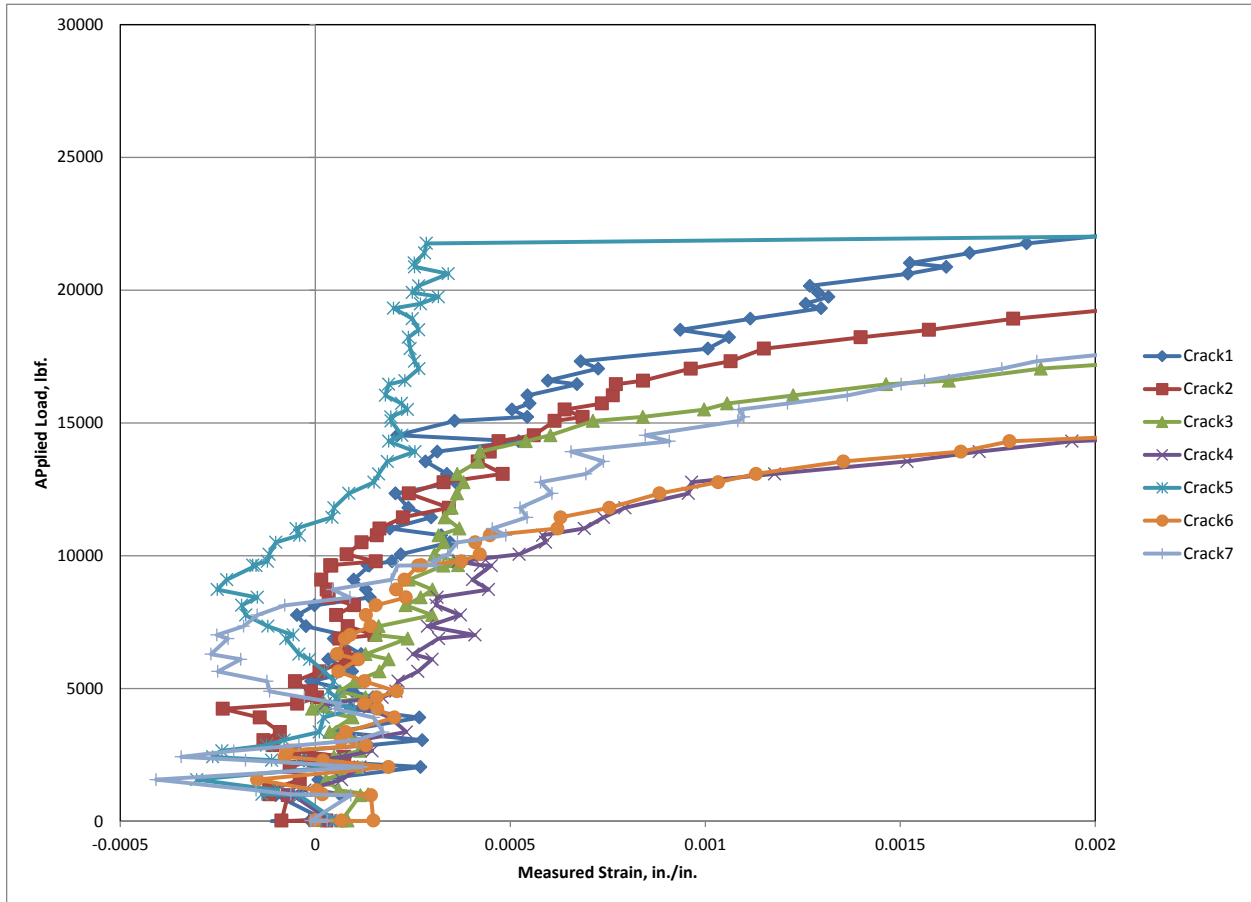


Figure 49. Virtual gage measurements across cracks indicated on Tie N10 strain map in Figure 34 zoomed to a lower strain range.

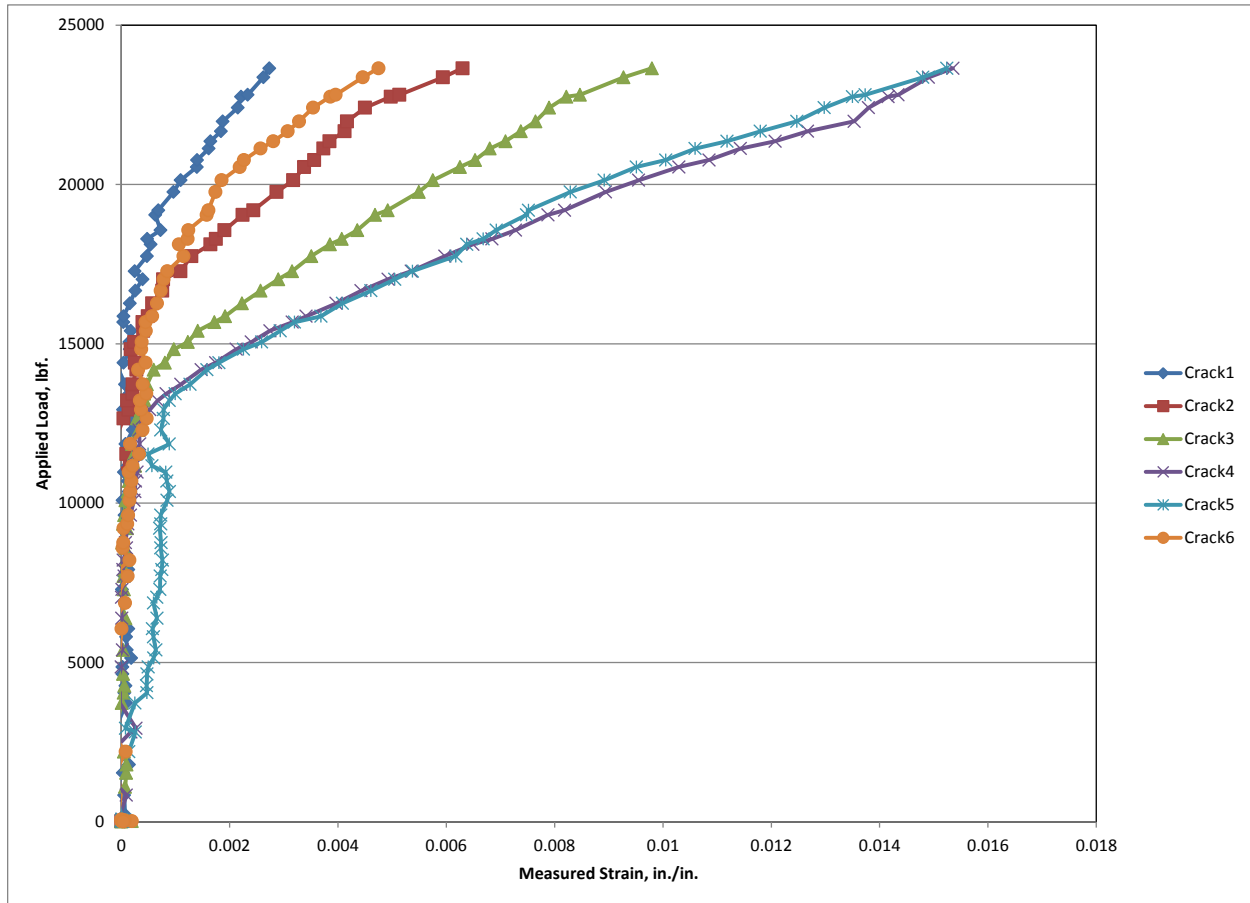


Figure 50. Virtual gage measurements across cracks indicated on Tie S3 strain map in Figure 35.

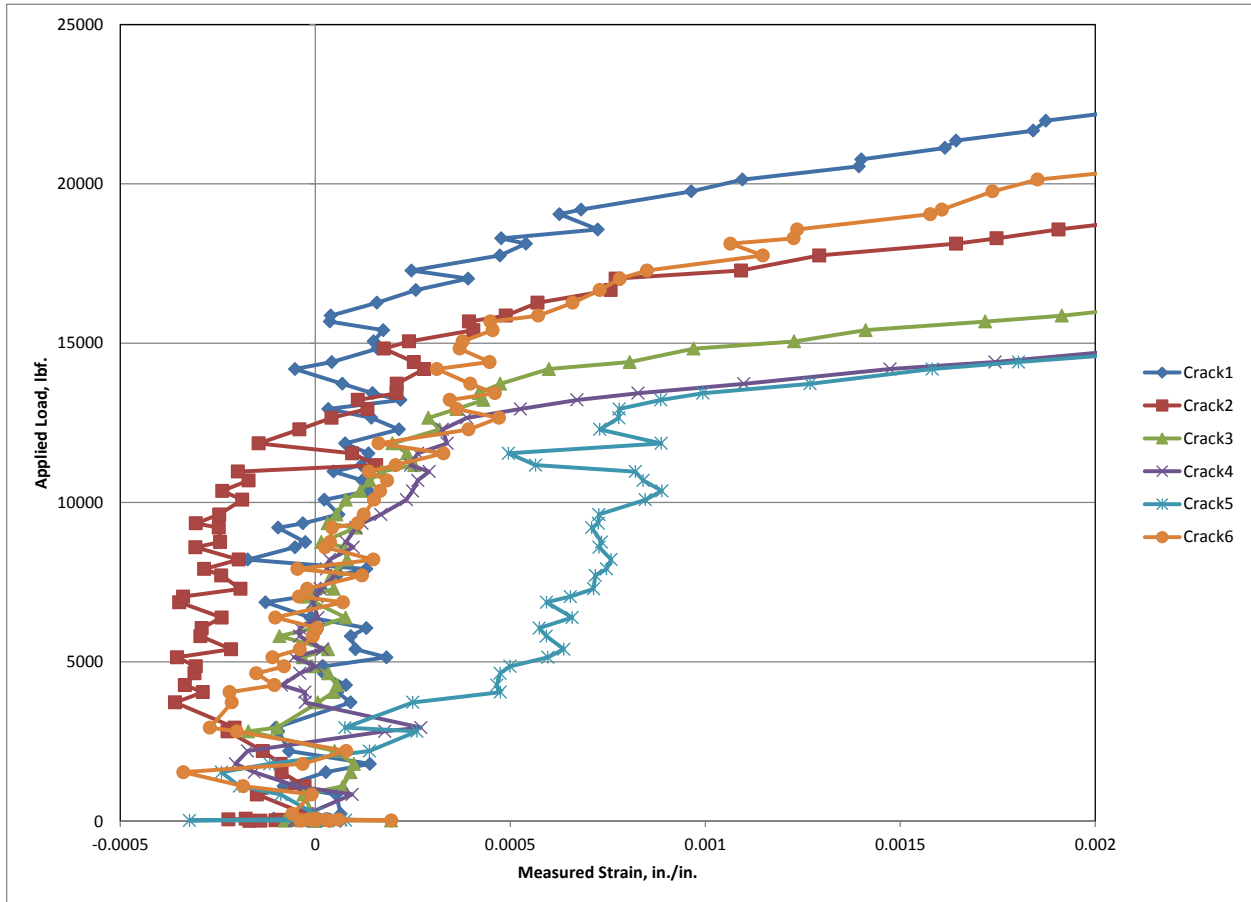


Figure 51. Virtual gage measurements across cracks indicated on Tie S3 strain map in Figure 35 zoomed to a lower strain range.



Figure 52. Abrasion test set-up.

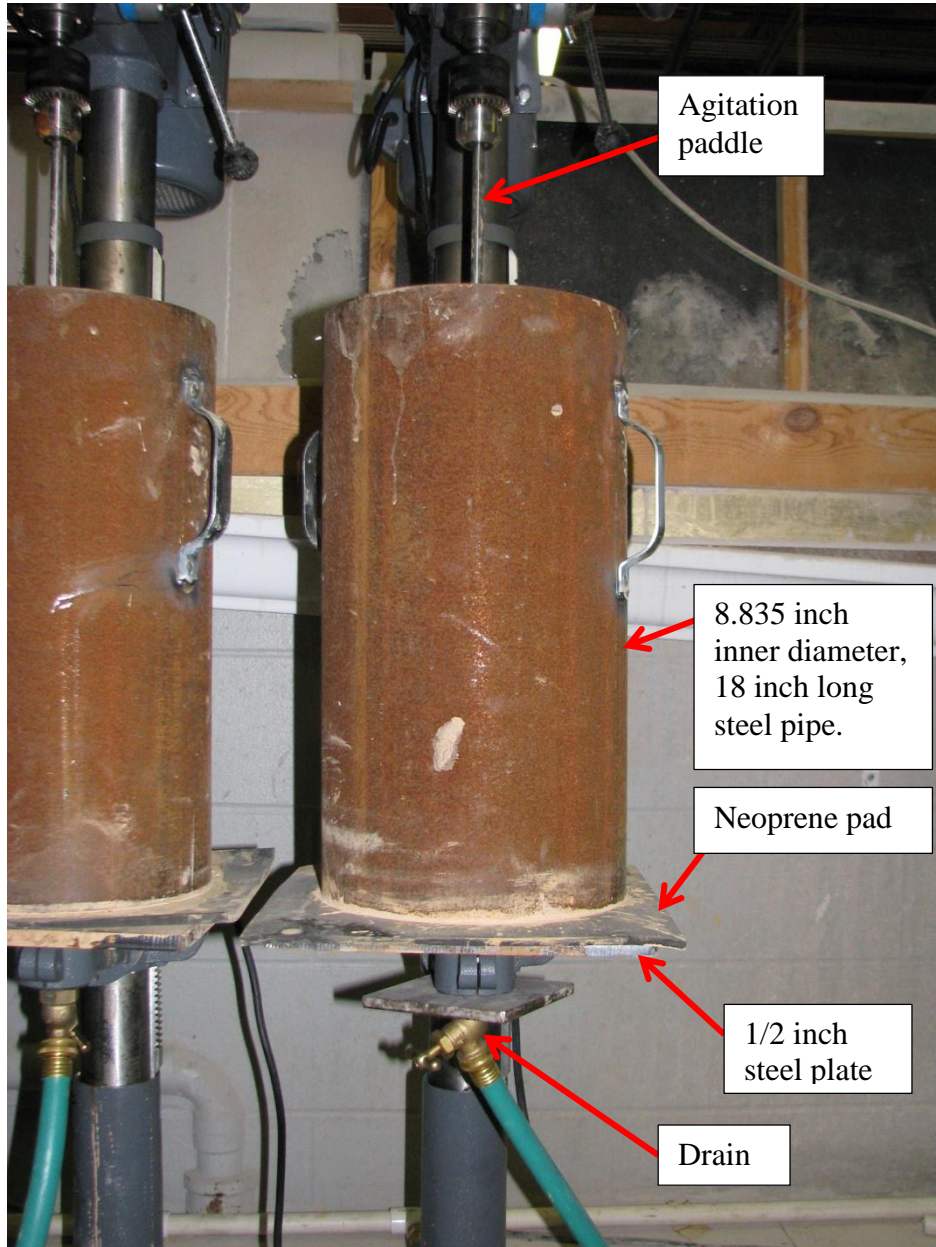


Figure 53. Close up view of abrasion test apparatus.

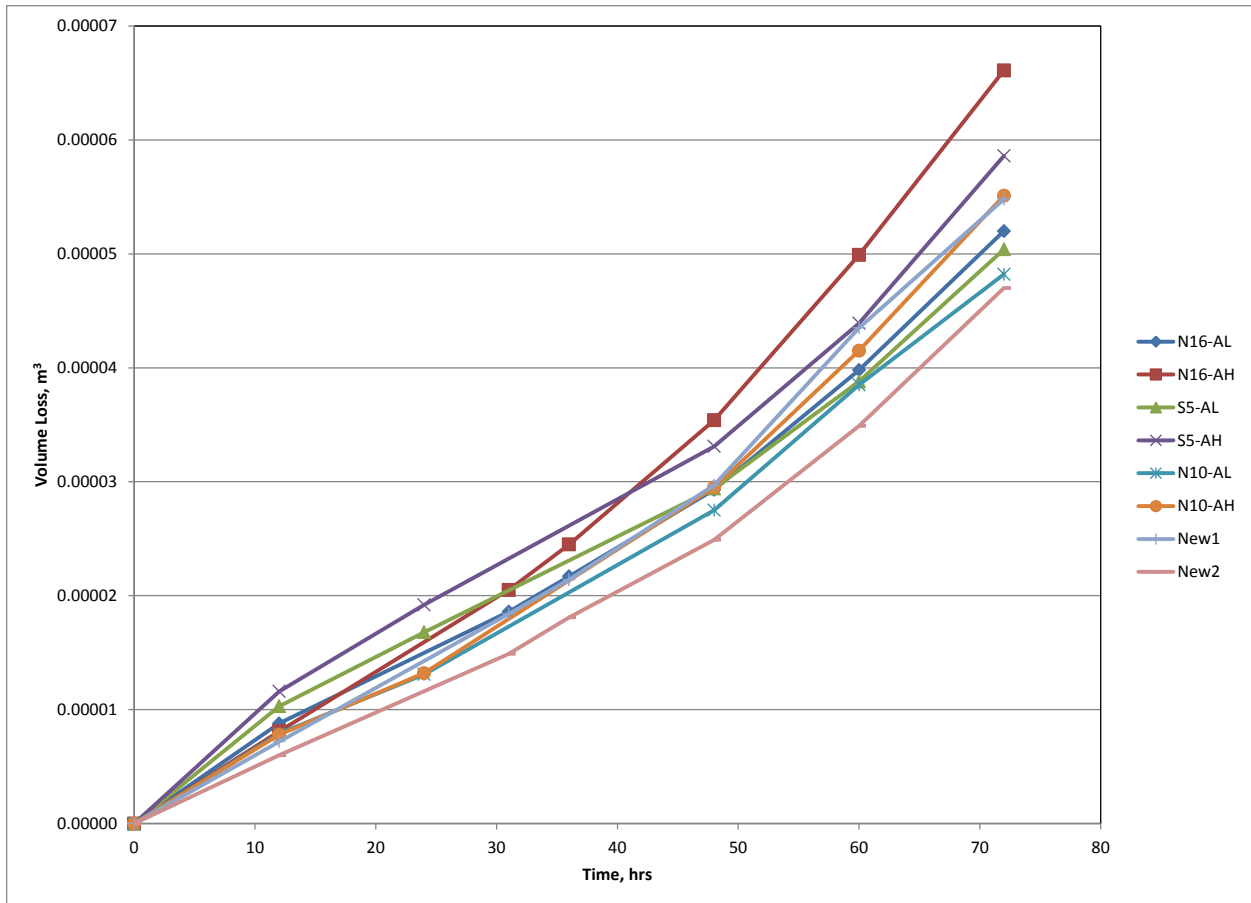


Figure 54. Volume loss versus time for each extracted core specimen obtained from the ties that were subjected to abrasion tests. The suffixes “AL” and “AH” refers to an abrasion specimen extracted from the in-service high and in-service low sides of the railroad ties. The railroad ties were obtained from a superelevated curved portion of the railroad tracks where the derailment had taken place, and therefore, one side of the ties sit at a higher elevation in service than the other side.

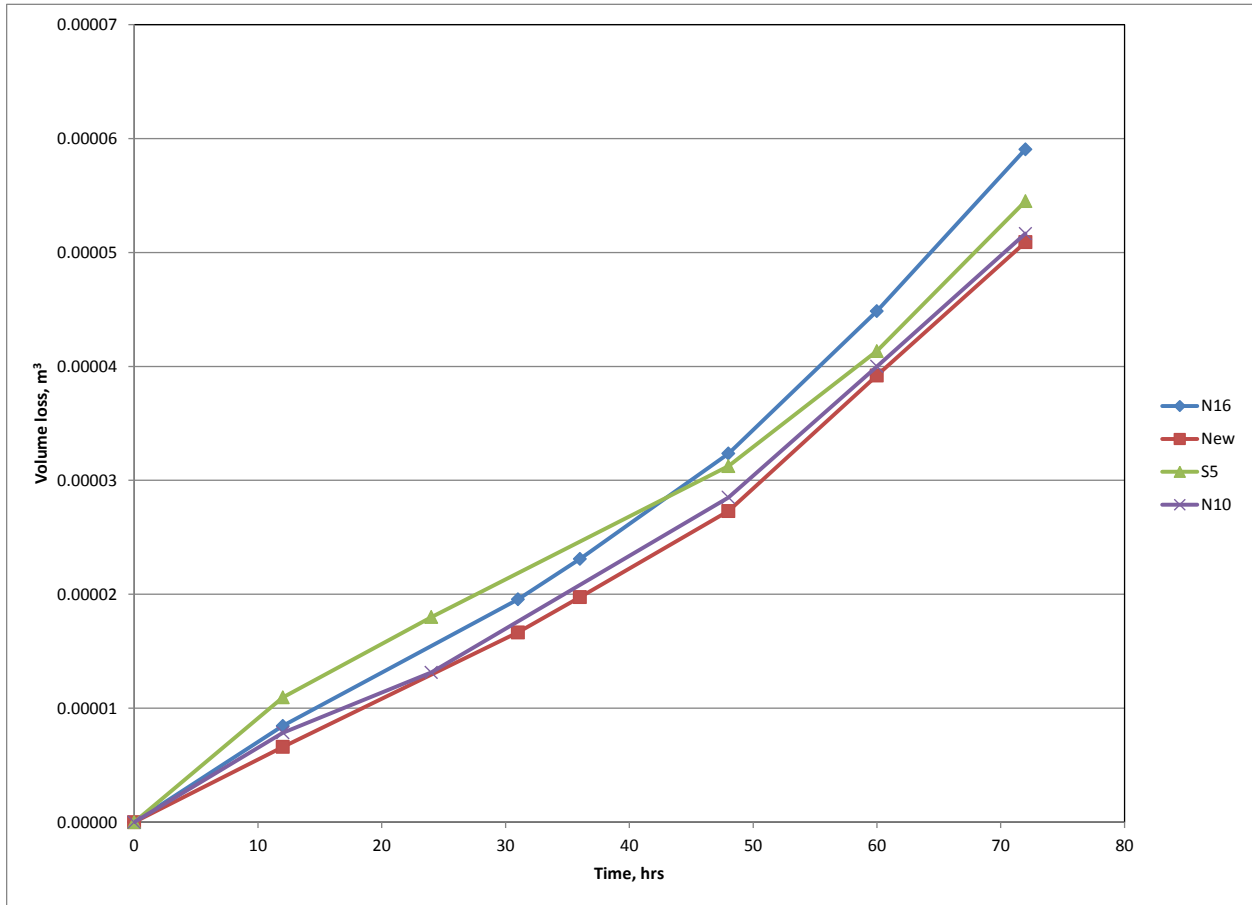


Figure 55. Average volume loss versus time for the two companion specimens for each tie that was subjected to abrasion tests.

APPENDIX A

APPENDIX B



Acct #: 093990
Customer: Wiss Janney Elstner Associates
Shipper #:
Address: 330 Pfingsten Road
 Northbrook, IL, 60062
Contact: Rob Schulman
PO #: 053900

Manufacturer: Agilent Technologies
Model: 34970A
Description: Data Acquisition/Switch Unit
Serial Number: MY44016020
Asset Number: MY44016020
Barcode:

As Received	As Returned	Action Taken	Cal Date:
In Tolerance X	In Tolerance X	Full Calibration X	08/03/2013
Out of Tolerance	Out of Tolerance	Special Calibration	Due Date: 08/03/2014
Malfunctioning	Malfunctioning	Oper. Verification	Temperature: 71.00 deg. F
Operational	Operational	Adjusted	Humidity: 37.00 %
Damaged	N/A	Repaired	Baro. Press.:
N/A		Charted	Procedure: DCN 01510
		Returned As Is	Reference: manufacturer's manual

Incoming Remarks:
No Power Cord.

Technical Remarks:

Calibration Standards Utilized					
Cert. #	Manufacturer	Model #	Description	Cal Date	Due Date
2526310014	Fluke	5700A	Multifunction Calibrator	07/30/2013	10/30/2013

The above identified unit was calibrated in our laboratory at the address shown below.

This report applies only to the item(s) identified above and shall not be reproduced, except in full, without the written approval of Trescal. This unit has been calibrated utilizing standards with a Test Uncertainty Ratio (TUR) of greater than 4:1 approximating a 95% confidence level with a coverage factor of k=2 unless otherwise stated above or as stated on the Report of Calibration. The calibration was performed using references traceable to the SI through NIST or other recognized national laboratory, accepted fundamental or natural physical constants, ratio type of calibration, or by comparison to consensus standards. Trescal's calibration program is in compliance with:

ISO/IEC 17025:2005, ANSI/NCSL Z540-1:1994, ANSI/NCSL Z540.3:2006, MIL STD 45662A, QD-4000:2011.

Trescal warrants all material and labor performed for ninety (90) days unless covered under a separate policy.

* Any number of factors may cause the calibrated item to drift out of tolerance before the interval has expired.

Technician Name/Date: Louis Davis, 08/03/2013

Signatory:

QA Approved:



ENGINEERS
ARCHITECTS
MATERIALS SCIENTISTS

Wiss, Janney, Elstner Associates, Inc.
330 Pflingsten Road
Northbrook, Illinois 60062
847.272.7400 tel | 847.291.9599 fax
www.wje.com
IAS Certification Number: TL165

Certificate of Calibration

Instrument Identification

Noun: LVDT
Manufacturer: Trans-Tek
Description: 1" LVDT

Model #: 353-000
Serial Number: 820125-29

Certification Information

Cal Date: 6/10/2014
Cal Due: 6/10/2015

Temp (F): 70.1
Humidity (%): 48

Calibration Data

Displacement (in.)	Trial 1 (V)	Trial 2 (V)	Trial 3 (V)	Fitted Values (V)	Fitted Error 1 (V)	Fitted Error 2 (V)	Fitted Error 3 (V)
0.000	0.000	-0.004	0.003	-0.005	0.005	0.001	0.008
0.100	-1.075	-1.081	-1.074	-1.102	0.027	0.021	0.028
0.200	-2.186	-2.196	-2.189	-2.199	0.013	0.003	0.010
0.300	-3.293	-3.300	-3.296	-3.296	0.003	-0.004	0.000
0.400	-4.396	-4.399	-4.398	-4.393	-0.003	-0.006	-0.005
0.500	-5.491	-5.497	-5.494	-5.490	-0.001	-0.007	-0.004
0.600	-6.591	-6.588	-6.589	-6.587	-0.004	-0.001	-0.002
0.700	-7.683	-7.675	-7.679	-7.684	0.001	0.009	0.005
0.800	-8.782	-8.762	-8.776	-8.782	0.000	0.020	0.006
0.900	-9.887	-9.870	-9.877	-9.879	-0.008	0.009	0.002
0.900	-9.890	-9.876	-9.878	-9.879	-0.011	0.003	0.001
0.800	-8.781	-8.778	-8.777	-8.782	0.001	0.004	0.005
0.700	-7.683	-7.682	-7.680	-7.684	0.001	0.002	0.004
0.600	-6.592	-6.590	-6.591	-6.587	-0.005	-0.003	-0.004
0.500	-5.495	-5.495	-5.495	-5.490	-0.005	-0.005	-0.005
0.400	-4.399	-4.401	-4.403	-4.393	-0.006	-0.008	-0.010
0.300	-3.295	-3.300	-3.326	-3.296	0.001	-0.004	-0.030
0.200	-2.192	-2.195	-2.235	-2.199	0.007	0.004	-0.036
0.100	-1.081	-1.081	-1.122	-1.102	0.021	0.021	-0.020
0.000	0.000	-0.004	-0.059	-0.005	0.005	0.001	-0.054

Expanded Uncertainty (V): 0.121
Excitation Voltage (V): 10.002

Coefficient A0 (V) = -0.005
Coefficient A1(V/inch) = 10.971
Voltage = A0 + A1*Displacement

Calibration Standards


Noun	Manufacturer	Model	Serial #	Cal Date	Cal Due
Micrometer	Mitutoyo	153-205	C14661	5/16/2014	5/16/2016

Remarks:

This instrument has been calibrated using standards with accuracies traceable to the National Institute of Standards and Technology.


The reported expanded uncertainty is based on Type A and Type B standard uncertainty multiplied by a coverage factor k=2, which for a normal distribution provides a level of confidence of approximately 95%.

Calibrator:

X 
R. Keesbury

Date: 6/11/14

Reviewed and Approved:

X 
John Pearson

Date: 6/10/14



ENGINEERS
ARCHITECTS
MATERIALS SCIENTISTS

Wiss, Janney, Elstner Associates, Inc.
330 Pfingsten Road
Northbrook, Illinois 60062
847.272.7400 tel | 847.291.9599 fax
www.wje.com
IAS Certification Number: TL165

Certificate of Calibration

Instrument Identification

Noun: LVDT
Manufacturer: Trans-Tek
Description: 1" LVDT
Model #: 353-000
Serial Number: 820125-49

Certification Information

Cal Date: 6/10/2014
Cal Due: 6/10/2015
Temp (F): 70.1
Humidity (%): 48

Calibration Data

Displacement (in.)	Trial 1 (V)	Trial 2 (V)	Trial 3 (V)	Fitted Values (V)	Fitted Error 1 (V)	Fitted Error 2 (V)	Fitted Error 3 (V)
0.000	0.000	0.000	-0.014	0.012	-0.012	-0.012	-0.026
0.100	1.097	1.093	1.084	1.099	-0.002	-0.006	-0.015
0.200	2.197	2.192	2.184	2.185	0.012	0.007	-0.001
0.300	3.293	3.290	3.283	3.271	0.022	0.019	0.012
0.400	4.377	4.376	4.372	4.357	0.020	0.019	0.015
0.500	5.456	5.455	5.458	5.443	0.013	0.012	0.014
0.600	6.528	6.531	6.534	6.530	-0.002	0.001	0.004
0.700	7.603	7.607	7.615	7.616	-0.013	-0.009	-0.001
0.800	8.681	8.694	8.697	8.702	-0.021	-0.008	-0.005
0.900	9.764	9.777	9.779	9.788	-0.024	-0.011	-0.009
0.900	9.765	9.793	9.791	9.788	-0.023	0.005	0.003
0.800	8.693	8.697	8.702	8.702	-0.009	-0.005	0.000
0.700	7.602	7.614	7.614	7.616	-0.014	-0.002	-0.002
0.600	6.531	6.535	6.536	6.530	0.001	0.005	0.006
0.500	5.457	5.457	5.457	5.443	0.014	0.014	0.013
0.400	4.377	4.374	4.373	4.357	0.020	0.017	0.016
0.300	3.288	3.283	3.285	3.271	0.017	0.012	0.014
0.200	2.190	2.185	2.186	2.185	0.005	0.000	0.001
0.100	1.089	1.083	1.086	1.099	-0.010	-0.016	-0.013
0.000	-0.006	-0.010	-0.012	0.012	-0.018	-0.022	-0.024

Expanded Uncertainty (V): 0.062
Excitation Voltage (V): 10.002
Coefficient A0 (V) = 0.012
Coefficient A1(V/inch) = 10.862
Voltage = A0 + A1*Displacement

Calibration Standards

Noun	Manufacturer	Model	Serial #	Cal Date	Cal Due
Micrometer	Mitutoyo	153-205	C14661	5/16/2014	5/16/2016

Remarks:

This instrument has been calibrated using standards with accuracies traceable to the National Institute of Standards and Technology.

The reported expanded uncertainty is based on Type A and Type B standard uncertainty multiplied by a coverage factor k= 2, which for a normal distribution provides a level of confidence of approximately 95%.

Calibrator:

X
R. Kessbury

Date:

Reviewed and Approved:

John Pearson

Date:

Certificate of Calibration

Instrument Identification

Noun: Load Cell
Manufacturer: Sensotec
Capacity (lb): 50000
Model #: SENSOTEC 41
Serial Number: 982893

Certification Information

Cal Date: 6/9/2014
Cal Due: 6/9/2015
Mode: Compression
Temp (F): 74
Humidity (%): 49

Calibration Data

Combined Curve Fit Analysis

Load (lb)	Run 1 (mV/V)	Run 2 (mV/V)	Run 3 (mV/V)	Fitted (mV/V)	Error 1 (mV/V)	Error 2 (mV/V)	Error 3 (mV/V)
0	0.00000	0.00000	0.00000	-0.00155	-0.00155	-0.00155	-0.00155
5000	0.30046	0.30057	0.30069	0.30109	0.00063	0.00052	0.00040
10000	0.60278	0.60297	0.60309	0.60373	0.00095	0.00076	0.00064
15000	0.90490	0.90500	0.90513	0.90637	0.00147	0.00137	0.00124
20000	1.20749	1.20752	1.20768	1.20901	0.00152	0.00149	0.00133
25000	1.51028	1.51031	1.51051	1.51165	0.00137	0.00134	0.00114
30000	1.81323	1.81335	1.81349	1.81429	0.00106	0.00094	0.00080
35000	2.11632	2.11631	2.11648	2.11693	0.00061	0.00062	0.00045
40000	2.41946	2.41958	2.41965	2.41956	0.00010	-0.00002	-0.00009
45000	2.72265	2.72267	2.72292	2.72220	-0.00045	-0.00047	-0.00072
50000	3.02607	3.02607	3.02624	3.02484	-0.00123	-0.00123	-0.00140
25000	1.51365	1.51355	1.51379	1.51165	-0.00200	-0.00190	-0.00214
0	0.00002	-0.00027	0.00007	-0.00155	-0.00157	-0.00128	-0.00162

Coefficient A0 = -1.55E-03
Coefficient A1 = 6.05E-05
mV/V Output = A0 + A1*Load

Standard Deviation (mV/V): 0.00122
Standard Deviation / Span: 0.040%
Full Scale Output (mv/V): 3.02484
lb / $\mu\epsilon$ Output: 8.26490
Expanded Uncertainty (mV/V): 0.00911
Expanded Uncertainty (lb): 125.0
Expanded Uncertainty / Span: 0.30%



Calibration Standards

Noun	Manufacturer	Model	Serial #	Cal Date	Cal Due
Load Cell	Interface	1620AJH-50k	102505	1/11/2012	1/11/2015



Remarks:

This instrument has been calibrated using standards with accuracies traceable to the National Institute of Standards and Technology. This calibration conforms to the ASTM Standard Practice E74, Calibration of Force Measuring Instruments for Verifying the Force Indication of Testing Machines.

The reported expanded uncertainty is based on Type A and Type B standard uncertainty multiplied by a coverage factor k= 2, which for a normal distribution provides a level of confidence of approximately 95%.

Calibrator: 
X 
R. Keesbury

Date: 6/9/14

Reviewed and Approved: 
X 
J. Pearson

Date: 6/10/14

Certificate of Calibration

Instrument Identification

Noun: CET Model #: PA-5
Manufacturer: Unimeasure Serial Number: 36040027
Description: CET-5"

Certification Information

Cal Date: 6/10/2014 Temp (F): 71.5
Cal Due: 6/10/2015 Humidity (%): 41

Calibration Data

Displacement (in.)	Voltage (mV/V)	Voltage (mV/V)	Voltage (mV/V)	Fitted Values(mV/V)	Fitted Error 1 (mV/V)	Fitted Error 2 (mV/V)	Fitted Error 3 (mV/V)
0.000	38.462	39.261	38.462	39.141	-0.679	0.120	-0.679
0.500	138.162	137.962	138.162	137.714	0.448	0.248	0.448
1.000	236.364	236.464	236.464	236.287	0.076	0.176	0.176
1.500	334.965	334.665	335.065	334.861	0.104	-0.195	0.204
2.000	433.566	433.467	433.167	433.434	0.132	0.033	-0.267
2.500	531.968	531.768	531.668	532.007	-0.039	-0.239	-0.339
3.000	630.769	630.470	630.370	630.581	0.189	-0.111	-0.211
3.500	729.471	729.171	728.871	729.154	0.317	0.017	-0.283
4.000	828.571	828.172	827.772	827.727	0.844	0.445	0.045
4.500	927.073	926.374	926.274	926.301	0.772	0.073	-0.027
4.500	926.773	926.274	926.074	926.301	0.473	-0.027	-0.227
4.000	828.272	827.972	827.373	827.727	0.544	0.245	-0.355
3.500	729.271	729.171	728.671	729.154	0.117	0.017	-0.483
3.000	630.470	629.970	629.670	630.581	-0.111	-0.611	-0.910
2.500	531.768	531.668	531.269	532.007	-0.239	-0.339	-0.739
2.000	433.367	433.167	432.867	433.434	-0.067	-0.267	-0.567
1.500	334.865	335.065	334.765	334.861	0.005	0.204	-0.095
1.000	235.964	236.364	236.264	236.287	-0.323	0.076	-0.024
0.500	138.062	137.862	137.962	137.714	0.348	0.148	0.248
0.000	39.760	39.461	39.361	39.141	0.620	0.320	0.220

Expanded Uncertainty (mV/V): 2.4658 Coefficient A0 (mV/V)= 39.141
Excitation Voltage(V): 10.010 Coefficient A1(mV/V/in)= 197.147
Displacement = A0 + A1*Voltage

Calibration Standards

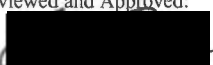
Noun	Manufacturer	Model	Serial #	Cal Date	Cal Due
Gage Block Set	Mitutoyo	516.935	095467 C10256	5/19/2014	5/19/2016

Remarks:

This instrument has been calibrated using standards with accuracies traceable to the National Institute of Standards and Technology.

The reported expanded uncertainty is based on Type A and Type B standard uncertainty multiplied by a coverage factor k= 2, which for a normal distribution provides a level of confidence of approximately 95%.

Calibrator: 
X 
R. Reesbury Date: 6/11/14

Reviewed and Approved:
X 
J. Pearson Date: 6/16/14

APPENDIX C

INTEROFFICE MEMORANDUM

Via: E-mail/Project folder

To: A. Koray Tureyen

From: Hugh (Xiaoqiang) Hou

Date: July 16, 2014

Project: NTSB Concrete Tie Testing and Petrography
WJE No. 2014.2701

Subject: Petrographic studies of concrete cores

As requested, petrographic studies and air-void analyses were conducted on concrete cores to assess the general characteristics of the concrete. The cores had been extracted from precast pre-stressed concrete railroad ties after the ties had been subjected to a flexural loading test (bend test). The petrographic studies were part of a broader evaluation of the concrete ties and were intended to assess aggregate types, air-void system parameters, depth of paste carbonation, and deterioration mechanisms that may affect the durability of the ties.

SAMPLES

Six 3.8-inch diameter concrete cores were received on June 19, 2014 for petrographic studies and air-void analyses. Each core represented the full thickness of the concrete tie. Core identifications, lengths, and brief descriptions of as-received cores are provided in Table 1. The appearance of the as-received cores is provided in Appendix A.

The core designated NEW represented a concrete tie that reportedly had never been installed. This core was intended to serve as a control. The remaining five cores represented concrete ties that had been installed in 1994 in a railroad track in the Bronx borough of New York, New York. Each core had been extracted over a vertical crack, which was either preexisting or had been induced, for Core NEW only, by the Tie Center Negative Moment Test (Bend Test) per American Railway Engineering and Maintenance-of-way Association "Manual for Railway Engineering," Chapter 30, Part 4, Concrete Ties.

Core lengths ranged from 7.0 inches (Core NEW) to 6.5 inches (S3, S4 and N10), and locally to 5.5 inches (S3). The top surface of each core (as-cast bottom surface) exhibited generally minor to moderate erosion and minor raveling/spalls near the crack. The bottom surface of each core (as-cast top surface) extracted from ties taken from service exhibited moderate to severe erosion and spalls, and was generally an uneven surface exposing polished or fractured aggregate particles. The original struck surface (cast top) was only observed on the bottom of the control core (New). Two layers of 7-wire strand reinforcement were generally present in each core. The reinforcement was free of significant corrosion and appeared to be in good condition. Horizontal cracks or fractures were observed at the locations of reinforcement, which are reportedly associated with coring and/or Bend Testing.

Table 1. General Characteristics of Cores

Core ID	Parent Tie	Max. Core Length (inch)	Concrete Loss* (inch)	End Surfaces and Major Characteristics	Appendix Figures
NEW	Never installed (control)	7.0	N/A	<ul style="list-style-type: none"> Flat cast top surface, no significant paste erosion Bottom surface uneven, struck or free surface Core broke into two segments at strand 2-inches from top surface (strand not submitted); fresh, clean fracture surface Upper core segment fractured at vertical crack; fracture surface fresh, clean Transverse crack at lower strand at 4.6 inches depth Short diagonal crack 1 inch above bottom surface 	A1 - A4
S3	Installed in track 1994	6.5	0.5	<ul style="list-style-type: none"> Top surface half moderately eroded on one side of vertical crack, remaining half spalled to 0.2 inch maximum depth Bottom surface uneven, partially eroded and partially spalled or fractured Core broke into three major segments at upper and lower strand, at depths of 2.2 and 4.5 inches; fracture surfaces fresh, clean Upper core segment broke at vertical crack; debris, discoloration and glossy appearance on crack surfaces Vertical crack extended to depth of lower strand 	A5 - A8
S4	Installed in track 1994	6.5	0.5	<ul style="list-style-type: none"> Flat cast top surface, minor paste erosion; minor raveling near vertical crack Bottom surface eroded, polished aggregates Core broke into two segments at strand, at depths 2.3 inches and 4.5 inches; fracture surface fresh, clean Vertical crack changed to diagonal between two layers of reinforcement Transverse cracks at reinforcement 	A9 - A12
S5	Installed in track 1994	6.9	0.1	<ul style="list-style-type: none"> Uneven top surface, minor erosion and raveling Bottom surface severely eroded and spalled, fractured and polished aggregate Vertical crack extended to lower strand Transverse cracks at reinforcement 	A13-A16
N10	Installed in track 1994	6.5	0.5	<ul style="list-style-type: none"> Top surface minor erosion, minor raveling and spalls near vertical crack Bottom surface severely eroded, polished aggregates Vertical crack extended to upper reinforcement, then diagonally crack exits core above lower reinforcement Transverse cracks at reinforcement 	A17-A20
N16	Installed in track 1994	6.9	0.1	<ul style="list-style-type: none"> Top surface minor erosion, small spalls and raveling near vertical crack Bottom surface slightly eroded Vertical crack extended to upper reinforcement Transverse cracks at reinforcement 	A21-A24

*Calculated by subtracting the maximum lengths of in-service cores from the length of Core NEW.

PETROGRAPHIC STUDIES

Petrographic studies were conducted using the methods and procedures described in ASTM C856-11, *Standard Practice for Petrographic Examination of Hardened Concrete*. The cores were photographed as received. Cores were briefly examined and reassembled using epoxy, as needed, to facilitate subsequent preparation. After the epoxy hardened, each core was cut in half longitudinally, generally parallel to the strand reinforcement and perpendicular to the major crack, using a water-cooled, continuous-rim, diamond saw blade. One resulting planar surface of each core was lapped using progressively finer silicon carbide abrasives to achieve a fine matte finish suitable for examination with a stereomicroscope. Lapping removes saw damage and exposes textural features such that contacts between layers and the edges of air voids, cracks, and aggregate constituents can be more easily observed. Photographs of lapped surfaces of the cores are shown in Figures 1 through 7. Fresh fracture surfaces were also prepared to study the physical characteristics of the concrete. Thin sections were prepared from each core to assess compositional and textural characteristics. Lapped and fracture surfaces were examined at magnifications up to approximately 50X using a stereomicroscope. The thin sections were examined using a petrographic (polarized-light) microscope at magnifications ranging from 50X to 630X. Microscopic examination and various tests are designed to elicit specific information about the composition and condition of the concrete. The observations are interpreted to derive conclusions about quality, performance, and probable cause of distress. Thin-section studies reveal details of crystal size, morphology, abundance, and distribution, leading to interpretations relating these data to certain features of the concrete and the conditions to which it has been exposed.

Air-void analysis was conducted on the lapped sections of the cores using the procedures and the modified-point-count method described in ASTM C457, *Standard Test Method for Microscopical Determination of Parameters of the Air-Void System in Hardened Concrete*.

Concrete Characteristics

Concrete mixes represented by the cores consisted of similar constituents in overall similar proportions and exhibited similar physical characteristics. The concrete was well consolidated. Concrete constituents were fairly uniformly distributed. Measured air contents and air-void system parameters are reported in Table 2. Selected petrographic observations are present in Table 3.

The concrete contains well-graded crushed carbonate rock (mainly dolostone) coarse and fine aggregates dispersed in an air-entrained portland cement paste (Figures 1 through 20). Nominal top size of the aggregate was 3/4 inch. Coarse and fine aggregates were similar and appeared to be from the same or similar source. The dolostone consisted of fairly hard, dense particles. No evidence of deleterious chemical reactions involving aggregate or paste was observed.

Paste qualities appear to be good overall. The paste is medium gray, hard, low in water absorbency and exhibits subvitreous luster on fresh fracture surfaces. No supplementary cementitious materials such as fly ash or ground slag were observed. Moderate amounts of cement-sized fragmental dolostone were observed in the paste (Figures 19 and 20). These fragments appeared to be similar to the aggregates in lithology and could indicate that the aggregates were dusty. The hydration of portland cement is advanced (Figure 20). Estimated water-to-cement ratio (w/c) is less than 0.38, which was assessed mainly based on the physical characteristics of the paste (Table 3). Paste-aggregate bond is tight. Fresh fractures created in

laboratory examinations and the preexisting crack surfaces mainly passed through aggregate particles (Figures A4, A12 and A24).

The depth of paste carbonation adjacent to a few near-to surface aggregate particles was locally up to 0.3 inch based on thin-section examinations. The typical depth of paste carbonation was less than 0.02 inch from top and bottom surfaces, and crack surfaces; the carbonation depth is considered negligible for 20-year-old concrete (Figure 8) and is indicative of dense paste.

No major cracks or significant microcracks were observed other than the vertical cracks that extend to the level of the top and/or bottom reinforcement, horizontal cracks at locations of reinforcement, and microcracks associated with the vertical and the horizontal cracks in each core.

Secondary deposits of calcium hydroxide and ettringite frequently lined air voids. Core NEW and Core N16 appeared to contain mainly calcium hydroxide in air voids. The remaining cores contained both calcium hydroxide and ettringite. No significant difference was observed in amounts of secondary deposits between the near-top region and the near-bottom region.

Air-Void System

The concrete contains abundant small spherical air voids that are characteristic of purposefully entrained air voids (Figures 9 through 18). Air-void system parameters are presented in Table 2. Typical appearance of the air-void systems is shown in Figure 18. Total air contents range from 3.1 percent (S3) to 7.8 percent (NEW). Measured spacing factors range from 0.0067 inch (NEW) to 0.0103 inch (S4). The air content of Core NEW is significantly higher, and the spacing factor is significantly lower than the other cores. The spacing factors in all cores except for NEW are similar, approximately 0.01 inch. The measured air content in S3 was the lowest of the cores, but the air voids are overall smaller. Minor air-void clustering was observed in each core (Figures 16 and 17). No significant reduction in air content was observed in the top or bottom regions of the concrete.

Table 2. Constituent Percentages and Air-Void System Parameters of Cores

Core	New	S3	S4	S5	N10	N16	ACI 201.2R-08 [#]
Air Content (A)	7.8	3.1	5.3	5.0	4.8	5.9	5.0 ± 1.5
Paste Content (p) %	30.7	29.6	27.4	31.8	29.7	28.6	
Fine Aggregate Content %	21.7	25.4	26.0	30.4	22.4	23.1	
Coarse Aggregate Content %	39.8	41.9	41.2	32.9	43.1	42.5	
Total Aggregate %	61.5	67.3	67.2	63.3	65.5	65.6	
Void Frequency (n, per inch)	11.4	5.4	6.1	7.3	6.8	6.9	
Paste-Air Ratio (p/A)	3.9	9.6	5.1	6.4	6.2	4.9	
Avg. Chord Length (inch)	0.0068	0.0057	0.0087	0.0068	0.0070	0.0085	
Specific Surface (in ² /in ³)	586	702	458	587	572	471	630 Min.
Spacing factor (inch)	0.0067	0.0089	0.0103	0.0088	0.0089	0.0097	0.008 Max.
[#] ACI 201.2R-08 recommended limits for concretes with nominal maximum aggregate size of 3/4 inch and moderate exposure to freezing and thawing.							

Concrete Distress and Deterioration

Cracks

Vertical cracks were typically less than 0.018 inch (0.45 mm) wide in the top region of the concrete and decreased in width with increasing depth. The cracks either terminated at the depth of the upper reinforcement (NEW and N16), or extended towards the depth of the lower reinforcement. The crack often changed direction from vertical to diagonal below the upper reinforcement. The cracks often branched near the upper reinforcement. The crack typically intercepted many aggregate particles, including a few large coarse aggregate particles in the top region (Figures 1 through 14), indicating that the crack developed after the concrete had gained significant strength and paste to aggregate bond. The vertical cracks in the cores extracted from in-service ties were partially filled to depths slightly greater than or equal to 1 inch (Figure 19). The crack-filling material often appeared layered and contained angular particles of carbonate and siliceous minerals non-uniformly dispersed in a very fine-grained matrix. Additional widening of the crack is suggested by separation of the crack-filling material.

The crack-filling material was not observed in the control core (NEW). The surface of the vertical crack in the control core was free of debris, non-discolored, and appeared fresh, consistent with a recent crack (compare Figure A4 vs. Figure A8).

The horizontal cracks at locations of reinforcement mainly intercepted aggregate particles and crack surfaces generally appeared to be free of significant debris or discoloration except for dried debris from coring (Figures A12 and A24).

Surface Erosion and Deterioration

The control core (NEW) is free of significant deterioration and erosion at the top and bottom surfaces. All of the cores extracted from the in-service railroad ties exhibited erosion and spalls to varying extents at both surfaces. The bottom surface of in-service ties typically exhibited more severe erosion and spalls compared to the top surface. Spalls and raveling on top surfaces of the in-service ties typically occurred within the vicinity of the vertical cracks. The top surface of these cores was generally smooth but often exhibited a few exposed aggregate particles. A few sub-horizontal, parallel cracks or microcracks were observed in the top surface region of in-service ties, only at the preexisting vertical crack (Figures 12, 13, and 15).

The original struck or free surface of the concrete (as-cast top, bottom in service) was only observed in the control core (NEW). The bottom surface of all of the cores except the control core was uneven and exhibited exposed coarse aggregate. The surface was either eroded and somewhat smooth or spalled and rough.

Polished aggregate particles were observed on bottom surfaces of the in-service cores (Figures A6, A10, A14, A18 and A22). This feature appears to be indicative of abrasion-related erosion. Assuming all ties had the same initial thickness as NEW (7 inches), concrete loss from the bottom surface at the locations where the cores were taken from the used ties ranged from 0.1 inch in S5 and N16 to 0.5 inch in S3, S4 and N10 (Table 1). The bottom end of Core S3 and S5 each exhibited a portion of fresh fractured surface, which appears to have been caused during the Bend Test from observations made on the ties. Loss of concrete from the top surface appeared to be localized and generally minimal.

SUMMARY AND DISCUSSION

Petrographic studies and air-void system analyses have been conducted on cores taken from concrete railroad ties to assess the general characteristics of the concrete with specific focus on aggregate types, air-void system parameters, depth of paste carbonation, and deterioration that may affect the durability of the ties.

Principal findings from the studies are provided in Tables 1, 2 and 3 and summarized below:

- Concretes represented by the cores were similar. Concrete in each core contained crushed carbonate rock (mainly dolostone) coarse and fine aggregates uniformly distributed in air-entrained portland cement paste. Maximum nominal top size of the aggregate was 3/4 inch. The aggregates appeared to be well graded and consisted of fairly hard, dense, durable stone.
- The concrete was well consolidated.
- No evidence of deleterious chemical reactions involving the aggregates and constituents of the paste was observed. Secondary deposits of calcium hydroxide, ettringite, or a mixture of calcium hydroxide and ettringite frequently lined the air voids. None of the deposits are associated with distress.
- The depth of paste carbonation was essentially negligible, typically less than 0.02 inch, and locally up to 0.3 inch around a few near-top aggregates based on thin-section examinations.
- Paste qualities appeared to be good overall with tight paste-aggregate bond. Estimated water-to-cement ratio (w/c) is less than 0.38. The estimation was based mainly on the physical characteristics of the concrete. The manufacture of concrete ties generally involves heat-curing. Heat-curing may significantly reduce the abundance of residual portland cement and increase the abundance of calcium hydroxide, compared to concrete cured at non-elevated temperatures.
- Measured air-void system parameters are provided in Table 2, along with applicable limits recommended by ACI 201.2R-08 for concretes with nominal maximum aggregate size of 3/4 inch and moderate exposure to freezing and thawing. Based on the measured air-void system parameters and comparisons to those recommended in ACI 201.2R-08, the air-void system parameters are less than optimal for freeze-thaw durability. With the possible exception of Cores S4 and N16, however, the air-void system parameters appear to be sufficiently close to ACI requirements. In addition, dense, low w/c, low absorption paste generally provides additional protection from frost damage. Thus, the lack of freeze-thaw related general damage in the cores obtained from the railroad ties is not surprising.
- The vertical and near-top sub-horizontal cracks in the cores extracted from ties removed from service appear to have formed after the concrete had gained significant strength and paste-to-aggregate bond. Features consistent with plastic-stage cracks were not observed. Vertical cracks in all of the in-service ties contained a crack-filling material composed of angular mineral and rock particles dispersed in a very fine-grained matrix. The mineral and rock particles are not constituents of the tie concrete, suggesting that the source of the crack-filling material is external to the concrete.
- The top and bottom surfaces of all ties except the control sample (NEW) exhibited surface erosion of varying extents. Generally, no extensive concrete loss was observed from the top surface. Polished aggregate particles observed on the bottom surfaces of the in-service ties appeared to be indicative of abrasion-related erosion. The loss of concrete in the cores taken from the in-service ties ranged from 0.1 inch to 0.5 inch.
- The horizontal cracks at the levels of strand were likely caused by the core removal process and/or the flexural loading tests.

Table 3. Selected Petrographic Observations

Core ID	Coarse and Fine Aggregates	Paste Characteristics					Paste-Aggregate Bond	Depth of Paste Carbonation (inches)*	Secondary Deposits
		Color and Luster	Hardness	Water Absorptivity	Estimated UPC and Calcium Hydroxide** %	Estimated w/c**			
NEW	Crushed dolostone	Gray and subvitreous	Hard	Low	4 to 6 6 to 9	< 0.38	Tight	<0.02	Mainly CH
S3	Crushed dolostone	Gray and subvitreous	Hard	Low	3 to 5 6 to 9	< 0.38	Tight	<0.02	CH and Ettringite
S4	Crushed dolostone	Gray and subvitreous	Hard	Low	4 to 6 7 to 10	< 0.38	Tight	<0.02	CH and Ettringite
S5	Crushed dolostone	Gray and subvitreous	Hard	Low	3 to 5 7 to 10	< 0.38	Tight	<0.02	CH and Ettringite
N10	Crushed dolostone	Gray and subvitreous	Hard	Low	3 to 5 6 to 9	< 0.38	Tight	<0.02	CH and Ettringite
N16	Crushed dolostone	Gray and subvitreous	Hard	Low	4 to 6 6 to 9	< 0.38	Tight	<0.02	Mainly CH

*locally up to 0.3 inch around a few near-top aggregate particles. **Manufacturing concrete cross-ties generally involves heat curing, which typically decreases the abundance of residual portland cement and increases the abundance of calcium hydroxide compared to non-heat-cured concrete. Therefore, estimation of w/c in the studies was mainly based on the physical characteristics of the concrete.

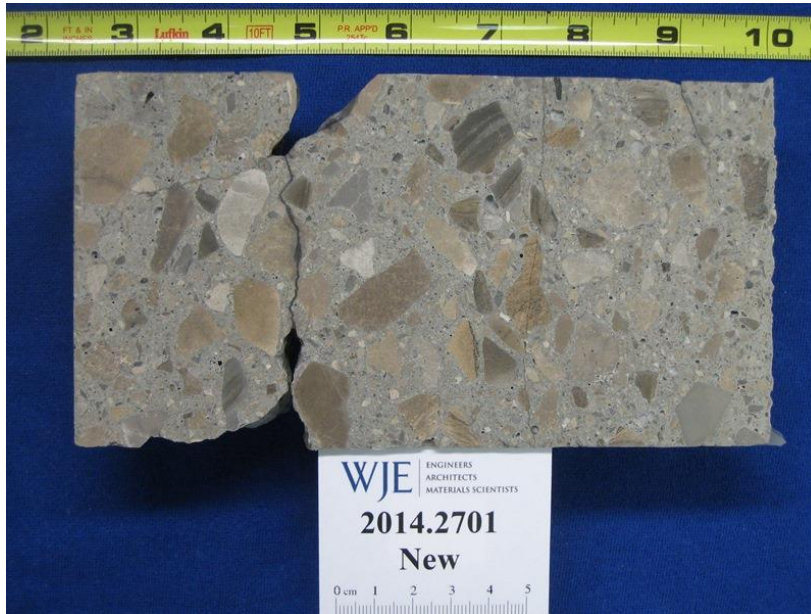


Figure 1. Core NEW. Lapped cross section illustrating the appearance of the concrete. In-service top end is on left. The yellow ruler in the photo was not at the same focal plane as concrete surface and should not be used to measure length of core. Same for Figures 2 through 8.



Figure 2. Core S3. Lapped cross section illustrating the appearance of the concrete. In-service top end is on left.

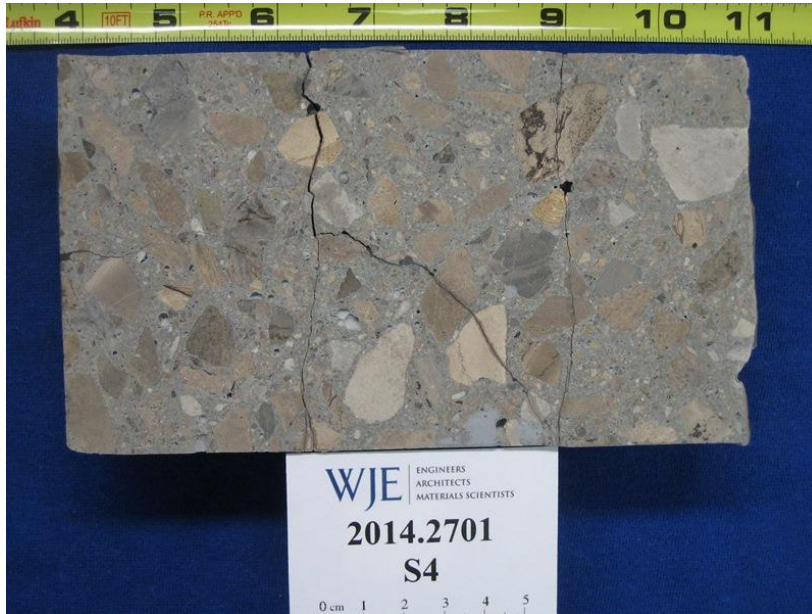


Figure 3. Core S4. Lapped cross section illustrating the appearance of the concrete. In-service top end is on left.



Figure 4. Core S5. Lapped cross section illustrating the appearance of the concrete. In-service top end is on left.



Figure 5. Core N10. Lapped cross section illustrating the appearance of the concrete. In-service top end is on left.



Figure 6. Core N16. Lapped cross section illustrating the appearance of the concrete. In-service top end is on left.

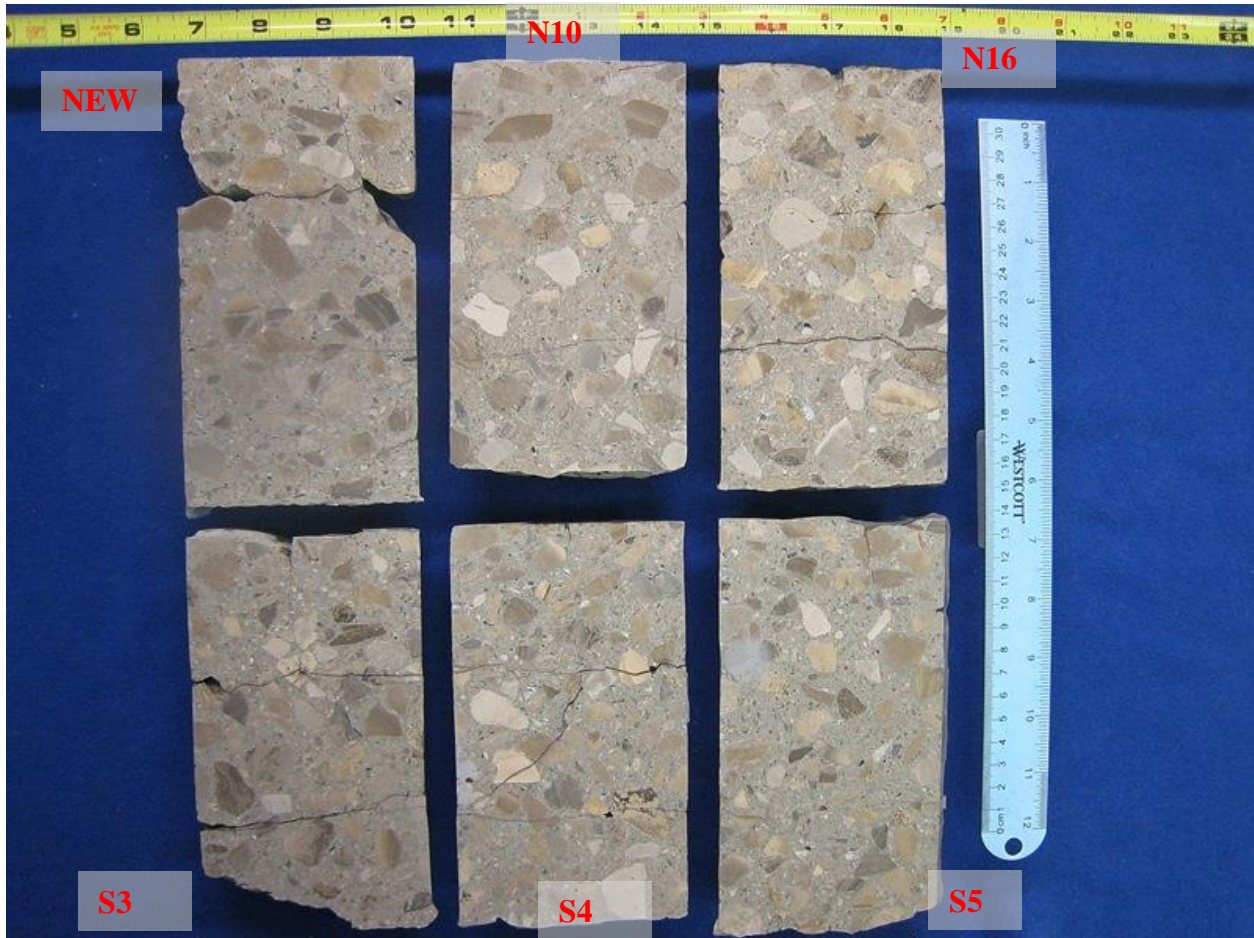


Figure 7. Lapped core sections illustrating the overall similar appearance of the concrete.

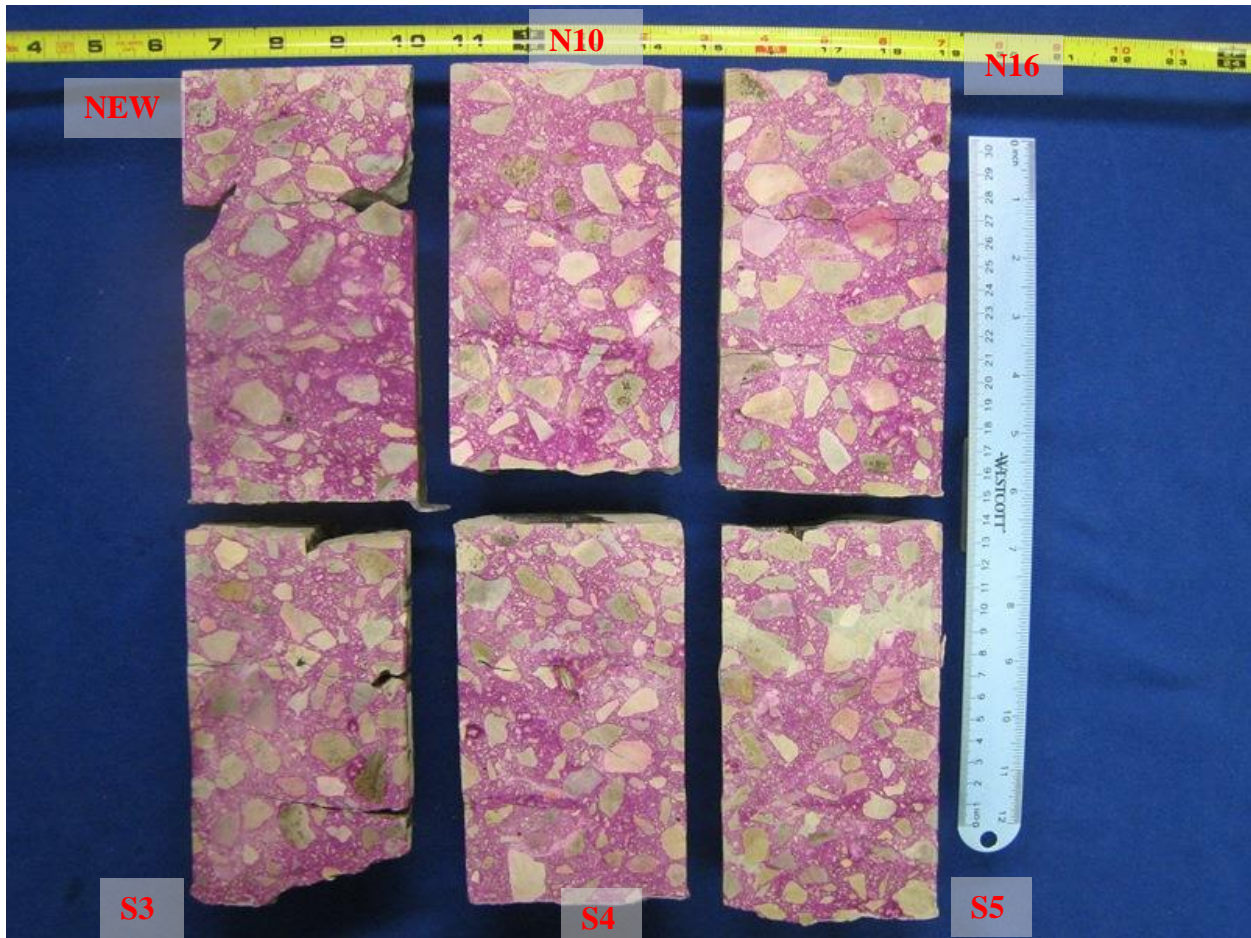


Figure 8. Saw-cut sections stained with phenolphthalein pH indicator solution. Only surficial carbonation was detected.



Figure 9. Core NEW. Close-up view showing vertical crack passing through a coarse aggregate particle, and example of air-void system in the near-top region. Epoxy was applied to the crack surfaces to reassemble the core.

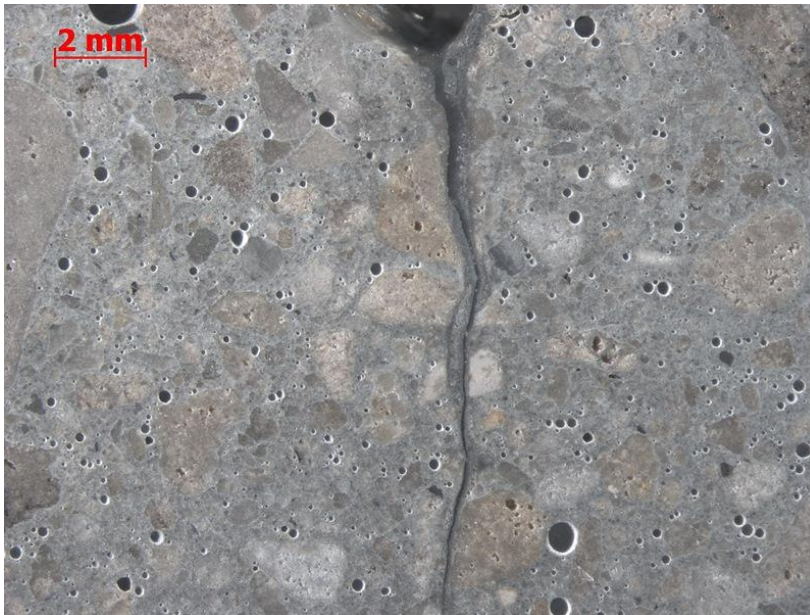


Figure 10. Core S3. Close-up view showing a vertical crack, and example of air-void system in near-top region. Epoxy was applied to the crack surfaces to reassemble the core.

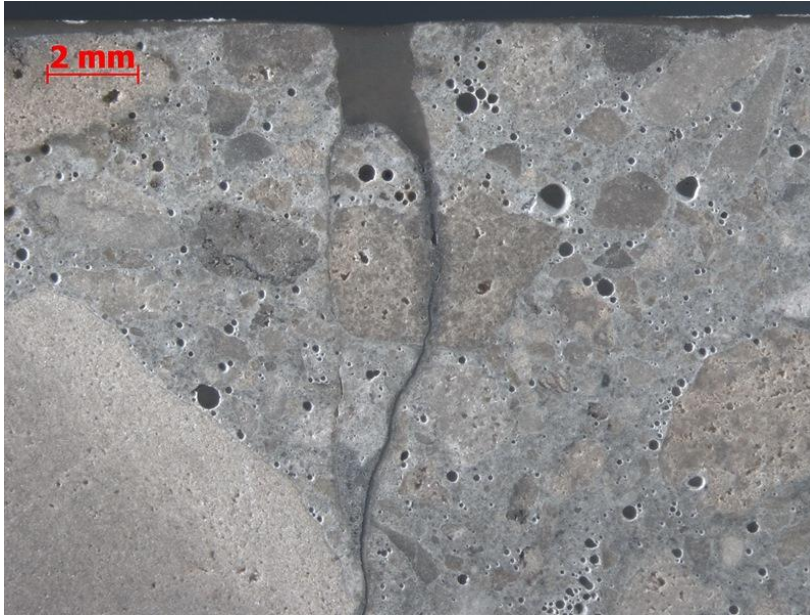


Figure 11. Core S4. Close-up view showing a vertical crack passing through a coarse aggregate particle, and example of air-void system in the near-top region. Epoxy was applied to the top surface to preserve the texture.



Figure 12. Core S5. Close-up view of near-top region showing a vertical crack and sub-horizontal cracks (red arrow). The vertical crack passes through a coarse aggregate particle. Epoxy was applied to the top surface to preserve the texture.



Figure 13. Core N10. Close-up view showing a vertical crack that passes through a coarse aggregate particle, and example of air-void system in the near-top region. Red arrows show discontinuous sub- horizontal cracks. Epoxy was applied to top surface to preserve the texture.

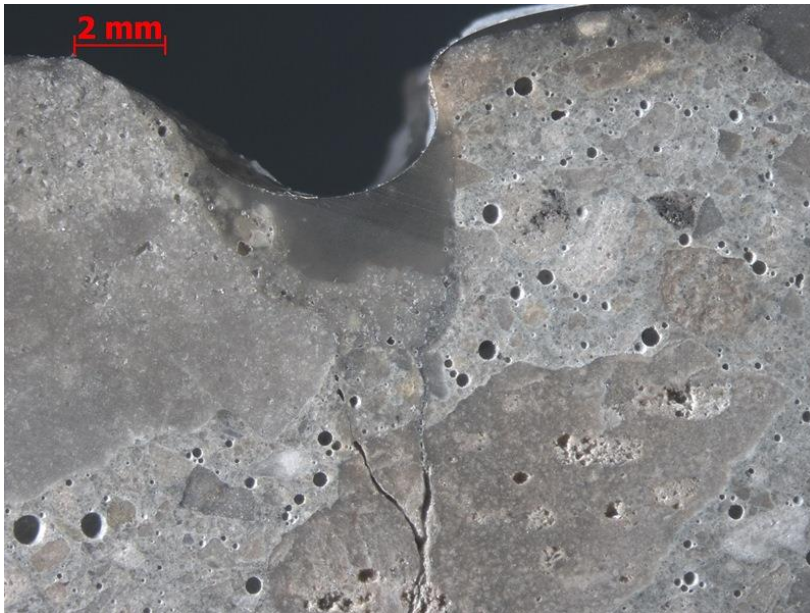


Figure 14. Core N16. Close-up view showing a vertical crack passing through a coarse aggregate particle, and example of air-void system in near-top region. Epoxy was applied to top surface to preserve the texture.

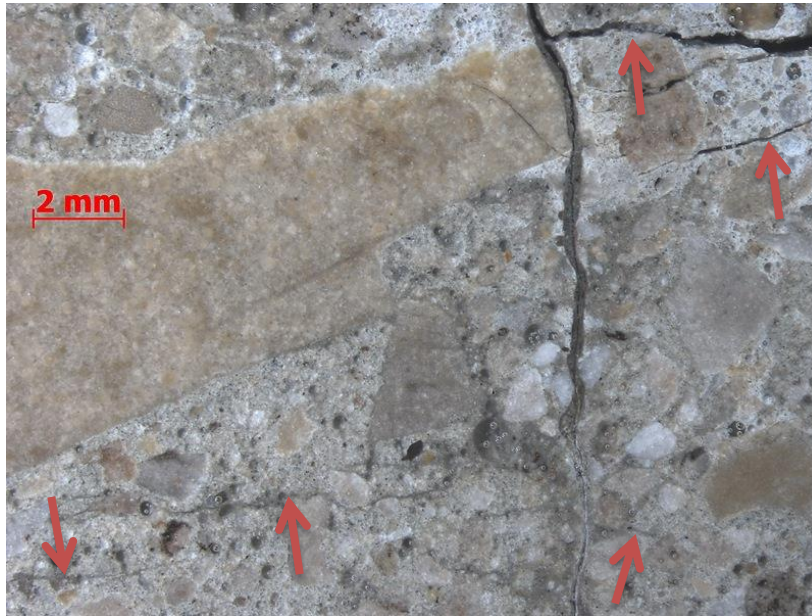


Figure 15. Core N10. Region at depth interval from 0.2 to 0.7 inch. Arrows show sub-horizontal cracks in the near-top region.

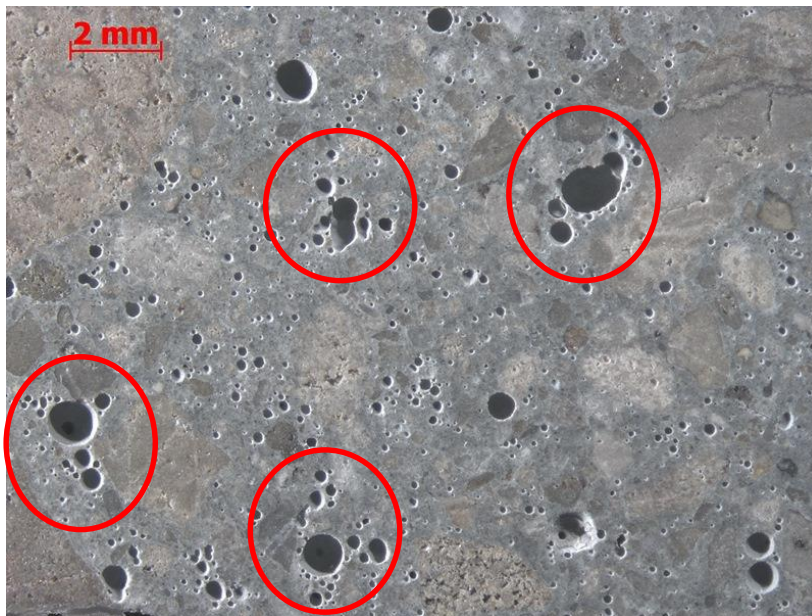


Figure 16. Core S4. A region at depth of approximately 5 inch. Examples of small air clusters are circled.

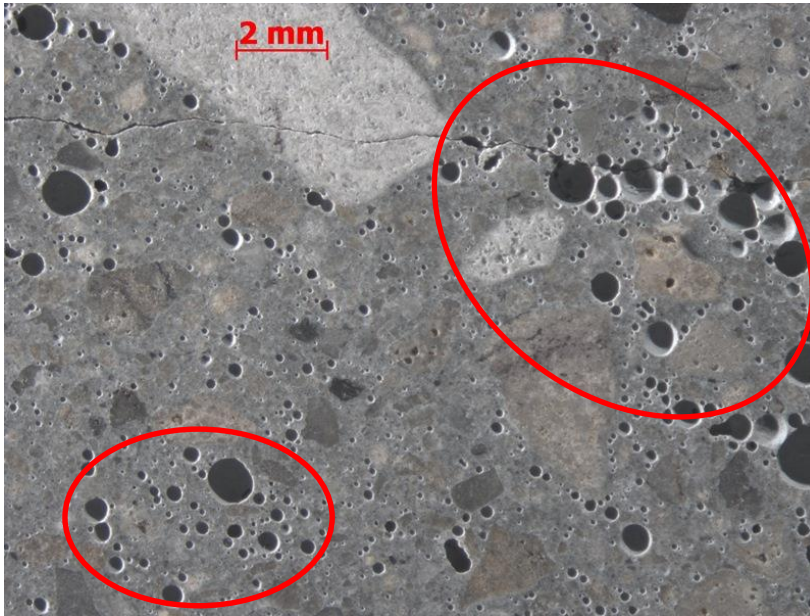


Figure 17. Core S5. Region at depth interval from 1.6 to 2.4 inches. Larger clusters of air voids are circled. The crack is a portion of the vertical crack.

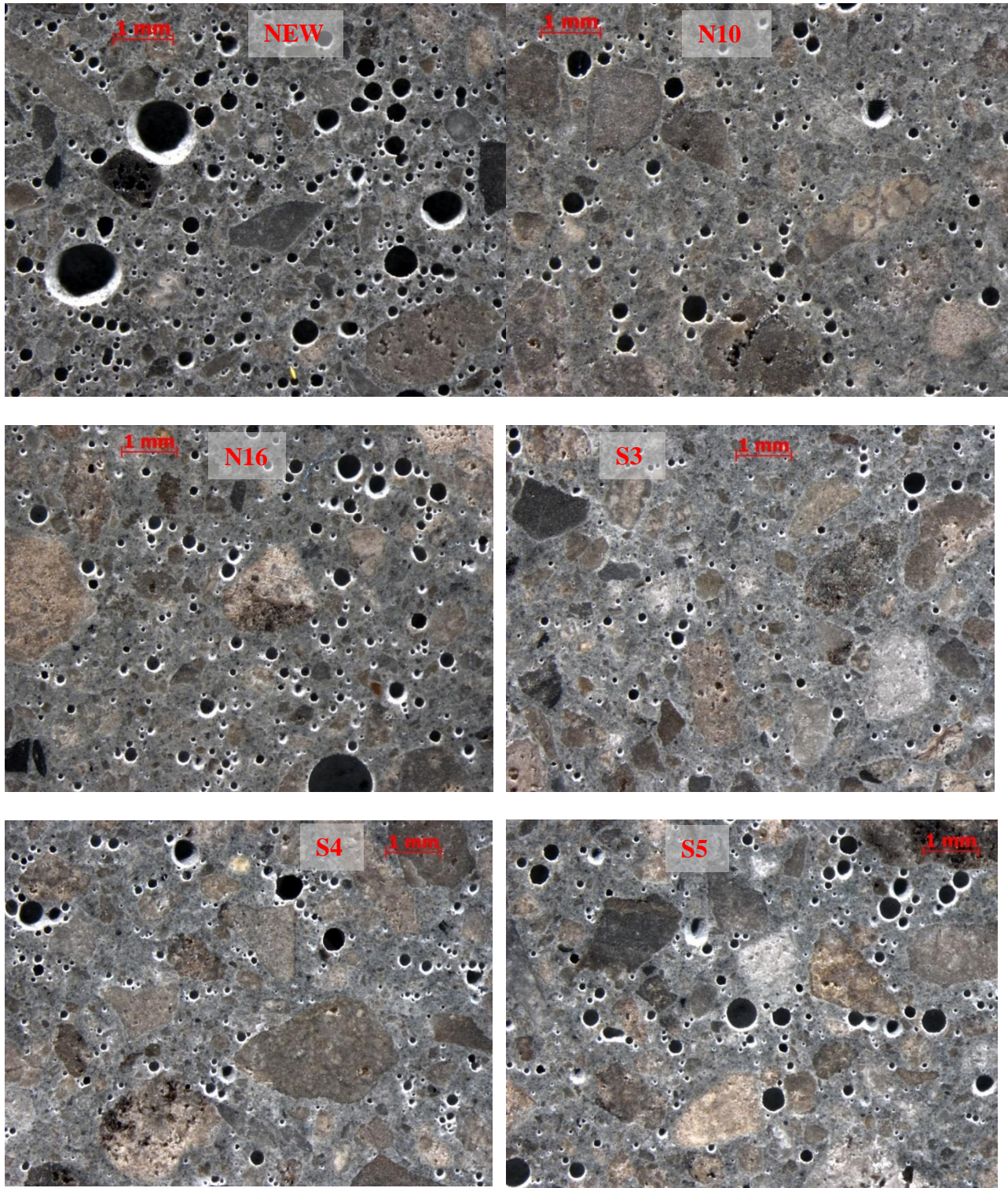


Figure 18. Typical appearance of the air-void systems in the indicated concrete cores.

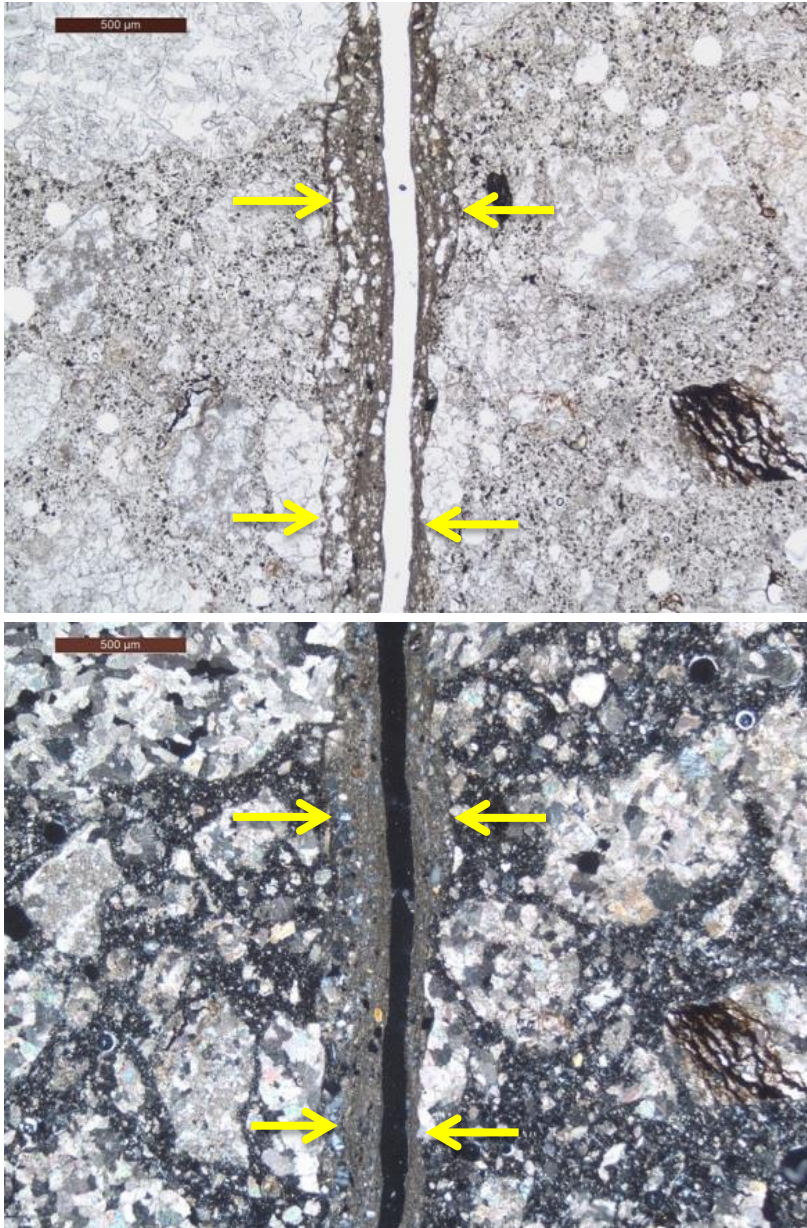


Figure 19. Core S3. Region 1 inch below the top surface is shown. Arrows show a crack-filling material. No significant carbonation was observed on the crack surface. Upper photo, plane-polarized light. Lower photo, cross-polarized light.

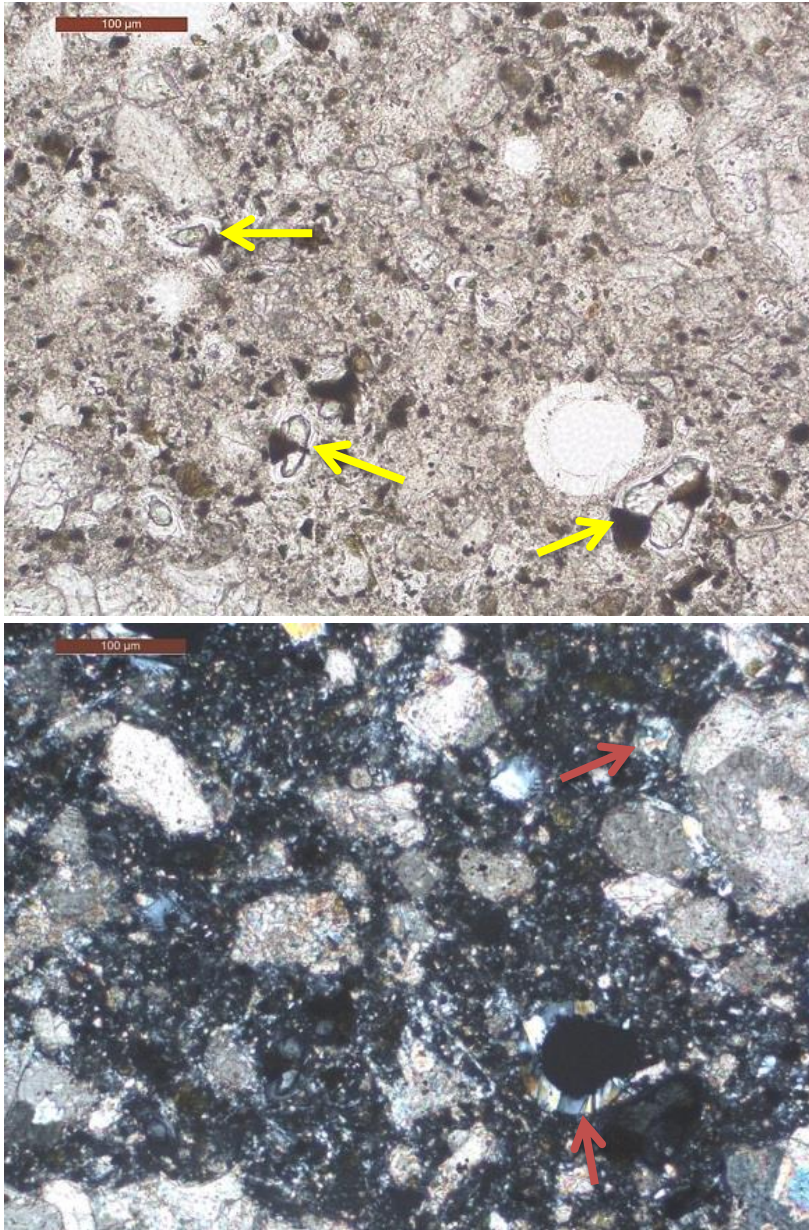


Figure 20. Core NEW. Yellow arrows show examples of residual portland cement particles in the paste. Cement-sized fragmental carbonate particles are frequently observed (bottom photo, bright pink-yellow). Red arrows show examples of secondary portlandite (calcium hydroxide). Upper photo, plane-polarized light. Lower photo, cross-polarized light.

APPENDIX A: PHOTOGRAPHS OF AS-RECEIVED CORES

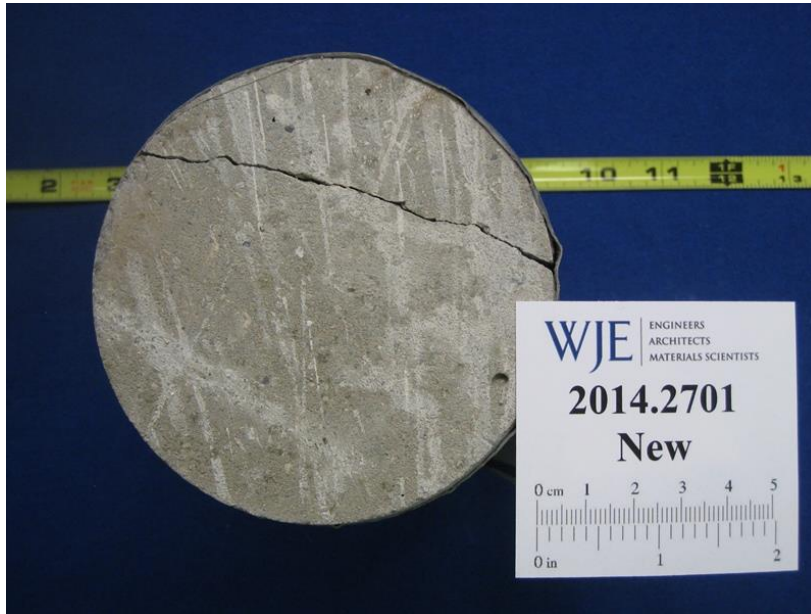


Figure A1. Core NEW, top surface. The yellow ruler in the photo was not at the same focal plane as concrete surface and should not be used to measure length of core. Same Figures A2 through A7, A9 through A16, A19 through A24.

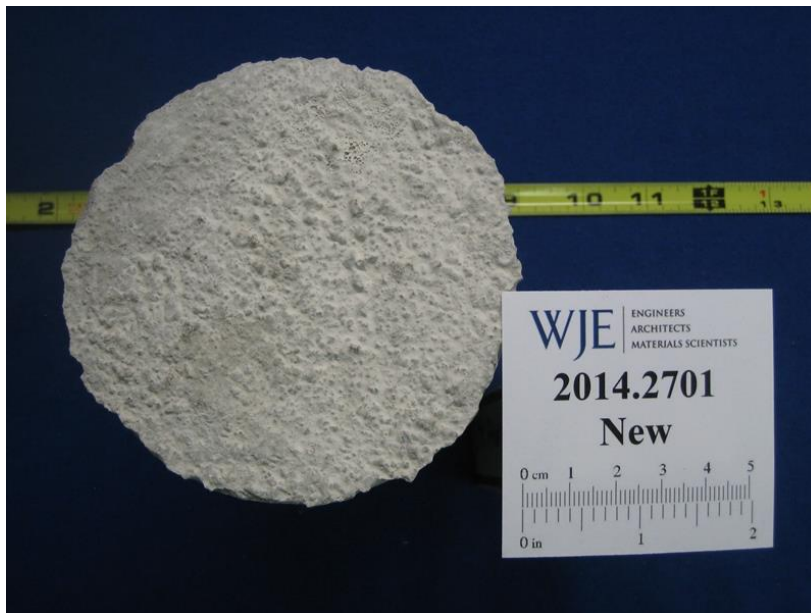


Figure A2. Core NEW, bottom surface



Figure A3. Core NEW, side view. Top surface (cast bottom) is on left.



Figure A4. Core NEW, opened fracture surface of the upper segment. The fracture appears to be fresh.

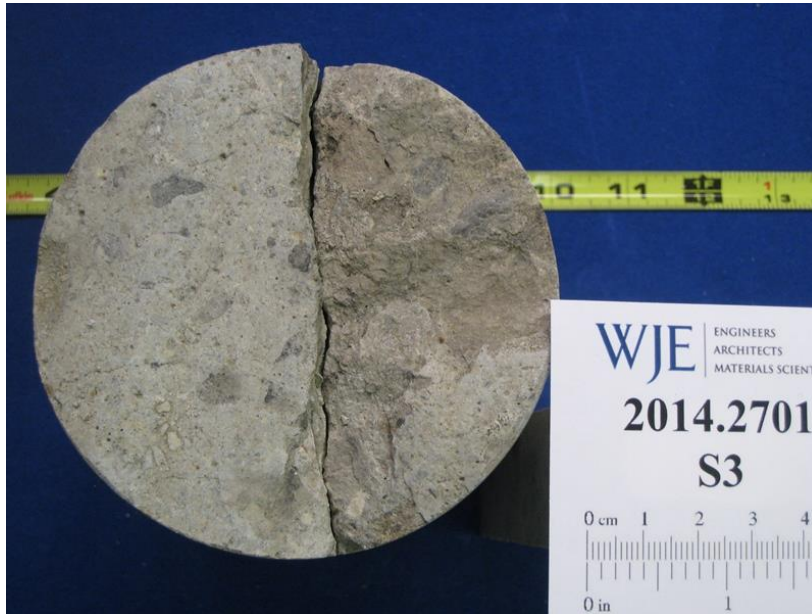


Figure A5. Core S3, top surface.



Figure A6. Core S3, bottom surface.



Figure A7. Core S3, side view, top surface is on left.



Figure A8. Core S3, fracture surface of the upper segment. Fracture does not appear to be recent.

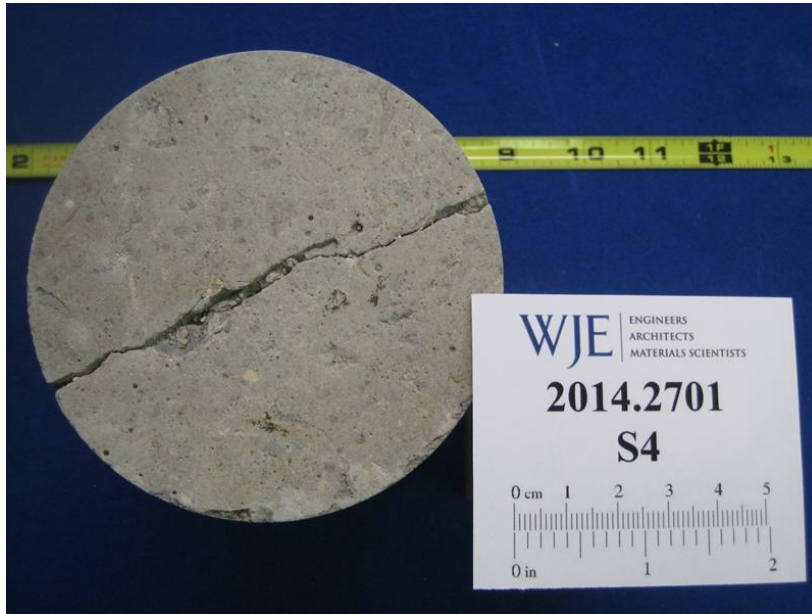


Figure A9. Core S4, top surface.

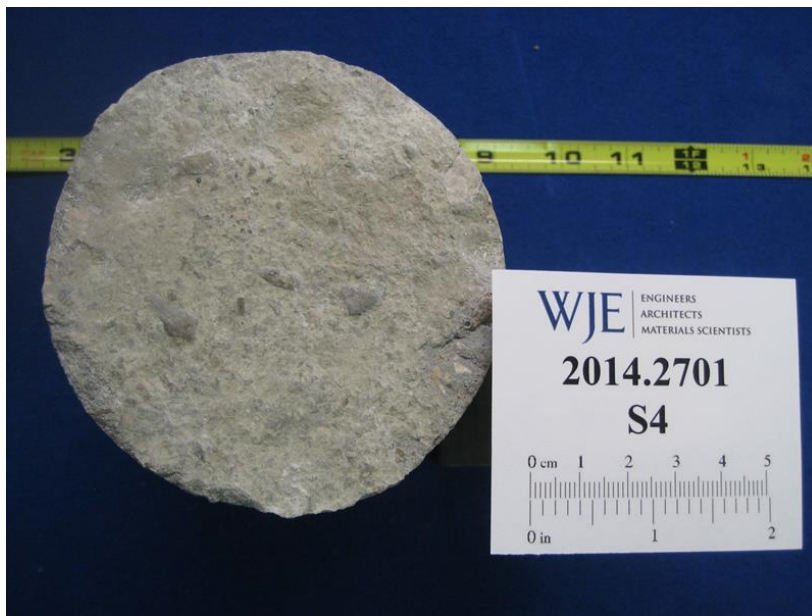


Figure A10. Core S4, bottom surface.

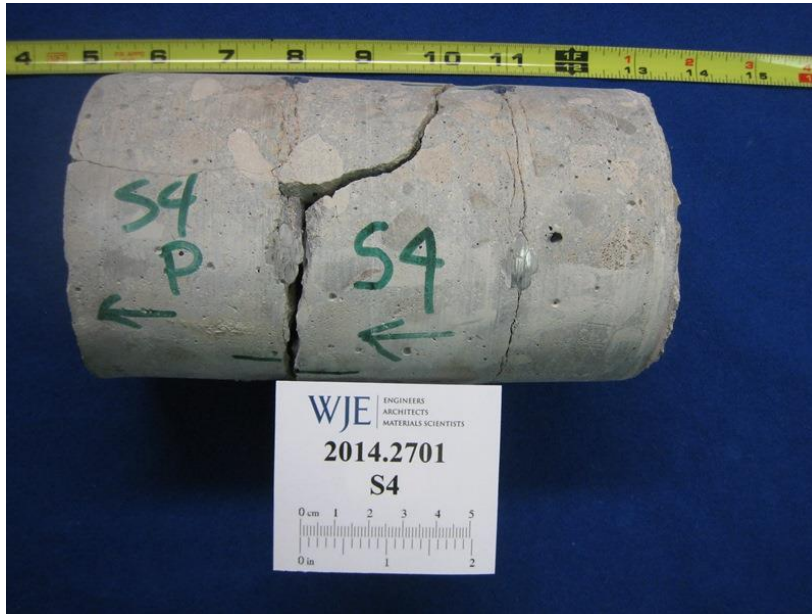


Figure A11. Core S4, side view. Top surface is on the left.



Figure A12. Core S4, matching fracture surface.



Figure A13. Core S5, top surface.



Figure A14. Core S5, bottom surface.



Figure A15. Core S5, side view A. Top surface is on left.



Figure A16. Core S5, side view B. Top surface is on left.



Figure A17. Core N10, top surface.

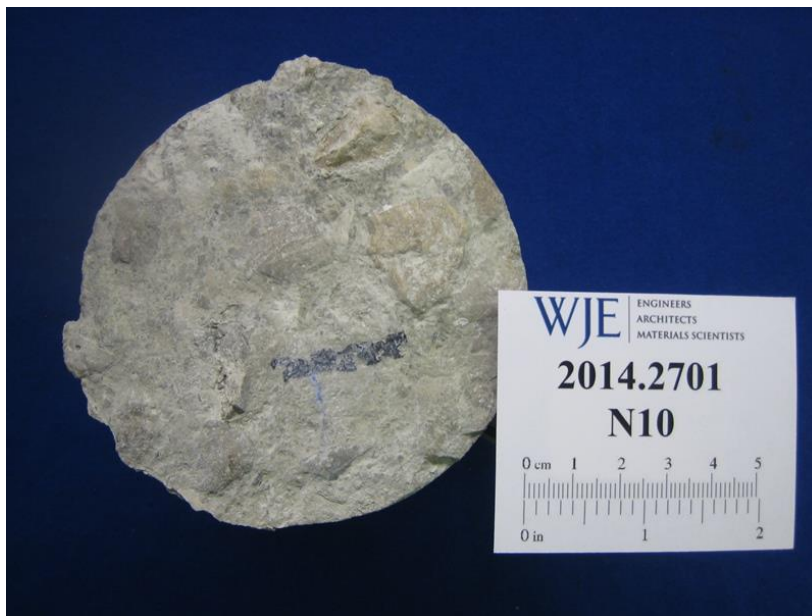


Figure A18. Core N10, bottom surface.



Figure A19. Core N10, side view A. Top surface is on left.



Figure A20. Core N10, side view B. Top surface is on left.



Figure A21. Core N16, top surface.



Figure A22. Core N16, bottom surface.



Figure A23. Core N16, side view, top surface is on left.



Figure A24. Core N16, fracture surface at reinforcement.